

# Chemical Composition of Selected Metal Poor Stars

A thesis

Submitted For The Degree of

Doctor of Philosophy

in Faculty of Science

By

AMBIKA. S



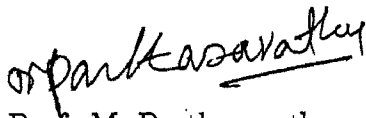
Department of Physics  
Indian Institute of Science

Bangalore-560 012, India

July 2004

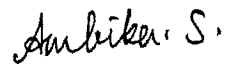
## Declaration

I hereby declare that this thesis, submitted to Physics Department, Indian Institute of Science, for the award of a Ph.D. degree, is a result of the investigations carried out by me at Indian Institute of Astrophysics, Bangalore, under the Joint Astronomy Programme, under the supervision of Professor Parthasarathy. The results presented herein have not been subject to scrutiny for the award of a degree, diploma, associateship or fellowship whatsoever, by any university or institute. Whenever the work described is based on the findings of other investigators, due acknowledgment has been made. Any unintentional omission is regretted.



Prof. M. Parthasarathy,

(Thesis Supervisor),



Ambika.S

(Ph.D. Candidate)

Department of Physics  
Indian Institute of Science  
Bangalore 560 012, India  
July, 2004

*To my family*

## Acknowledgments

I would like to take this opportunity to thank my institute IIA, and people here who have directly or indirectly helped me in pursuing my research work.

I specially thank my thesis supervisor Prof. Parthasarathy. He gave me enough space for independent thinking and advised me whenever necessary. The useful discussions I had with him were of immense help.

I am thankful to Dr. W. Aoki and Dr. B.E. Reddy for obtaining the spectra at our request and for helpful comments during the analysis.

I acknowledge, Dr. John Lester at the university of Toronto, Canada, who has kindly provided me the Unix version of the WIDTH9 program. I would like to thank Dr. Dorman and Dr. Behr for helpful information and comments on HB stars and their evolution and Dr. Moehler for her constructive criticism. Dr. Ferraro is acknowledged for kindly providing the B, V magnitudes of M13 stars.

This research has extensively made use of the NASA ADS literature archives, NASA/ IPAC Extragalactic Database (NED), CDS (simbad) database and *vizier* services. These services are acknowledged.

I thank the conveners of Joint Astronomy Program (JAP), Prof. Arnab and Prof. Jog, my co-guide for their kind help in JAP related matters.

I thank the director of IIA for extending the facilities in IIA for my research. Members of Board of Graduate Studies and Prof. A. V. Raveendran are acknowledged. Mr. Nathan and Mr. A.V. Ananth are thanked for their co-operation regarding the computer facilities. Ms. Vagiswari and Mrs. Christina are acknowledged for their help with the library facilities. It is in VBO Kavalur, that I got the experience in observational astronomy. I thank all the VBO (Kavalur) staff for their kind support.

I would like to thank all my IIA friends : my batchmates, juniors, seniors and library trainees (ofcourse, Shalini !) who made my stay in IIA a pleasant one. I am just mentioning few names, from whom I got academic benefit : Helping hand of Chai and Girish during our coursework time and later during the project time, Dharam's co-operation during guide hunting days, Nagaraj's company during the

days of programming, useful tips of Reddy, Sivarani, Pandey and Aruna at times, trouble shooting skills of Baba Varghese whenever I got struck with any software (even while writing thesis !), Srik's & Sankar's e-help, which never made me realize their absence : all these friends have taught me, what learning and sharing is all about. Specially Geetanjali, who introduced me to IRAF and IDL, with whom I had many useful discussions, made the things at IIA look different because of her constant friendship.

I also would like to thank friends in IISc and friends in other JAP related institutes for their friendship and the word of encouragement at times.

Lots of memories haunt, when I climb my first step in the ladder. My school teachers at Bharatmata Vidyamandir, who taught me in my mothertounge are fondly remembered. Their patience to listen and answer any nonsense question of a kid, kept the curiosity and questioning attitude of the child alive. I would like to acknowledge the unseen person Dr. Vasudev, who used to write weekly science articles in 'Prajaa-vani' for children. His articles inspired me in my childhood to choose basic science as my career, against the current of applied sciences.

I acknowledge my lecturer K. L. S. Sharma of Jain College and Dr. C. R. Ramaswamy from Bangalore University for their mesmerizing lectures and encouragement. Madam R.C. Usha from Vijaya High School, who showed me the virtue of discipline in any work, is always remembered. If I happen to meet her any time, would like to say, we are not Rathan of Kabuliwala as she used to imagine us.

Manjula, because of whose persistence I took the entrance examination and landed up in a research institute, is greatly acknowledged.

I thank my all my family members, aunts and uncles, for their constant encouragement. Thanks are also due for my cousins and friends. From the past couple of years, whenever we meet, they had only one mantram to chant : "*Inno aagilvaa* (still not over) ?". So folks, your consistent *encouraging words (!?)* are greatly thanked ! Finally it is coming to an end : -).

My parents and brother, who were often the targets of my frustration during the course and who patiently waited with a hope that I will finish 'someday', are greatly sympathized and thanked.! I also thank the person, to whom the headache later got transfered and who acted as a catalyst, making me wind up the course faster.

# Contents

---

<b>1</b>	<b>General Introduction</b>	<b>1</b>
1.1	Kinematics . . . . .	3
1.2	Surveys : . . . . .	4
1.2.1	Current Understanding . . . . .	5
1.3	Stellar evolution . . . . .	6
1.3.1	Main sequence . . . . .	6
1.3.2	Subgiant . . . . .	8
1.3.3	Red Giant Branch (RGB) . . . . .	8
1.3.4	Horizontal Branch (HB) . . . . .	9
1.3.5	Post-HB evolution : Asymptotic Giant Branch (AGB) . . . . .	9
1.3.6	Evolution of high mass stars . . . . .	11
1.4	Abundance variation of elements with respect to metallicity . . . . .	11
1.4.1	Light elements: He, D, Li, Be, B . . . . .	13
1.4.2	CNO abundances . . . . .	14
1.4.3	$\alpha$ -elements . . . . .	15
1.4.4	Odd- $z$ elements . . . . .	15
1.4.5	Fe peak elements . . . . .	15
1.4.6	The neutron capture elements . . . . .	16
1.4.7	Abundance of heavy elements . . . . .	18

<b>2</b>	<b>Observations and Analysis</b>	<b>22</b>
2.1	Observations and description of selected stars: . . . . .	22
2.1.1	ZNG 4 in M13 . . . . .	22
2.1.2	LSE 202 . . . . .	23
2.1.3	BPS CS 29516-0041 (CS 29502-042), BPS CS 29516-0024 and BPS CS 29522-0046 . . . . .	23
2.2	Data Reduction: . . . . .	24
2.3	Analysis . . . . .	26
2.3.1	Atmospheric Models . . . . .	26
2.3.2	Line information (atomic data) . . . . .	27
2.3.3	Spectral analysis code . . . . .	28
2.4	Determination of atmospheric Parameters . . . . .	29
2.4.1	Effective Temperature . . . . .	29
2.4.2	Gravity . . . . .	30
2.4.3	Microturbulent Velocity . . . . .	31
<b>3</b>	<b>Chemical composition of UV-bright star ZNG 4 in the globular cluster M13 *</b>	<b>32</b>
3.1	Abstract . . . . .	32
3.2	Introduction . . . . .	33
3.3	Observations . . . . .	34
3.4	Analysis . . . . .	35
3.4.1	Radial velocity . . . . .	35
3.4.2	Atmospheric parameters . . . . .	35
3.4.3	Balmer Lines . . . . .	38
3.5	Results . . . . .	39



3.6	Discussion . . . . .	43
3.7	Evolutionary status of post-HB Star . . . . .	46
3.8	Conclusions . . . . .	47
<b>4</b>	<b>Abundance analysis of the metal poor giant : LSE-202</b>	<b>56</b>
4.1	Abstract . . . . .	56
4.2	Introduction . . . . .	57
4.3	Observations . . . . .	58
4.4	Analysis . . . . .	59
4.5	Results . . . . .	61
4.5.1	Radial velocity . . . . .	61
4.5.2	Atmospheric parameters and abundances . . . . .	62
4.5.3	Non LTE corrections . . . . .	62
4.5.4	Hyperfine structure effects : . . . . .	64
4.5.5	Elemental abundances . . . . .	64
4.5.5.1	Lithium Abundance . . . . .	64
4.5.5.2	CNO elements . . . . .	65
4.5.5.3	Odd z elements . . . . .	65
4.5.5.4	$\alpha$ -elements . . . . .	66
4.5.5.5	Fe peak elements . . . . .	66
4.5.5.6	Heavy elements . . . . .	67
4.5.5.7	r-process elements . . . . .	68
4.6	Discussion and Conclusions . . . . .	69
<b>5</b>	<b>High resolution spectroscopy of metal poor halo giants :</b>	
	<b>CS 29516-0041, CS 29516-0024 and CS 29522-0046</b>	<b>89</b>
5.1	Abstract . . . . .	89
5.2	Introduction . . . . .	90

5.3	Observations and Analysis . . . . .	92
5.3.1	Determination of atmospheric parameters . . . . .	93
5.4	BPS CS 29516-0041 (CS 29502-042) . . . . .	96
5.4.1	Radial velocity . . . . .	96
5.4.2	Atmospheric parameters . . . . .	96
5.4.3	Abundances . . . . .	96
5.4.3.1	Comparison with the results of Cayrel et al. (2004) . . . . .	98
5.5	BPS CS 29516-0024 . . . . .	99
5.5.1	Radial velocity . . . . .	99
5.5.2	Atmospheric Parameters . . . . .	99
5.5.3	Abundances . . . . .	101
5.5.3.1	Comparison with the study of Cayrel et al. (2004) . . . . .	103
5.6	BPS CS 29522-0046 . . . . .	104
5.6.1	Radial velocity . . . . .	104
5.6.2	Atmospheric parameters . . . . .	104
5.6.3	Abundances . . . . .	106
5.7	Conclusions . . . . .	107
<b>6</b>	<b>Summery and Conclusions</b>	<b>120</b>
6.1	ZNG 4 in M13 . . . . .	121
6.2	LSE 202 . . . . .	123
6.3	BPS CS objects . . . . .	124
	<b>References</b>	<b>127</b>
	<b>List of Publications</b>	<b>134</b>

# Chapter 1

## General Introduction

---

The extremely metal poor (EMP) stars are the oldest objects known in our galaxy. It is necessary to know their chemical composition in order to observe the products of Big Bang nucleosynthesis, to understand the earliest episodes of star formation (or star formation history of our galaxy) and regarding the first heavy element producing objects. The study of their chemical composition, serve as a tool to constrain the model of stellar nucleosynthesis, yields of Type I and Type II supernovae and there by Galactic chemical evolution (chemical enrichment history of our galaxy).

Theories of Big Bang nucleosynthesis suggest that, it was mainly hydrogen, helium and little amount of elements upto boron which were synthesized primordially. Other metals (elements heavier than lithium) were formed from the nucleosynthesis and evolution of initial stellar generations (Spite & Spite (1985), Cayrel 1996).

There have been several models which are constructed to interpret the chemical evolution of the Galaxy (Eggen et al. 1962, Trimble 1983, Edmunds and Pagel 1984). The basic points in these scenarios are : about 15 billion years ago, the galaxy was a cloud (or several clouds) basically made up of hydrogen and helium. The first generation of stars (Population III) stars were formed basically from these two elements. They built heavy elements in their interiors and when they exploded as supernovae (SNe), they released these elements into the galactic (interstellar) matter [Burbridge et al. (B<sup>2</sup>FH) 1957, Wallerstein et al. 1997]. The Galaxy, thus got

enriched little by little.

The stars, that formed from the (ISM) clouds which contained the ejecta of first generation of stars, were called Population II stars. If the star formation is triggered by shockwaves of supernova explosions, the composition of the formed star must be a mixture of the ISM and supernova products. The abundance analysis of the metal poor stars reveal the presence of large dispersions in heavy elements. This could be interpreted as the incomplete mixing of the interstellar medium (ISM). But each type of elements, like  $\alpha$  process, Fe peak and neutron capture elements show an unique dispersion (McWilliam et al. 1995, Cayrel et al. 2004), which cannot be simply explained by inhomogeneity of the ISM. (The topic is discussed further, later in the chapter). These facts imply mixing of ejecta from small number of SNe into the parent clouds. The study of the chemical composition of the metal poor stars can thus provide information about the yield of the SNe.

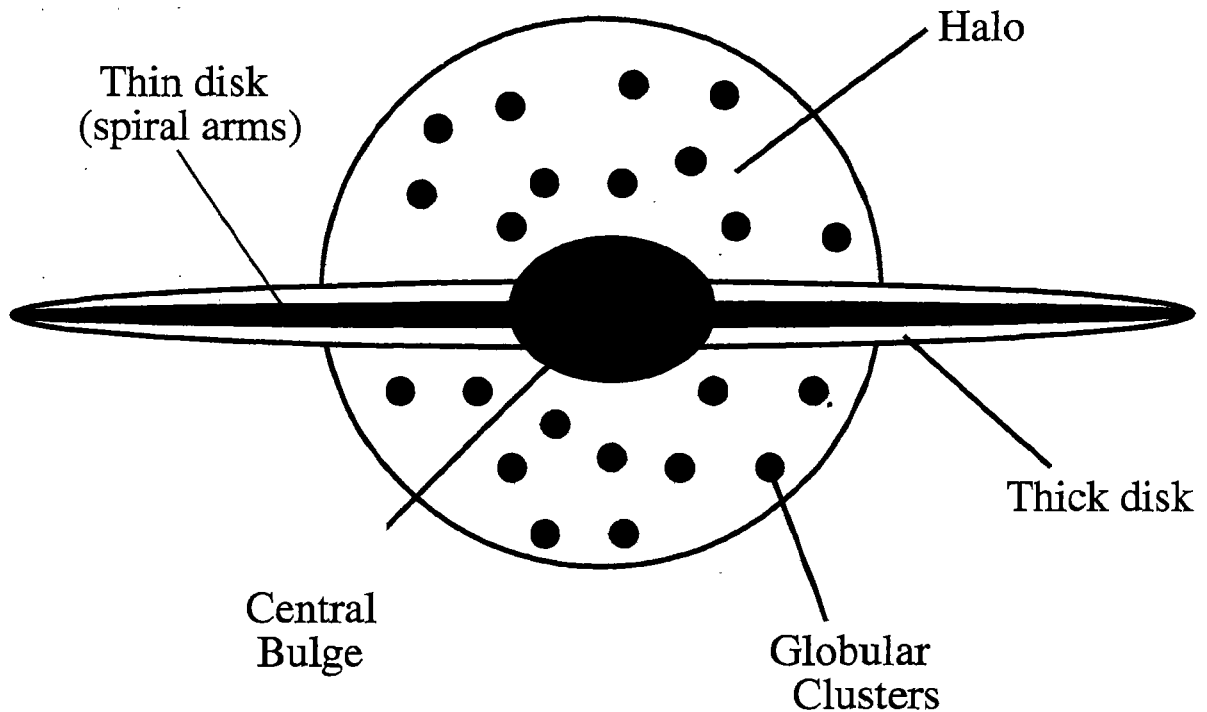


Figure 1.1: Schematic diagram of our galaxy, viewed edge on, showing its components.

The schematic diagram of our galaxy is shown in figure 1.1. Stars in the thin disk (Population I) have solar metallicity.

The stars in globular clusters are moderately metal poor ( $-2.5 < [\text{Fe}/\text{H}] < -0.4$ )<sup>1</sup>. Being in the cluster environment, the stars in the globular clusters (GC) must have undergone several episodes of star formation and thus are slightly enriched in metals. These stars in GCs give unique information about age of the cluster, as all the stars have same distance, same time of formation and similar chemical composition. In this regard, extremely metal poor stars can be defined as the stars which are more metal poor than the stars in the most metal poor globular clusters ( $[\text{Fe}/\text{H}] < -2.5$ ).

The most metal poor stars are mainly located in the galactic halo. Compared to the galactic disk, galactic halo has a smaller density of gas (interstellar matter) which may be due to the collapse of the Galaxy (Eggen et al. 1962). Therefore less stars are formed per unit volume, so that the metal enrichment of the halo is much smaller than that of the disk. This collapse can also explain the kinematical properties of the stars of the halo and of the disk.

Stars in the thick disk were presumed to have a metallicity linking Population I and II (with  $-1.0 < [\text{Fe}/\text{H}] < -0.3$ ). But Morrison et al. (1990), Beers and Sommen Larsen (1995) have reported the metallicity of the thick disk going down to -2.0 or even lower.

## 1.1 Kinematics

The kinematics of very metal poor stars are quite different from the stellar population in the solar neighborhood. Eggen et al. (1962) have observed that: (i) these stars move in a highly elliptical orbits instead of circular (ii) their velocity perpendicular to galactic plane (W) is larger than normal star and (iii) their angular momentum with respect to the galactic center is smaller than the angular momentum of stars with circular orbits. From the proper motion study of these stars, Majewski (1992) has claimed the halo to be slightly retrograde. Figure 1.2 shows the evolution of

---

<sup>1</sup>Generally the abundance of iron  $[\text{Fe}/\text{H}]$  is considered to be the metallicity of the star.

We adopt the usual spectroscopic notations :  $\log \epsilon(\text{A}) = \log_{10}(\text{N}_\text{A}/\text{N}_\text{H}) + 12.0$  and that  $[\text{A}/\text{B}] = \log_{10}(\text{N}_\text{A}/\text{N}_\text{B})_\star - \log_{10}(\text{N}_\text{A}/\text{N}_\text{B})_\odot$  : where A and B are two different elements and  $\text{N}_\text{H}$  is the number density of hydrogen.

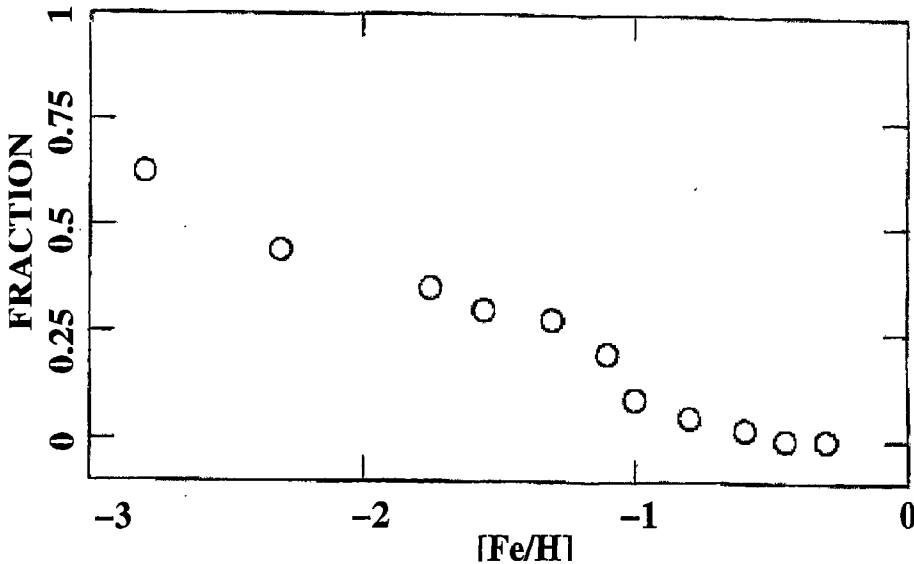


Figure 1.2: Evolution (trend) of proportion of retrograde orbits with  $[\text{Fe}/\text{H}]$  (Carney et al. 1994)

proportion of retrograde orbits as a function of metallicity in the survey of Carney et al. (1994). The transition from the galactic halo to the galactic disk is fairly abrupt, with not a single retrograde orbit at  $[\text{Fe}/\text{H}] > -0.5$ .

## 1.2 Surveys :

Surveys of these metal poor stars fall into two categories. One is based on their kinematical studies (proper motion surveys) and low resolution spectroscopy (spectroscopic surveys).

Sandage and coworkers (1986, 1987) studied 1125 high proper motion stars from the UVW velocity component and ultraviolet excess in these stars. They have derived the metallicity from  $\delta(U - B)$  excess. The probability of finding metal poor stars increases by several hundred times in these kinds of surveys but the output sample will be kinematically biased.

The other category consists of stars observed spectroscopically down to a limiting magnitude in a given field of the sky. It was first carried out by Bond (1980, 1981),

whose survey covered 5000 square degrees of the sky, down to  $B = 11.5$ . This survey discovered 100 metal poor stars with 3 stars of metallicities equal to or below  $[\text{Fe}/\text{H}] = -3.0$ . These observations proved that simple model of galactic evolution cannot work. The simple model of galactic evolution assumes a (i) closed box model with no infall or loss of matter, (ii) instantaneous recycling and mixing of elements and (iii) constant nuclear yields. If this model were to hold good, then Bond's survey should have revealed many more very metal poor stars than what was observed.

One more major attempt was started by Beers, Preston and Shectman (1985, 1992, known as BPS survey), which is still on going. They used a 4 degree objective prism in combination with a narrow band filter with band pass of  $150 \text{ \AA}$ , centred at Ca II doublet at 3933, 3968  $\text{ \AA}$  (Ca II H and K lines), using 61 cm Curtis Schmidt telescope at CTIO or Burrell Schmidt telescope at KPNO. The stars with weak or absent Ca II H and K lines were identified by visual inspection of plates, then followed up with slit spectroscopy of the most promising candidates. The limiting magnitude of the survey was  $B=16$ . The above mentioned survey resulted in the discovery of more than 100 new metal poor stars with  $[\text{Fe}/\text{H}] \leq -3.0$

Similar to this, is the digitized Hamburg/ESO objective-prism survey (Christlieb et al. 2001). But these surveys so far have discovered quite many extreme metal poor stars but not a single Population III (zero metal) star. HE0107-5240 is the most metal poor star (with  $[\text{Fe}/\text{H}] = -5.3$ ) known till date (Christlieb et al. 2004).

### 1.2.1 Current Understanding

Several scenarios have been invoked for not finding a true Population III star, yet. One scenario is (Yoshi 1981, Yoshi et al. 1995) that, these stars are contaminated by a small amount of interstellar matter accreted, when they are orbiting in an already enriched gas during the 10 Gyr. Second scenario is (Truran and Cameron 1971), low mass cut off of IMF in zero metal environment may be above  $0.9 M_{\odot}$ . In that case, an observable first generation star cannot exist till now. Lastly, that these stars may be existing but the surveys might not have covered it so far.

## 1.3 Stellar evolution

In a young open cluster like Hyades, stars are aligned diagonally in a color-magnitude diagram called Main Sequence, where stars are burning hydrogen to helium in their core. But the color-magnitude diagram of an old globular cluster looks very different. In figure 1.3, color magnitude diagram of a globular cluster is displayed. The upper part of the diagonal main sequence (which should be comprised of newly born O-type and B-type stars) is clearly absent.

The position of the star in the color-magnitude diagram of the cluster indicates its evolutionary state : Main Sequence (core hydrogen burning), Subgiant (shell hydrogen burning), Giant (phase after the exhaustion of hydrogen burning, where expansion provides gravitational stability, till the state of He-flash), Horizontal Branch (core helium burning and shell hydrogen burning), Asymptotic Giant branch (instability similar to giant branch, after core helium exhaustion, with double shell burning) and Planetary Nebulae (central hot star ionizing the dust envelope ejected during the AGB phase).

### 1.3.1 Main sequence

In this phase, energy is liberated in the core of the star from the nuclear fusion of hydrogen into helium (in the low mass stars ( $< 2.3M_{\odot}$ ) through p-p chain and in higher mass stars through CNO cycle). Nuclear timescale is of the order of  $10^{10}$  years for  $1M_{\odot}$  stars. This is much longer than the free fall time scale and Kelvin-Helmholtz time scale (of the order of  $10^7$  years) which characterizes pre main sequence evolution. This explains, why most of the solar neighborhood stars are observed to be main-sequence stars.

Further stellar evolution, off the main sequence depends on the initial mass of the star on the main sequence.



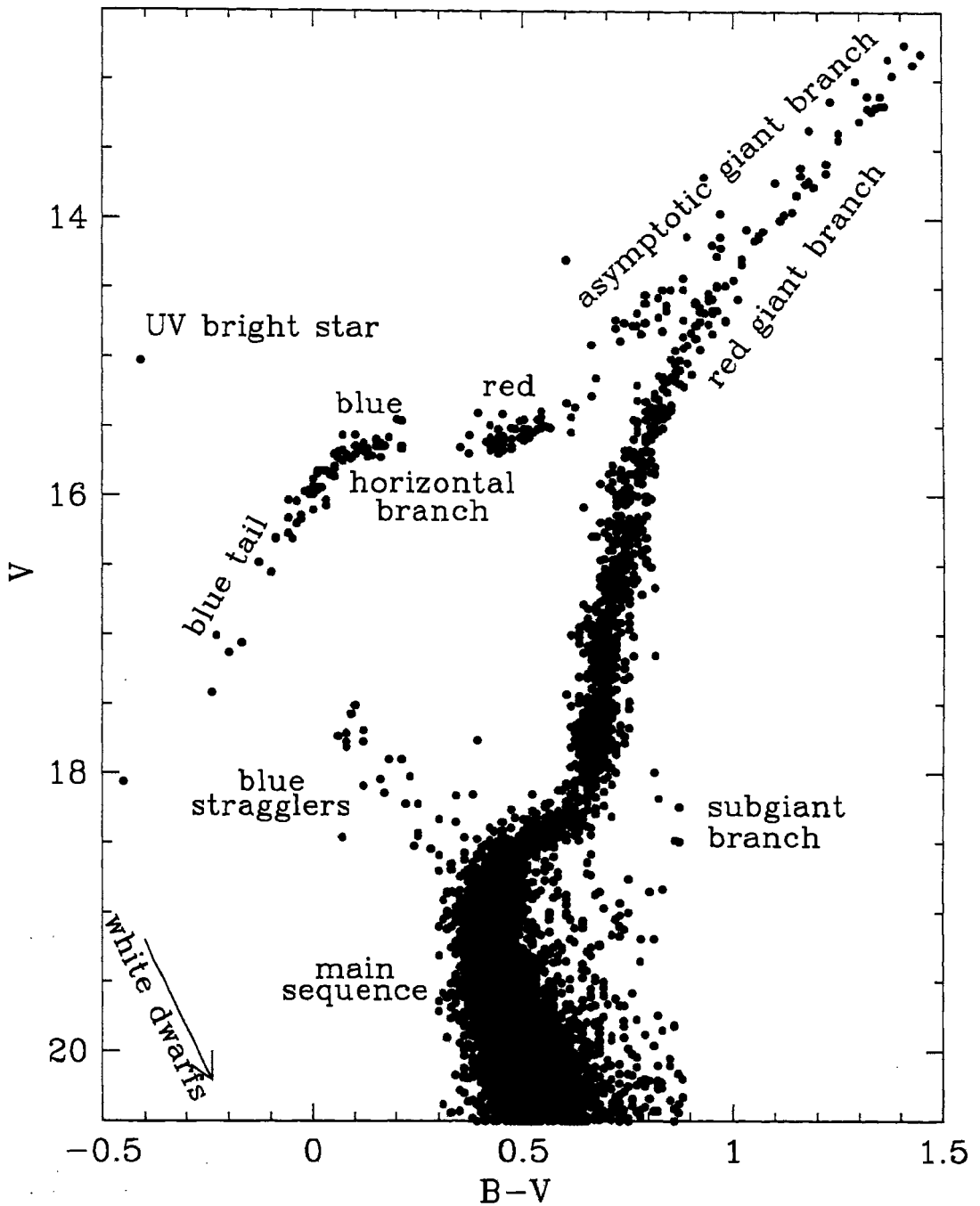


Figure 1.3: Color magnitude diagram (CMD) of a globular cluster showing the stars in different evolutionary states.

### 1.3.2 Subgiant

After the exhaustion of hydrogen core, low and intermediate mass stars would move towards the right in the H-R diagram, burning hydrogen in the shell and dumping He further into the core. As the core mass increases, the core gravitationally contracts to support the outer envelope of the star. Thus the gravitational field felt by the hydrogen shell gets stronger and stronger. To counterbalance the pressure in the shell, according to perfect gas law, density and temperature will increase, which in turn increases the rate of hydrogen burning in the shell. But as long as the envelope is radiative, it can carry a limited luminosity, as the photon diffusion rate is fixed for a star of given mass. Therefore, all the luminosity generated in the shell does not reach the surface. The remaining luminosity will heat up the intermediate layers, causing them to expand, thereby increasing the radius. This constant  $L$  followed by increase of  $R$  will lead to decrease of  $T$ , in accordance with the relation  $L = 4\pi R^2 \sigma T_e^4$ . The locus of points during this redward phase of evolution is known as subgiant branch.

### 1.3.3 Red Giant Branch (RGB)

The ability of the photospheric layers to prevent the free streaming of photons drops rapidly with the decreasing temperature. Hence,  $T_{\text{eff}}$  cannot continue to fall down as there is a temperature barrier. This forces the star to travel vertically upward in the H-R diagram (increase of luminosity). The stellar radius increases to typically 100 solar radii and the entire envelope of the star becomes convective (red giant branch, RGB). Many elements which are synthesized are brought to the surface due to first dredge up. The surface abundances are modified as follows.

- 1)  ${}^4\text{He}$  remains constant, as the surface abundance is already large.
- 2)  ${}^{14}\text{N}$  is enhanced. The conversion of  ${}^{14}\text{N}$  to  ${}^{15}\text{O}$  is the slowest step in the CNO cycle, and the processed material therefore appears mostly in the form of  ${}^{14}\text{N}$ .
- 3)  ${}^{12}\text{C}$  is highly depleted. As the processed material is mostly in the form of  ${}^{14}\text{N}$ , and the total abundance of C, N, and O remains constant, the  ${}^{12}\text{C}$  abundance will decrease as the cyclic reaction proceeds.
- 4) The  ${}^{16}\text{O}$  abundance remains constant as it is not directly involved in the CNO

cycle, although some will be processed into  $^{14}\text{N}$  (Becker & Iben 1979).

Also, there is mass loss occurring at this phase as these stars with very low gravity cannot retain coronal gas, unlike the Sun.

### 1.3.4 Horizontal Branch (HB)

In the case of low mass stars, after the star reaches the tip of the RGB, He ignites under degenerate conditions with a “flash” to remove the degeneracy. After the completion of He-flash, the star has a core which is stably fusing helium to carbon and a hydrogen shell surrounding it. This state of core-He burning and shell hydrogen burning is called Horizontal Branch (HB). Location of a star on the HB, not only depends upon its initial mass and chemical composition, but also on the mass lost by the star in its ascent of the RGB. In the case of massive stars, they have a convective core and not helium degenerate core. The central temperature reaches  $10^8$  K faster than in low mass stars and burning of the central He sets in earlier.

### 1.3.5 Post-HB evolution :

#### Asymptotic Giant Branch (AGB)

Once the He in the core of HB gets exhausted, the star is left with carbon-oxygen core surrounded by He and hydrogen shells (double shell burning state). The inert core continues to contract as in previous case, with energy generation in two shell sources. With the rapidly rising luminosity, the star will ascend the giant branch again (Asymptotic giant branch: AGB). Surface abundances get altered again due to second dredge up. Surface abundance changes are similar to those produced in the first dredge-up, with a further enhancement of  $^{14}\text{N}$  and depletion of  $^{12}\text{C}$ . During thermally pulsating state (TP-AGB), when helium sporadically burns via the triple- $\alpha$  process ( $3\ ^4\text{He} \rightarrow\ ^{12}\text{C}$ ), the star will expand and hydrogen shell burning ceases. A strong convection zone is again produced, bringing further products of nucleosynthesis to the stellar surface.

The third dredge-up mixes (*i*) freshly produced carbon from He burning and

(ii) freshly produced s-process elements (formed via slow neutron capture) into the envelope. After few pulse cycles, this converts the chemistry of the stellar surface from an oxygen rich one into a carbon rich one for all stars whose initial masses are in  $1M_{\odot} < M_{*} < 5M_{\odot}$  range.

Also heavy mass loss (of the order of few  $M_{\odot}$ ) will occur on AGB that they become planetary nebulae illuminated by hot central core with mass less than  $1.4 M_{\odot}$ . From the central stage of planetary nebulae, the exposed core burns out its hydrogen and helium shells, loses the extended envelope and descends in the HR diagram and will end up as white dwarf.

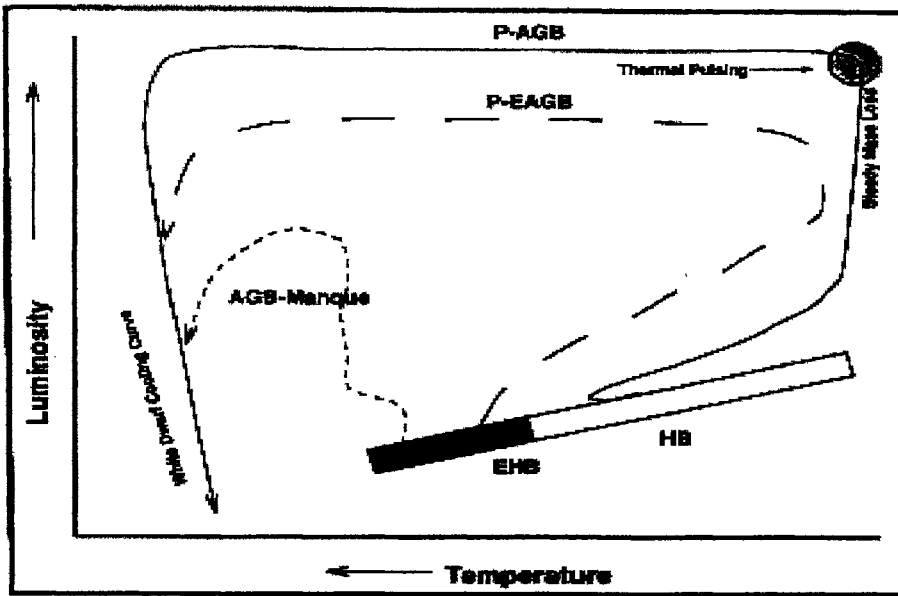


Figure 1.4: Different types of post-HB evolutionary sequences are represented schematically (Dorman et al. 1993). “EHB” stars have, too small envelope masses to reach the end stages of normal AGB evolution.

However, there are other possibilities for post-HB evolution (Greggio & Renzini 1990, Dorman et al. 1993). Figure 1.4 shows the schematic diagram of post-HB evolution. The normal AGB sequence is shown as a solid line. But if the HB envelope mass is less than some critical mass plus an amount to allow for mass loss ( $M_{\text{env}}^0 < M_{\text{env}}^{\text{TP}} + \delta M_{\text{AGB}}$ ), then it will never become a “classic” thermally pulsating AGB (TP-AGB) star. These are referred as extreme HB stars (EHB). The two

evolutionary track morphologies of this class of objects are thus.

1. Models that evolve through the early stages of the AGB but not the TP stage, which is shown by the long-dashed curve in the Figure 1.4. The evolutionary tracks for these models peel away from the lower AGB before the TP phase, as the envelope is consumed from below by nuclear burning and probably from above by stellar winds. They are referred to as post-early AGB (P-EAGB) models.
2. The least massive of the EHB models never develop extensive outer convection zones and stay at high  $T_{\text{eff}}$  ( $\geq 20,000$  K) during their evolution. Such models are known as “AGB-manque” (or failed AGB) sequences. It is shown by the short-dashed curve in the diagram.

### 1.3.6 Evolution of high mass stars

In higher mass stars (with  $M_{\star} > 10M_{\odot}$ ), Hydrogen exhaustion is followed by core helium ignition. Similarly He exhaustion is followed by carbon-oxygen core igniting. Thus the star will evolve further by exhaustion of fuel in the core, core-contraction, core ignition converting the ash to new fuel. The end product will be iron at the core, which is surrounded by more and more shell sources like an onion ring [Shu (1982), Carrol & Ostlie (1996)], which is shown in figure 1.5. Once Fe is produced at the core, further fusion is not possible, as it is the stablest element. So, after the core contraction when temperature of the order of several billion K is reached, it follows Thermodynamic behavior of matter, requiring more unbound particle. (The explosion is Type II Supernova). Thus it disintegrates to alpha particles, which further disintegrate, absorbing core's heat. The free electrons are captured by protons to form huge mass of neutrons at nearly nuclear density.

## 1.4 Abundance variation of elements with respect to metallicity

After the discovery of metal poor stars from objective-prism surveys, there have been subsequent follow up of these stars from high resolution echelle data (McWilliam et

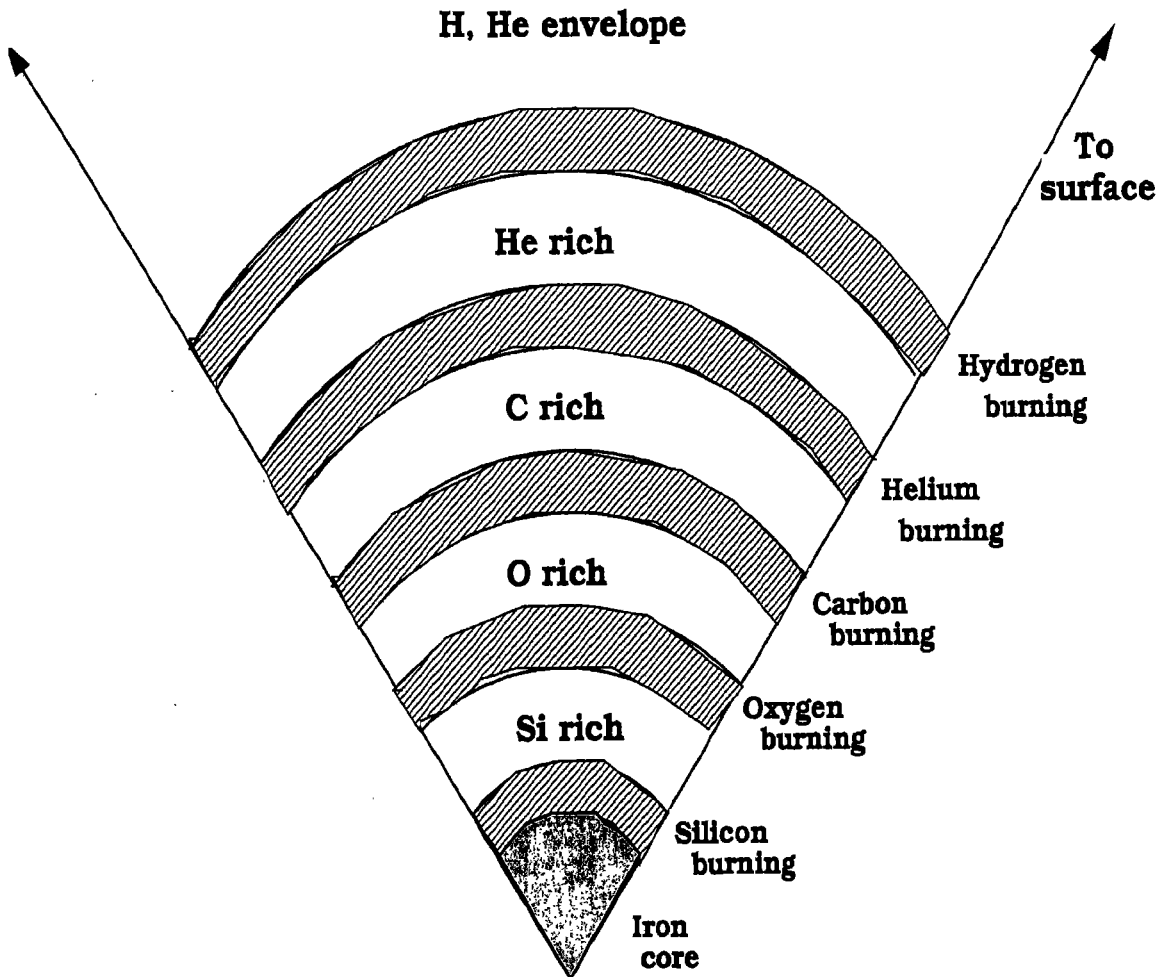


Figure 1.5: The onion like interior of a massive star that has evolved through core silicon burning. Inert regions of the processed material are sandwiched between the nuclear burning shells. The drawing is not to scale.

al. 1995, Ryan et al. 1996, Honda et al. 2004, Cohen et al. 2004). These groups have carried out the systematic survey of elemental abundances in the case of EMP stars.

In traditional spectroscopic analysis of metal poor stars, the mean abundance ratio of the chemical elements is discussed as a function of overall metallicity, usually measured by the iron abundance  $[\text{Fe}/\text{H}]$ . The results are then compared with the predictions of models of nucleosynthesis and chemical evolution of the galaxy. Thus, they provide constraints on the site and mechanism of nucleosynthesis. Some of the overall trends shown by the elements are briefly discussed below.

#### 1.4.1 Light elements: He, D, Li, Be, B

Among the light elements, helium abundance has not been directly determined in cool dwarfs. Deuterium lines are also not observable, as the primordial deuterium gets destroyed during the contraction phase towards the main sequence. Be, B lines have extremely low abundance in the Sun and are not produced in SNe II.

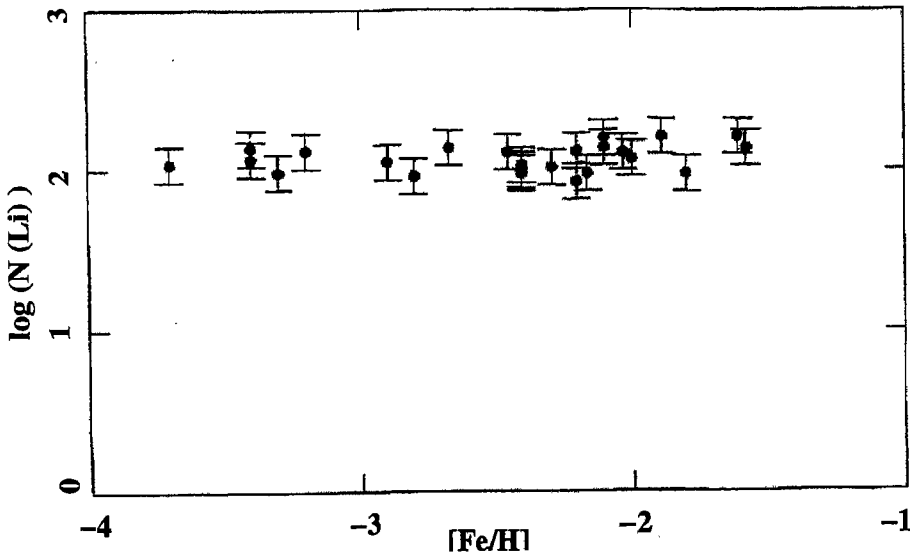


Figure 1.6: Evolution of Li abundance as a function of  $[\text{Fe}/\text{H}]$  (Spite et al. 1996). The abundance remains constant from  $[\text{Fe}/\text{H}] = -1.5$  down to  $[\text{Fe}/\text{H}] = -4.0$ .

But in the case of lithium, it is not as fragile as D and is not destroyed in the atmospheres of the halo dwarfs. Thus the Li line has been observed in halo stars (Spite and Spite 1982).

Now it is known that the Li abundance in dwarfs remain at the value of 2.1, even at the lowest metallicities. (figure 1.6) and this unique behavior of Li is a splendid confirmation of the prediction of the hot Big Bang cosmology.

However, Ryan et al. (1999) reported that the Spite lithium plateau in metal poor turn off stars show slight post-primordial enrichment. They conclude that the primordial value for Li abundance could be 2.00 dex. Also, the observed scatter in Li abundances in these (metal poor stars) are minimal ( $< 0.031$  dex). Stars cooler than the Spite plateau ( $5000 \text{ K} < T_{\text{eff}} < 5500 \text{ K}$ ) show depletion of Li by  $\approx 0.27$  dex per 100 K (Ryan et al. 1998).

## 1.4.2 CNO abundances

$[\text{C}/\text{Fe}]$  and  $[\text{N}/\text{Fe}]$  have no clear trend with  $[\text{Fe}/\text{H}]$  at low metallicity whereas, O stays overabundant with Fe by 0.5 dex, down to lowest observed metallicities.

Some stars exhibit anomalous strong G bands, characteristic of subgiant CH stars. Also there are stars with moderate to strong CN bands with  $[\text{Fe}/\text{H}] < -2.5$  and having GP index upto 7.79. Carbon enhancements in these stars are presumed to be because of the mass loss from the binary companion which has undergone AGB phase and which is now in a cool white dwarf state.

Recently study of 25 EMP giants without anomalous G-band by Cayrel et al. (2004) has yielded a mean value of  $[\text{C}/\text{Fe}] \approx 0.2$  dex with a dispersion of 0.37 dex. For O, they obtain a mean value of  $[\text{O}/\text{Fe}] \approx 0.7$  dex with a dispersion of 0.17 dex.

It is understood that Type II supernovae are responsible for the generation of significant quantities of oxygen, while Type I supernovae are responsible for the creation of most of the Fe observed.



### 1.4.3 $\alpha$ -elements

This includes Mg, Si, S, Ca and Ti. These  $\alpha$  elements closely follow oxygen as predicted by the theory (Arnett 1971), but with a smaller enhancement ( $< 0.5$  dex). (It must be noted that Mg and Ca have more accurate determination of abundances than Si). Mg is produced with core Ne-burning and shell C burning. Si and Ca are formed during Si and O burning and Ti during complete and incomplete S-burning. But Most of the  $\alpha$  elements show identical abundance ratios despite of the sites that they have been produced.

### 1.4.4 Odd-z elements

This includes Na, Al and K. The prediction of the explosive nucleosynthesis (Arnett 1971) is that the odd elements should be over deficient at low metallicities. This is confirmed for Na and K, from the observation of Cayrel et al. (2004). But Al does not show any trend in their sample and abundance scatter of this element from star to star is large.

### 1.4.5 Fe peak elements

The iron peak elements do not exactly follow Fe. At very low metallicity Cr and Mn tend to be more deficient than Fe by 0.5 dex or so, where as Co has an inverse behavior; being overabundant by a factor of 0.5 dex. Ni is also slightly overabundant, but not as much as Co.

Among iron peak elements, Cr and Mn are built up mainly by incomplete explosive Si burning, whereas Fe, Co, Ni and Zn are produced in the complete explosive Si burning. (Umeda & Nomoto 2002). Among them, Cr and Mn are found to be more deficient than Fe by 0.5 dex or so. [Cr/Mn] ratio is close to solar value in most metal poor stars though Mn is an odd-z element and Cr is an even-Z element. Ni is thought to be produced in the same nuclear process. But [Ni/Fe] seemed to increase slightly with decreasing metallicity in the survey by McWilliam et al. (1995). Recent analysis of metal poor giants by Cayrel et al. (2004) reveals [Ni/Fe] to be almost constant

( $\approx 0$ ) with decreasing metallicity.

Co shows an inverse trend compared to Cr and Fe, being overabundant by a factor of 0.5 dex (McWilliam et al. 1995, Cayrel et al. 2004). In the case of Zn, this trend of [Zn/Fe] ratio increasing with decreasing [Fe/H] is even more pronounced.

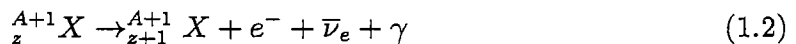
### 1.4.6 The neutron capture elements

When nuclei progress with higher number of protons, it causes a high coulomb potential barrier. Thus it becomes difficult for other other charged particles like protons,  $\alpha$ -particles etc to react with them. But this limitation does not exist when neutrons collide with these nuclei. Consequently, nuclear reaction involving neutrons can occur at low temperature assuming that free neutrons are present in the gas.

The reaction with neutrons



result in more massive nuclei that are either stable or unstable against beta-decay reaction



If the beta-decay half life is short compared to the time scale for neutron capture, the neutron-capture reaction is said to be slow process or an “s-process” reaction. s-process reactions tend to yield stable nuclei, either directly or secondarily via beta decay. On the other hand, if the half life for the beta-decay is long compared to the time scale of neutron capture, the neutron-capture reaction is termed as a rapid process or “r-process” and results in neutron-rich nuclei. These processes do not play significant role in energy production. But they (neutron-capture processes) are understood to be responsible for the synthesis of the bulk of the heavy elements in the mass region  $A \geq 60$ .

The r-process nuclei are effectively primary nucleosynthesis products, formed under dynamic conditions in an environment associated with the evolution of massive stars ( $M_* \geq 10M_\odot$ ) to supernova explosions of Type II.

There is increasingly strong evidence that the r-process isotopes (identified in solar-system) are the products of two distinct class of r-process events, for the region  $A \leq 130 - 140$  and  $A \geq 130 - 140$ . The helium and carbon shells of massive stars undergoing supernova explosions can give rise to significant neutron productions, via  $^{13}\text{C}(\alpha, n)^{16}\text{O}$ ,  $^{18}\text{O}(\alpha, n)^{21}\text{Ne}$  and  $^{22}\text{Ne}(\alpha, n)^{25}\text{Mg}$ . This shock processing of the helium and/or carbon shells in Type II supernovae may produce r-process nuclei in the mass range of  $A \leq 130 - 140$ . Supernovae (Type II) of certain mass range or neutron star mergers appear to be the promising candidates for the production of nuclei in the mass range  $A \geq 130 - 140$ . But the details remains to be worked out.

The s-process nuclei are understood to be products of neutron captures on pre-existing silicon-iron “seed” nuclei, occurring at hydrostatic burning conditions in both he-burning cores of massive stars and particularly the themally pulsing helium shells of asymptotic giant branch (AGB) stars. In this case (s-process), the two astrophysical environments are as follows. The thermally pulsing helium shells of AGB stars provide an environment in which the  $^{13}\text{C}(\alpha, n)^{16}\text{O}$  reaction can operate to produce s-process nuclei in the heavy region through lead to bismuth (the “main” component). The helium burning core of massive stars ( $M \geq 10M_{\odot}$ ) provide an environment in which the  $^{22}\text{Ne}(\alpha, n)^{25}\text{Mg}$  reaction can operate to produce s-process nuclei through mass region  $A \approx 90$  (the “weak” component). But the efficiency of production of s-process nuclei decreases at low metallicities (below  $[\text{Fe}/\text{H}] \approx -2.0$ ) as a result of increased abundance of nuclei from Ne to Ca relative to iron. In principle, this process can be a source of the lightest s-process nuclei, after significant production of iron seed nuclei has occurred.

In this scenario, the first heavy ( $A \geq 60$ ) elements introduced into the interstellar medium (ISM) of our galaxy are expected to have been r-process nuclei formed in association with massive stars ( $M \geq 10M_{\odot}$ ), on timescales  $\tau_{*} \leq 10^8$  yr. On the other hand, most of the s-process nuclei which operates predominantly in low mass ( $M \approx 1 - 3M_{\odot}$ ) stars are first introduced into the ISM on timescales of ( $\approx 10^9$  yr) characteristic lifetimes of their stellar progenitors (Truran et al. 2002).

### 1.4.7 Abundance of heavy elements

In the solar system, 85% of the barium is thought to have been produced by s-process nucleosynthesis and 15% by the r-process where as, element europium has 3% and 97% fractions for s and r-processes respectively. Thus, the  $[Ba/Eu]$  abundance ratio provides information about neutron-capture processes that formed the heavy elements.

However, there is a large scatter in abundances of r-process and s-process elements in metal poor stars. This star-to-star scatter could be explained as due to local inhomogeneities resulted because of contributions from individual nucleosynthetic (SNe) events and they suggest an early, unmixed chemically inhomogeneous galaxy. Ishimaru & Wanajo (1999) have tried to explain the observed large dispersions in  $[Eu/Fe]$  for halo stars, converging with increasing metallicity, with their theoretical models (Figure 1.7).

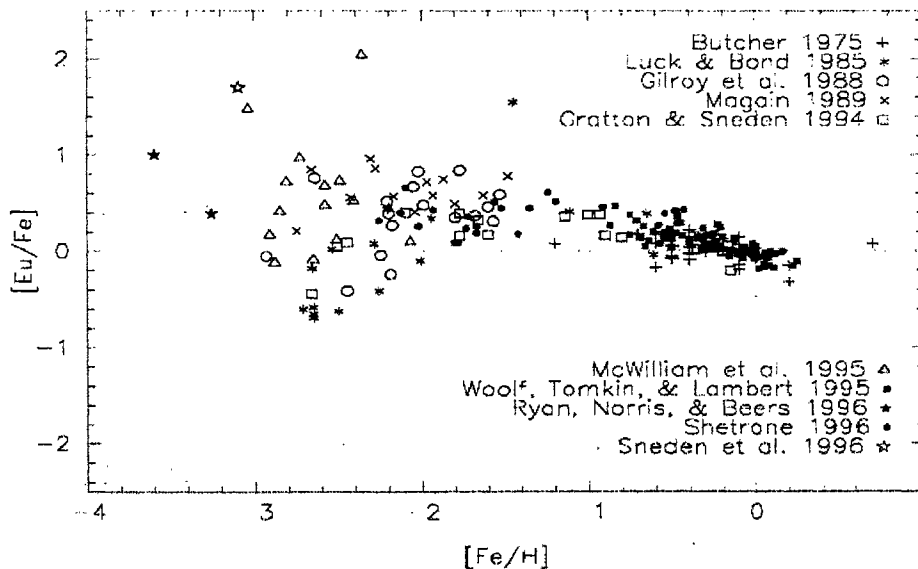


Figure 1.7: Evolution of Eu as a function of metallicity. Figure is taken from Ishimaru & Wanajo (1999)

They constrain the mass range of SNe for the r-process site to be either stars of  $8-10 M_{\odot}$  or  $> \approx 30 M_{\odot}$ . Thus the study of r-process elements in extreme metal poor stars can speak about the yield of the individual supernova.

Spite & Spite (1978) noted a systematic decreasing trend of s-process elements relative to Fe, with respect to decrease in  $[\text{Fe}/\text{H}]$ . On the other hand,  $\text{Eu}/\text{Fe}$  ratio revealed a nearly solar or higher, even for stars at very low metallicity ( $-3 \leq [\text{Fe}/\text{H}] \leq -2$ ) (Figure 1.7). This indicated the presence of r-process in these stars and the trend in s-process elements were interpreted on the basis of their level of production in r-process. Observations of Truran (1981), Sneden & Parthasarathy (1983) further demonstrated that the heavy elements in earlier generation stars can be dominated by r-process elements than s-process elements. The recent detection of low Eu abundances in EMP stars by Ishimaru et al. (2004) demands further understanding of r-process sites.

Ryan et al. (1998) have noted the large variations in  $[\text{Sr}/\text{Fe}]$ , for stars at the same  $[\text{Fe}/\text{H}]$  (Figure 1.8). In contrast,  $[\text{Ba}/\text{Fe}]$  shows a well defined enrichment history (Figure 1.9). So they conclude that these two elements are produced by different mechanisms.

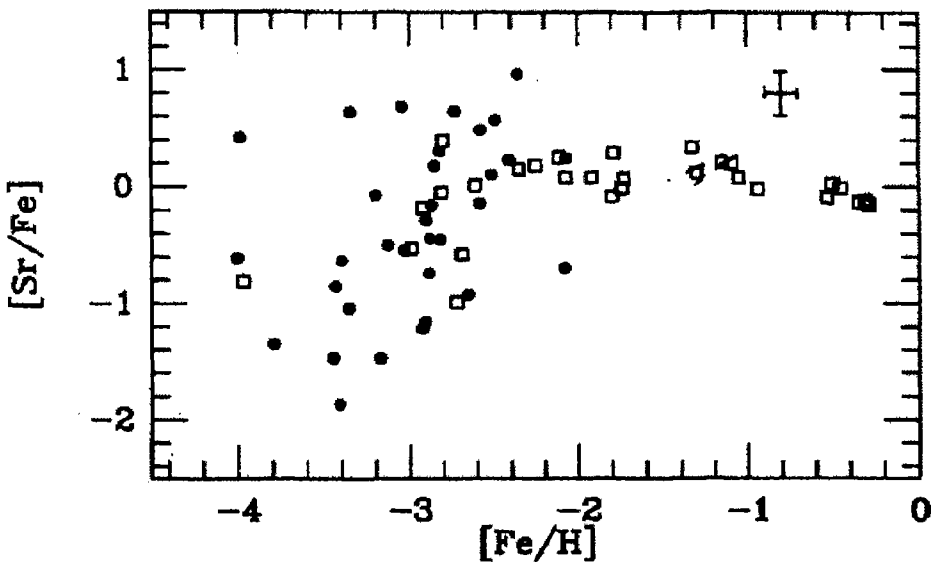


Figure 1.8: Evolution of Sr as a function of  $[\text{Fe}/\text{H}]$  of the star. Figure is taken from Ryan et al. (1996).

The high Sr abundance could have been produced by low-metallicity high mass stars, which later did not contribute to the evolution of Sr in the galaxy. The stars

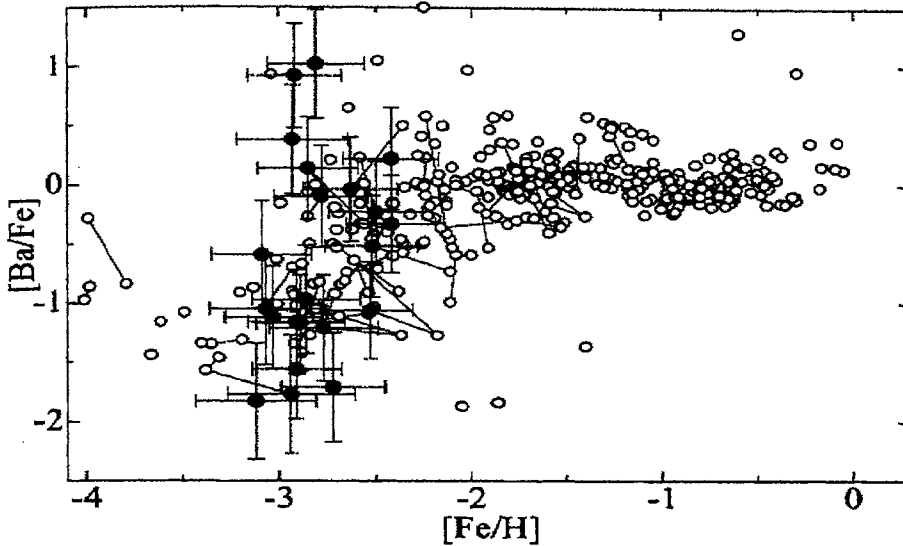


Figure 1.9: Figure is from Honda et al. (2004), where Ba abundances are plotted as a function of metallicity of the star.

with low Sr abundance might be exhibiting the normal value where as the origin of high Sr abundance in some stars could be attributed to a weak s-process present in them.

Many stars with enhanced G-band exhibit strong Sr II line at  $\lambda$  4554 Å and  $\lambda$  4215 Å. So, abundance of Sr in large number of metal poor stars is needed for statistics. The enhancement of s-process elements in stars is interpreted as a result of mass transfer in a binary system from a previous asymptotic giant branch (AGB) companion.

Aoki et al. (2000) have obtained the Pb abundance in a carbon rich star LP 625-44 ( $[Fe/H] = -2.7$ ) to be  $[Pb/Fe] = 2.65$ . The enhancement of Pb in this star is nearly same as that of Ba ( $[Ba/Fe] = 2.74$ ). This contradicts the theoretical models (Gallino et al. 1998, Busso et al. 1999), which estimate the enhancement of Pb by a factor of about two orders of magnitude larger than that of Ba for this metallicity. These observations put strong constraints on the model and suggest to investigate sites of alternative s-process nucleosynthesis (or reconsider the assumption concerning the  $^{13}C$ -rich s-processing site). However, observations of very metal poor star CS 29497-030 (Sivarani et al. 2004) yields a very high Pb abundance ( $[Pb/Fe] = +3.5$ ) and

also with respect to second peak s-process elements (like Ba, La) and fits into the newly introduced classification of lead (Pb) stars. These observations also show that there is scatter in [Pb/Fe] ratio from star to star at lower metallicities. Thus, further observation of this element in other metal poor stars are required to constrain the theoretical models.

Also, detection of radio active r-process elements, specially Th and U, whose half lives ( 14 Gyr for  $^{232}\text{Th}$  and 4.5 Gyr for  $^{238}\text{U}$  ) are shorter than the age of the universe (  $\approx 15$  Gyr ), helps in determining a lower limit on the age of the Galaxy, thereby the age of the universe (cosmochronometry). Comparing the abundance ratios U/Th when both are detected, or by comparing their abundance with a stable r-process elements like Eu, to the predicted ratios from theoretical models would determine the length of time from the era of nucleosynthesis when these elements were created, to the present. These stellar chronometric age estimates are critically dependent on accurate stellar abundance determination and well-determined theoretical nucleosynthesis predictions of the initial abundances of the radio active elements. This would require a detailed understanding of nucleosynthesis inside the star, supernova yields of these elements and accurate measurement of reactional cross-sections for the species.

Thus, a more accurate abundance determination of these heavy metals in large number of stars are required to understand the nucleosynthesis processes that occurred in the earlier generation of stars that existed before the presently observed metal poor stars.

# Chapter 2

## Observations and Analysis

---

### 2.1 Observations and description of selected stars:

#### 2.1.1 ZNG 4 in M13

The object (RA ( $16^h41^m37.528^s$ ) and DEC ( $+36^030'43.86''$ ) (2000) ) was termed as “UV bright star” by Zinn et al. (1972), as the star was brighter in the U band than other cluster stars. Cudworth and Monet (1979) have done the photographic photometry of the star and derive  $V = 13.78$  and  $(B - V) = 0.23$ . The recent CCD photometry of M13 cluster center was carried out by Paltrinieri et al. (1998), who give  $B=14.096$  and  $V=13.964$ . In order to understand the evolutionary status of UV bright stars, we started a program to obtain high resolution spectra of UV bright stars in selected globular clusters and ZNG 4 in M13 was the first target of our observation.

The high resolution spectra of ZNG 4 in M13 was obtained at Subaru 8m telescope using HDS spectrograph (Noguchi et al. 2002), which uses grating of  $31 \text{ grooves-mm}^{-1}$  and  $2.2K \times 4K$  CCD of  $13.5 \mu\text{m} \times 13.5 \mu\text{m}$  pixel size. Spectra were obtained at two different settings, covering the range from  $4142 \text{ \AA} - 5401 \text{ \AA}$  and  $5587.8\text{\AA} - 6813.4\text{\AA}$ . An exposure time of 20 min was given and the spectra had a S/N ratio of 35.



### 2.1.2 LSE 202

LSE 202 was discovered in The Luminous Stars Extension (LSE) survey for OB stars by Drilling and Bergeron (1995), along with a small number of bright metal deficient candidates (most of which were likely to be giants). We took up a program to analyze the high resolution spectra of these candidate giants, in order to understand the chemical composition of thick disk stars. LSE 202 was the first star observed under this program.

Beers et al. (2002) have carried out medium resolution (1-2 Å) spectroscopy and broadband (UBV) photometry for a sample of 39 bright stars. For LSE 202 they obtain,  $V = 10.66$ . Correcting for the interstellar extinctions value ( $E(B-V) = 0.04$ ), they estimate  $(B-V)_0$  as 0.71. Radial velocity was obtained using the line-by-line and cross-correlation techniques (Beers et al. 1999) and the value given is  $-384 \text{ km s}^{-1}$ . They have estimated the metallicity by spectroscopic and photometric method and they suggest a value of  $[Fe/H] = -2.19$  and they classify it as a halo star.

The spectra of the star LSE 202 was obtained with 4 exposure times (Two of them with 1500 s integration time and two others with 1800 s integration time) with the McDonald Observatory 2.7 m telescope with an Echelle spectrograph and  $2048 \times 2048$  CCD detector. Spectra are from 3750 Å to 10100 Å with gaps between the orders.

### 2.1.3 BPS CS 29516-0041 (CS 29502-042), BPS CS 29516-0024 and BPS CS 29522-0046

These stars were discovered in HK objective-prism/interference-filter survey, started in 1978 by Preston and Shectman (Beer, Preston and Shectman, 1985, 1992). The UBV photometry of these objects have been done by Norris et al. (1999). Bonifacio et al. (2000) have done the UBV photometric follow up of these stars together with the medium resolution spectroscopy (either with 2.1 m telescope at the Kitt Peak National Observatory, using the GoldCam spectrometer and the 2.5 m Isaac Newton Telescope on La Palma, using the intermediate dispersion spectrograph).

For BPS CS 29516-0041, they obtain  $V = 12.78$ ,  $(B - V)_0 = 0.53$  and  $(U - B)_0 = -0.08$  (by adopting a reddening estimate of  $E(B - V) = 0.07$ ).  $[\text{Fe}/\text{H}]$  is estimated to be  $-2.45$ . The star seem to to have the luminosity of supergiant class suggesting low surface gravity.

Photometry of BPS CS 29516-0024 yields  $V = 13.57$ . Reddening estimate of  $E(B - V) = 0.10$  yields  $(B - V)_0 = 0.76$  and  $(U - B)_0 = 0.13$ . Metallicity is estimated to be  $[\text{Fe}/\text{H}] = -2.86$  and the star is classified as a giant.

They obtain,  $V = 12.74$ ,  $(B - V)_0 = 0.39$  and  $(U - B)_0 = -0.20$  for BPS CS 29522-0046, with an  $E(B - V)$  value of 0.10. It is estimated to have the  $[\text{Fe}/\text{H}]$  value of  $-3.24$  and luminosity class of a turnoff star.

High resolution spectra of these objects were obtained at CTIO 4m telescope, Chile, using echell spectrograph with a grating of 31.6 l/mm and CCD (of size 2K - 6K) was used. The obtained spectra have 45 orders with wavelength range from 4940 Å to 8200 Å.

BPS CS 29516-0041 was observed on 21st June, 2002 with 45 minute exposure time. Signal to noise ratio (S/N) of the spectrum was about 45.

BPS CS 29516-0024 was observed on 22nd June, 2002 with two exposure times each of 45 minute. S/N of each of the spectrum was around 50.

BPS CS 29522-0046 was also observed on 22 June, 2002 with two exposure times of 30 minute each, which yielded a S/N ratio of 60 for each spectrum.

Table 2.1 gives observational information of the stars mentioned above.

## 2.2 Data Reduction:

Reduction of raw spectroscopic images consists of instrumental calibration ( which includes bias and and dark frame subtraction and flat field correction of object images), extraction of one-dimensional spectra, and wavelength calibration. These tasks were performed using Image Reduction and Analysis Facility (IRAF) packages.

The bias frames taken on each night were averaged using the task *zerocombine*.

Table 2.1: Brief information of the stars observed

Object Name	RA (2000)	DEC	l	b	V <sub>magn</sub>	(B - V)
ZNG 4 (in M13)	16 <sup>h</sup> 41 <sup>m</sup> 37.52 <sup>s</sup>	+36 <sup>o</sup> 30'43.86"	59 <sup>o</sup> .08	+40 <sup>o</sup> .93	13.964	0.13
LSE 202	17 <sup>h</sup> 58 <sup>m</sup> 28.27 <sup>s</sup>	+30 <sup>o</sup> 31'11.9"	56 <sup>o</sup> .28	+24 <sup>o</sup> .03	10.66	0.83
BPS CS 29516-0041 (BPS CS 29502-0042)	22 <sup>h</sup> 21 <sup>m</sup> 48.6 <sup>s</sup>	+02 <sup>o</sup> 28'47"	66 <sup>o</sup> .35	-43 <sup>o</sup> .36	12.78	0.60
BPS CS 29516-0024	22 <sup>h</sup> 26 <sup>m</sup> 15.1 <sup>s</sup>	+02 <sup>o</sup> 51'49"	67 <sup>o</sup> .77	-43 <sup>o</sup> .92	13.57	0.86
BPS CS 29522-0046	23 <sup>h</sup> 44 <sup>m</sup> 59.6 <sup>s</sup>	+08 <sup>o</sup> 46'53"	96 <sup>o</sup> .47	-50 <sup>o</sup> .65	12.74	0.49

The resultant bias frame is subtracted from the object and flat field frames using the task *ccdproc* in CCDRED package. The bias subtracted flatframes are median combined with *flatcombine* task and normalized by *apnorm* in the SPECRED package. The pixel-to-pixel variations across the CCD chip are removed by dividing the object frames by normalized flat field frame. This is again done using *ccdproc*. As the dark counts were negligible compared to bias counts, we did not use dark frames.

Extraction of the one-dimensional spectrum is carried out by the task *apall* in SPECRED (ECHELLE) package. This task also has an option to remove cosmic-ray hits on the spectrum. The resultant is a one-dimensional spectrum with counts versus pixel number and which is free of cosmic rays.

For wavelength calibration, a comparison spectra which is extracted similarly for each slit is required. The emission lines in the arc spectrum (Thorium-Argon in our case), are identified using the atlas of Thorium-Argon spectra. The dispersion correction (wavelength solution) is determined from the arc spectrum by using Legendre polynomial of the order 2 or 3. The wavelength correction is determined by using *identify* in SPECRED or *ecidentify* in ECHELLE package. Finally each individual object spectrum is wavelength-corrected using the task *dispcorrection*. Output is the spectrum with counts versus wavelength.

Telluric features in the spectrum of the star are removed by dividing the spectrum of the star by that of a rapidly rotating hot (A or B type) star, observed near the

same air mass and reduced in same method. In these hot stars, any weak line present will get highly broadened due to rapid rotation and will be close to the continuum level. Telluric features are removed from the regions 6100Å, 6500Å, 7100Å, 7400Å and 8700Å.

Equivalent widths of the lines were measured using *splot* package in IRAF. The absorption line were fitted by a Gaussian profile (in the case of broadened lines like balmer line profiles, total area under the continuum was considered). If the absorption profile is not symmetric and has only left or right wing, then we have considered the right half width or left half width of the half flux points respectively to construct the Gaussian profile. Blended lines were deblended using the routines available in the *splot* package.

## 2.3 Analysis

### 2.3.1 Atmospheric Models

We have carried out analysis of the spectra using LTE model atmosphere and spectrum synthesis.

The Local Thermodynamic Equilibrium (LTE) of the model atmosphere of the stellar photosphere, makes the following assumptions.

- a) It has a steady state atmosphere.
- b) The energy source lies well below the atmosphere and there is no incoming energy from above. This suggests, the flux of energy is constant with the depth of the atmosphere. It is usually specified by effective temperature, flux =  $\sigma T_{\text{eff}}^4$ ,  $\sigma$  being equal to  $5.6697 \times 10^{-5}$ .
- c) The atmosphere is thin compared to the radius of the star, therefore it is plane parallel.
- d) There is no relative motion of the layers in the normal direction and no net acceleration in the atmosphere. Hence the pressure balances the gravitation attraction.

$$\rho \frac{d^2 r}{dt^2} = -\rho g + \frac{dP}{dr} = 0 \quad (2.1)$$

where  $\rho$  is the density and  $g = GM_*/R_*^2$  is the gravitational acceleration, which is assumed constant as the atmosphere is thin.  $M_*$  and  $R_*$  are the mass and radius of the star respectively.

The assumptions of local thermodynamic equilibrium (LTE) are essentially that all transitions are only due to collisions between absorbers and that radiation is unimportant in determining energy level populations. This is fine in very dense regions where collisions are likely to dominate, but not in the case of photospheres of stars where densities are lower. Since resonance lines for alkali elements form in these outer layers, NLTE effects are thought to be important. Therefore non-LTE correction for resonant lines need to be considered.

For our studies we have mainly made use of Kurucz's ATLAS (1993) model atmospheres. The Kurucz ATLAS program calculates stellar atmospheres in radiative and convective equilibrium for the complete range of stellar temperature in steps of 250 K and  $\log g$  from 0 to 5.0 in steps of 0.5. It assumes the atmosphere to be plane parallel, horizontally homogeneous, in steady-state. (Line opacity is treated as line absorption distribution functions). The program considers detailed statistical equilibrium calculations for each element (Line blanketed atmosphere).

### 2.3.2 Line information (atomic data)

The physical data required in abundance analysis are the lower excitation potential of the line and the oscillator strength (gf value) of the line. The observed systematic line to line scatter in the elemental abundances could be attributed to the uncertainty in gf-values. Thus the reliable experimentally determined atomic data is essential for stellar spectroscopy.

For the object ZNG 4 in M13, we obtained the line information from Vienna Atomic Line Database (VALD) ( <http://www.astro.univie.ac.at/vald> ). We have also made use of the line list obtained using version 43 of the Synspec code of Hubeny and Lanz which is distributed as part of their TLUSTY model atmosphere program. ( <http://tlusty.gsfc.nasa.gov/Synspec43/synspec-line.html> ) and the information from the Kurucz linelist ( <http://kurucz.harvard.edu/linelists.html> ).

For other stars, we have mainly used the line information from the compilation of Luck and Bond, supplemented with line information from VALD.

### 2.3.3 Spectral analysis code

For all the cool giants, we carried out the spectrum analysis using latest (2002) version of MOOG, an LTE stellar line analysis program (Snedden 1973). Determination of elemental abundances using these codes is described by Castelli and Hack (1990). Since ZNG 4 in M13 is a warm star, indicating a temperature of 8500 K, along with MOOG we also used the Kurucz WIDTH program (Kurucz CDROM 13, 1993) for verification.

In MOOG, we have used the routine *abfind*, for abundance analysis and *synth* for spectrum synthesis.

The subroutine *abfind* compares the equivalent width of a given unblended line with the equivalent width calculated for a given atmospheric model. (Previous to this step, lines were identified using Moore's Multiple Table (1945) and their equivalent width were measured using *splot* in IRAF). It requires line data (with information on each line : about the wavelength, excitation potential for lower and upper level and the transition probability or the oscillator strength) as the input. The code basically solves the radiative transfer problem for spectral lines under the LTE assumptions and calculates line depths and equivalent widths for a given stellar atmospheric model for each individual line as a function of abundance. For a given stellar model, it does numerous iterations and the abundance is modified until the computed equivalent width matches with that of the observed equivalent width. Weak lines are more useful in determining the abundance, as their equivalent width does not get affected by variation of microturbulence, damping constants and Non-LTE. For blended lines, subroutine *blends* can be used, provided we know the abundance of the other element which is blended with the line (element) of our considerations.

The spectrum synthesis routine *synth* needs extensive line lists for each element in the different ionization states, with known laboratory wavelengths, excitation potential and oscillator strengths (gf-values). Kurucz website provides the database

for both atomic and molecular lines ( <http://kurucz.harvard.edu/linelists.html> and <http://kurucz.harvard.edu/molecules.html> ). Apart from the linelist, the inputs are stellar atmosphere model, abundances of relevant elements, beginning and end points of the spectrum, step size in the spectrum and width of the spectrum to be considered at each point. Also, we need to feed rotational velocity of the star, macroturbulent velocity and full width half maximum (FWHM) of instrumental Gaussian profile.

Given these as the inputs, MOOG calculates the continuum flux at each point separated by a step size. The code must be run several times by adjusting the input abundances of elements till the computed spectrum matches the observed one. By comparing the computed spectrum from *synth* with the observed spectrum, it is possible to derive line identification, microturbulent velocities, Doppler shifts and abundance from single and blended lines.

## 2.4 Determination of atmospheric Parameters

### 2.4.1 Effective Temperature

Initial estimation of  $T_{\text{eff}}$  of the stars was done from photometry. B and V values of ZNG 4 in M13 was obtained from Paltrinieri et al. (1998). For LSE 202, Beers et al. (2002) have derived B, V colors. For other stars, we took the photometric values from Bonifacio et al. (2000). The observed (B-V) color was corrected for extinction using galactic extinction estimates from Schlegel et al. (1998). NED (NASA Extragalactic Database) provides the galactic extinction calculator which transforms the coordinates of the object and calculates the galactic extinction ( <http://nedwww.ipac.caltech.edu/forms/calculator.html> ). We transformed the intrinsic B-V values of the star  $[(B - V)_0]$  to  $T_{\text{eff}}$  using empirical calibrations of (B-V) color versus  $T_{\text{eff}}$  (Flower, 1996). However, the empirical formula for (B-V) vs  $T_{\text{eff}}$  are derived from observations for Population I stars and is not adequate to use for stars with  $[\text{Fe}/\text{H}]$  ranging from  $-1.5$  to  $-3.0$ . Hence for halo stars, we made use of the calibrations given by Alonso et al. (1999).

Temperature of the star can also be deduced from Balmer line profiles. Kurucz

has synthesized Balmer profiles for various models of Population I and Population II atmospheres. However, the balmer line profiles are more sensitive to  $T_{\text{eff}}$  mainly in A and F stars only. We made use of it, in the case of ZNG 4 in M13 but for other stars, as it did not show good agreement.

The spectroscopic determination of temperature of the star uses the method of “excitation potential balance”. This measurement uses excitation potential ( $\chi$ ) of different transition of the same spectral species. If the assumed model temperature is correct, then the abundances derived from several different lines should not show any trend as a function of  $\chi$ . ie  $d \log \epsilon / d\chi = 0$ . If the assumed temperature is too high, then the models will overpopulate the levels with large  $\chi$  and the  $\log \epsilon$  derived from these levels will be too low, such that  $d \log \epsilon / d\chi < 0$ . If the assumed temperature is too low, converse will happen.

## 2.4.2 Gravity

One can deduce the value of  $\log g$  from the mass and radius relation. The equational form which represents the relation is as follows:

$$\log g = \log(M/M_{\odot}) - 10.62 - \log(L/L_{\odot}) + 4 \log T_{\text{eff}} \quad (2.2)$$

But for all the stars, luminosity and mass are not known. It can work only in the case of Population II post-AGB stars which have typical mass ( $M/M_{\odot} = 0.6$ ) and luminosity ( $L/L_{\odot} = 10^3$ ).

Balmer line profiles can also be used to estimate the gravity. But in the case of giants which have extended atmosphere, this might not give the correct result. Also the region of metal line formation might not coincide with that of Balmer line origin. So, it is not safe to use it for determination of gravity in the case of giants.

The other spectral absorption-line indicator to determine the photospheric parameters for the star is “ionization balance” approach. This assumes that the element abundances calculated from two different ionization stages of same element - for example, Fe I and Fe II - should be the same. If the values are not equal, it implies that the model atmosphere and spectral synthesis program are assuming an incorrect tem-



perature and gravity, so the predicted population of each ionization state is erroneous. If the abundances  $\log \epsilon(\text{FeI}) > \log \epsilon(\text{FeII})$ , then the temperature must be too high or the model gravity must be too low. (If  $\log \epsilon(\text{FeI}) < \log \epsilon(\text{FeII})$ , then the converse holds good). If we have fixed the temperature by the earlier technique of “excitation potential balance”, we can vary the gravity till we get  $\log \epsilon(\text{FeI}) = \log \epsilon(\text{FeII})$ .

### 2.4.3 Microturbulent Velocity

The microturbulent velocity ( $V_t$ ), which regulates the line formation mechanism for a given transition can influence the derived abundance ( $\log \epsilon$ ). Thus both excitation potential balance and ionization balance methods require an appropriate value for ( $V_t$ ). The value of  $V_t$  is determined in a manner similar to excitation potential balance. If the wrong ( $V_t$  is used for the abundance analysis, then the abundances derived from stronger lines will be systematically offset from those of weaker lines. So, we plot  $\log \epsilon$  for each line of a given species as a function of equivalent width ( $W_\lambda$ ), and vary  $V_t$  till we obtain  $d \log \epsilon / dW_\lambda = 0$ .

The last parameter which needs to be defined is the metallicity. Since the atmospheric structure is strongly dependent on the opacity and thus metallicity, it is important that the models in the analysis should consider an appropriate metallicity.

In practice, we iterate between a ( $T_{\text{eff}}$ ,  $\log g$ ) solution and recalculation of  $V_t$  and  $[\text{Fe}/\text{H}]$ , using many model atmospheres till all the parameters are stabilized.

# Chapter 3

## Chemical composition of UV-bright star ZNG 4 in the globular cluster M13 \*

---

### 3.1 Abstract

We present a detailed model-atmosphere analysis of ZNG 4, a UV-bright star in the globular cluster M13. From the analysis of a high resolution ( $R \approx 45,000$ ) spectrum of the object, we derive the atmospheric parameters to be  $T_{\text{eff}} = 8500 \pm 250$  K,  $\log g = 2.5 \pm 0.5$ ,  $V_t = 2.5 \text{ kms}^{-1}$  and  $[\text{Fe}/\text{H}] = -1.5$ . Except for magnesium, chromium and strontium, all other even  $Z$  elements are enhanced with titanium and calcium being overabundant by a factor of 0.8 dex. Sodium is enhanced by a factor of 0.2 dex. The luminosity of ZNG 4 and its position in the color-magnitude diagram of the cluster indicate that it is a Supra Horizontal Branch (SHB) (post-HB) star. The underabundance of He and overabundances of Ca, Ti, Sc and Ba in the photosphere of ZNG 4 indicate that diffusion and radiative levitation of elements may be in operation

---

<sup>0\*</sup> Based on observations obtained with the Subaru 8.2m Telescope which is operated by the National Astronomical Observatory of Japan.

in M13 post-HB stars even at  $T_{\text{eff}}$  of 8500K. Detailed and more accurate abundance analysis of post-HB stars in several globular clusters is needed to further understand their abundance anomalies.

## 3.2 Introduction

The term “UV-bright stars” was introduced by Zinn et al. (1972) for stars in globular clusters that lie above the horizontal branch (HB) and are bluer than red giants. The name resulted from the fact that, in the U band, these stars were brighter than all other cluster stars. Further investigations showed that this group of stars consist of blue horizontal branch (BHB) stars, supra horizontal branch stars (SHB), post asymptotic giant branch stars (post-AGB), post-early AGB (P-EAGB) stars and AGB-manque stars (de Boer 1985, 1987, Sweigart et al. 1974, Brocato et al. 1990, Dorman et al. 1993 and Gonzalez & Wallerstein 1994).

To derive the chemical composition of UV-bright stars in globular clusters and to understand their evolutionary stages, we started a program to obtain high resolution spectra of these objects in selected globular clusters with the High Dispersion Spectrograph (HDS, Noguchi et al. 2002) of the 8.2m Subaru Telescope. We selected a few UV-bright stars in the globular cluster M13 from the papers of Zinn et al. (1972) and Harris et al. (1983) to derive their chemical composition. In this paper we report the analysis of a high resolution spectrum of the UV-bright star ZNG 4 (RA ( $16^{\text{h}}41^{\text{m}}37^{\text{s}}.528$ ) and DEC ( $+36^{\circ}30'43.86''$ ) (2000) ) (Zinn et al. 1972) in M13 as the first target of our program.

M13 (NGC 6205) is a nearby well studied globular cluster with a distance modulus of  $(m - M)_0 = 14.42$  m and metallicity of  $[\text{Fe}/\text{H}] = -1.51$  (Kraft and Ivans 2003). The position of ZNG 4 in the color-magnitude diagram of M13 (Paltrinieri et al. 1998) is shown in Figure 3.1. Many of the globular clusters show a prominent gap in the blue tail of the HB, which is presumed to be due to differential mass loss on the Red Giant Branch (RGB). In M13 it is observed at  $T_{\text{eff}} = 10000\text{K}$  (Ferraro et al. 1997). High resolution spectroscopic studies of M13 BHB stars lying on either side of the

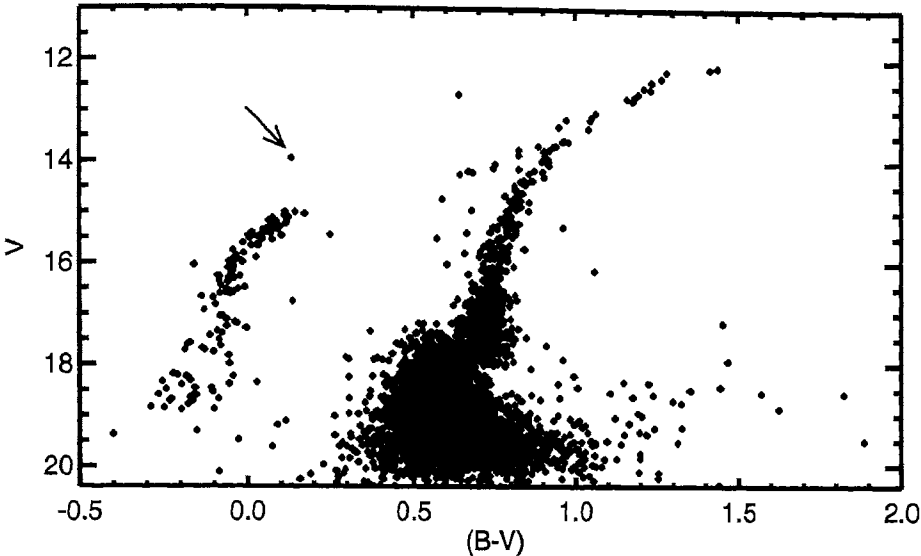


Figure 3.1: Color magnitude diagram (CMD) of globular cluster M13 obtained by Paltrinieri et al. (1998). The arrow indicates the position of ZNG 4 in the CMD.

gap were carried out by Peterson et al. (1983, 1995) and Behr et al. (1999, 2000a). They found anomalous photospheric abundances in BHB stars. These photospheric anomalies are most likely due to diffusion - the gravitational settling of helium and radiative levitation of the metal atoms in the stable atmosphere of hot stars. They found variations in the photospheric abundances and rotational velocities of BHB stars as a function of their effective temperatures.

### 3.3 Observations

We have obtained a high resolution ( $\frac{\lambda}{\Delta\lambda} \approx 45,000$ ) spectrum of ZNG 4 on 15th (UT:14h45m) April 2001 with the Subaru/HDS. The spectrum covering the wavelength range 4142 Å- 6814 Å was obtained in an exposure time of 20 minutes. There was no moon light problem during the observations and the sky background in the data was close to zero. We neglected the sky background in our data reduction.

The data was bias-subtracted, trimmed, flat-fielded to remove pixel to pixel variations, converted to a one-dimensional spectrum, and normalized to the continuum

using standard CCD data reduction package (NOAO IRAF). The spectrum has an average signal to noise ratio of 35. The reference spectrum of thorium-argon was used for the wavelength calibration.

The various orders in our echelle spectrum of ZNG 4 have well defined continuum and the normalization of the continuum was carried out using the IRAF echelle spectra reduction programs. The continuum level in the adjacent echelle orders to those containing the Balmer lines was useful in defining the continuum in the Balmer line regions and the profiles were normalized with a polynomial fit.

## 3.4 Analysis

The spectral lines were identified using Moore's atomic multiplet table (1945). Equivalent widths of the absorption lines were measured using the routines available in the SPLOT package of IRAF. The equivalent widths were measured by Gaussian fitting to the observed profiles (and a multiple Gaussian fit to the blended lines such as the Mg II lines at 4481 Å) and are given in Table 1.

### 3.4.1 Radial velocity

The radial velocity of ZNG 4 was derived from the wavelength shifts of many absorption lines. The average heliocentric velocity is found to be  $V_r = -257.56 \pm 1.08 \text{ kms}^{-1}$  which is in agreement with the value derived by Zinn (1974) ( $-253 \text{ kms}^{-1}$ ). It is also in agreement with the heliocentric velocities of M13 BHB stars derived by Behr et al. (1999) and Moehler et al. (2003).

### 3.4.2 Atmospheric parameters

For the initial estimate of effective temperature, we looked for the published CCD photometry of the star. Recent CCD photometry of M13 was carried out by Rey et al. (2001). However the ZNG 4 area of the cluster was not included in their observations (Rey : private communication ). We used the published CCD photometry of ZNG 4

by Paltrinieri et al. (1998), who give,  $B=14.096$  and  $V=13.964$ .  $(B-V) = 0.132$  and  $E(B-V) = 0.02$  (Kraft and Ivans 2003) will yield  $(B - V)_o = 0.112$  which corresponds to  $T_{\text{eff}} = 8373\text{K}$  (Flower 1996). However, the  $(B - V)_o$  and  $T_{\text{eff}}$  calibration given by Flower (1996) is for Population I stars.

For our analysis, excitation potential and oscillator strengths of the lines were taken from the Vienna Atomic Line Database (<http://www.astro.univie.ac.at/vald/>). We employed the latest (2002) version of MOOG, an LTE stellar line analysis program (Snedden 1973) and Kurucz (1993) grid of ATLAS models. MOOG has been used successfully in the analysis of the spectra of warmer stars with  $T_{\text{eff}} = 7900\text{ K}$  (Preston and Sneden 2000).

We have also analyzed the spectra using the Kurucz WIDTH program (Kurucz CDROM 13, 1993) for verification. We used the line list obtained using version 43 of the Synspec code of Hubeny and Lanz which is distributed as part of their TLUSTY model atmosphere program. (<http://tlusty.gsfc.nasa.gov/Synspec43/synspec-line.html>) and also the information from the Kurucz linelist (<http://kurucz.harvard.edu/linelists.html>).

The value of effective temperature was obtained by the method of excitation balance, forcing the slope of abundances from Fe I lines versus excitation potential to be zero. The surface gravity was then set by ionization- equilibrium, forcing abundances obtained from neutral (Fe I) and ionized (Fe II) species to be equal. The microturbulent velocity was estimated by demanding that there should be no dependence of the Fe I abundance upon equivalent widths of Fe I lines.

The plots of the abundances versus excitation potentials and abundances versus equivalent widths in the case of Fe I and Fe II lines are shown in Figure 3.2. Such plots were made by varying the  $T_{\text{eff}}$ ,  $\log g$  and  $V_t$  in steps of 250 K, 0.5 and 0.5  $\text{kms}^{-1}$  respectively to estimate the uncertainties in these parameters.

From our analysis, we find that  $T_{\text{eff}} = 8500\text{K}$ ,  $\log g = 2.5$ ,  $V_t = 2.5\text{kms}^{-1}$  and  $[\text{Fe}/\text{H}] = -1.5$  fit the data best (Figure 3.2). From the above mentioned method of analysis we find the uncertainties in  $T_{\text{eff}}$  to be 250 K,  $\log g = 0.5$  dex and  $V_t = 0.5\text{ kms}^{-1}$ . Uncertainties in derived abundances as a result of errors in the deter-

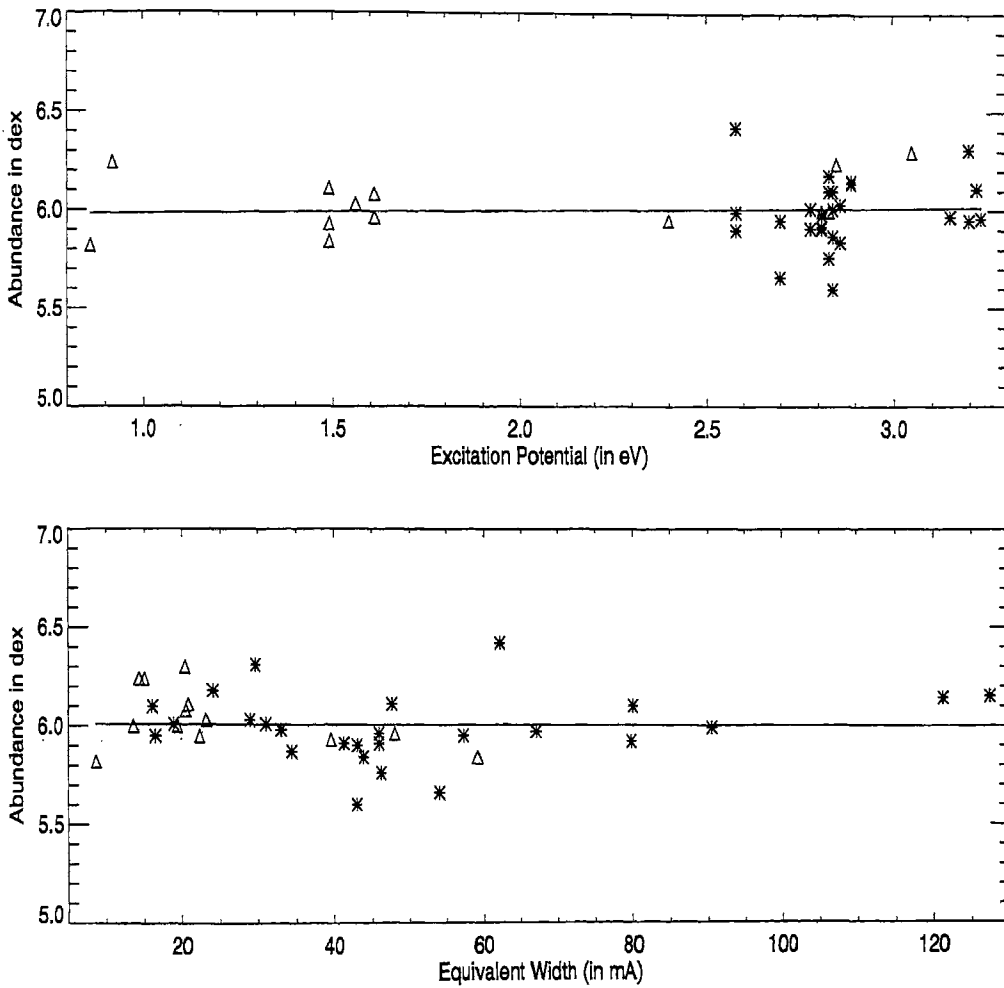


Figure 3.2: Top figure is the plot of the abundances from Fe lines versus excitation potential of the lines for the star ZNG 4 in M13. Figure at the bottom is the plot of the abundances from Fe lines versus their equivalent widths. Triangles represent the Fe I lines and stars denote the Fe II lines.

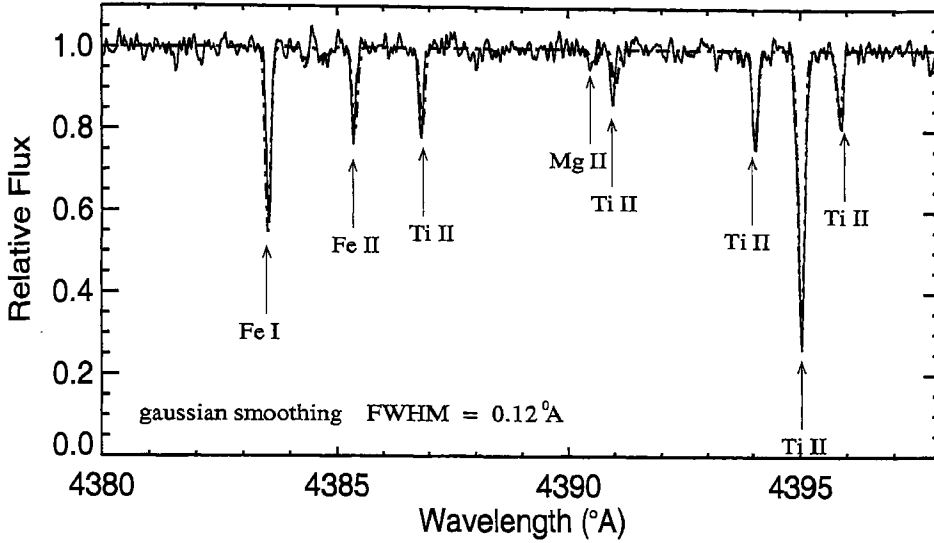


Figure 3.3: Synthetic spectrum calculated with the atmospheric parameters ( $T_{\text{eff}} = 8500 \text{ K}$ ,  $\log g = 2.5$ ,  $V_t = 2.5 \text{ kms}^{-1}$ ) and abundances (Tables 1 and 3.2) is overplotted on the observed spectrum of ZNG 4 in M13, in the  $4380 \text{ \AA} - 4400 \text{ \AA}$  region.

mination of the parameters and errors in the measurements of equivalent widths are found to be of the order of 0.2 dex.

Using the derived atmospheric parameters and abundances, a synthetic spectrum was generated and plotted over the observed spectrum for verification. The observed and synthetic spectra were found to match well with the above mentioned atmospheric parameters and the final abundances are given in Tables 1 and 3.2. A region of the observed and synthetic spectrum is shown in Figure 3.3. The abundances derived using MOOG (Tables 1 and 3.2) are in good agreement with the abundances derived using the WIDTH (Table 3.2).

### 3.4.3 Balmer Lines

We tried to estimate the  $T_{\text{eff}}$  and  $\log g$  from the analysis of Balmer lines in the spectrum of ZNG 4 using the Kurucz spectral atlas for Balmer lines (Kurucz CDROM 13, 1993).



We could not get a satisfactory fit between the observed and theoretical Balmer line profiles with the atmospheric parameters  $T_{\text{eff}} = 8500$  K,  $\log g = 2.5$ ,  $V_t = 2.5$  km s<sup>-1</sup> and  $[\text{Fe}/\text{H}] = -1.5$ . We also tried models that take into account the alpha element enhancements and no convective overshooting (ANOVER models: <http://kurucz.harvard.edu/grids/gridm15ANOVER/bm15ak2nover.dat>). They did not make any difference to the above mentioned atmospheric parameters (Figure 3.4). The best fit to  $H_\beta$  profile was obtained with the parameters  $T_{\text{eff}} = 8750$  K,  $\log g = 2.0$ ,  $V_t = 2.0$  km s<sup>-1</sup> and  $[\text{Fe}/\text{H}] = -1.5$  (Figure 3.4). However, the excitation balance and ionization equilibrium for Mg and Fe lines could not be achieved with the above parameters (see the last column in Table 3.2) and the abundances of Mg I, Mg II and Fe I, Fe II were found to differ significantly (Table 3.2). Therefore, we chose the model atmosphere determined from the analysis of metal lines (ie  $T_{\text{eff}} = 8500$  K,  $\log g = 2.5$ ,  $V_t = 2.5$  km s<sup>-1</sup> and  $[\text{Fe}/\text{H}] = -1.5$ ) to represent the atmosphere of the star.

The problem of fitting Balmer line profiles of HB stars has been mentioned by Grundahl et al. (1999) (and references therein). For stars being more luminous than HB stars, mass loss and/or extended atmosphere may influence the Balmer line profiles (Vink & Cassisi, 2002).

## 3.5 Results

The mean abundances of ZNG 4 relative to the Sun (Anders and Grevesse 1989) are given in Table 3.2, together with the number of lines used in the analysis and the standard deviation of abundances estimated from individual species.

Analysis of Mg lines gives  $[\text{Mg}/\text{H}] = -1.5$  which is the same as the M13 cluster metallicity. (The equivalent widths of the Mg II lines at 4481 Å (Table 1) were obtained by multiple gaussian fit to the lines in the observed spectrum). Silicon is overabundant compared to iron ( $[\text{Si}/\text{Fe}] = +0.4$ ). calcium and titanium are found to be overabundant ( $[\text{Ca}/\text{Fe}] = +0.8$  and  $[\text{Ti}/\text{Fe}] = +0.75$ ). There is a 0.5 dex difference in the abundances derived from the Ca I lines at 4226.73 Å and 4454.78 Å (Table 1).

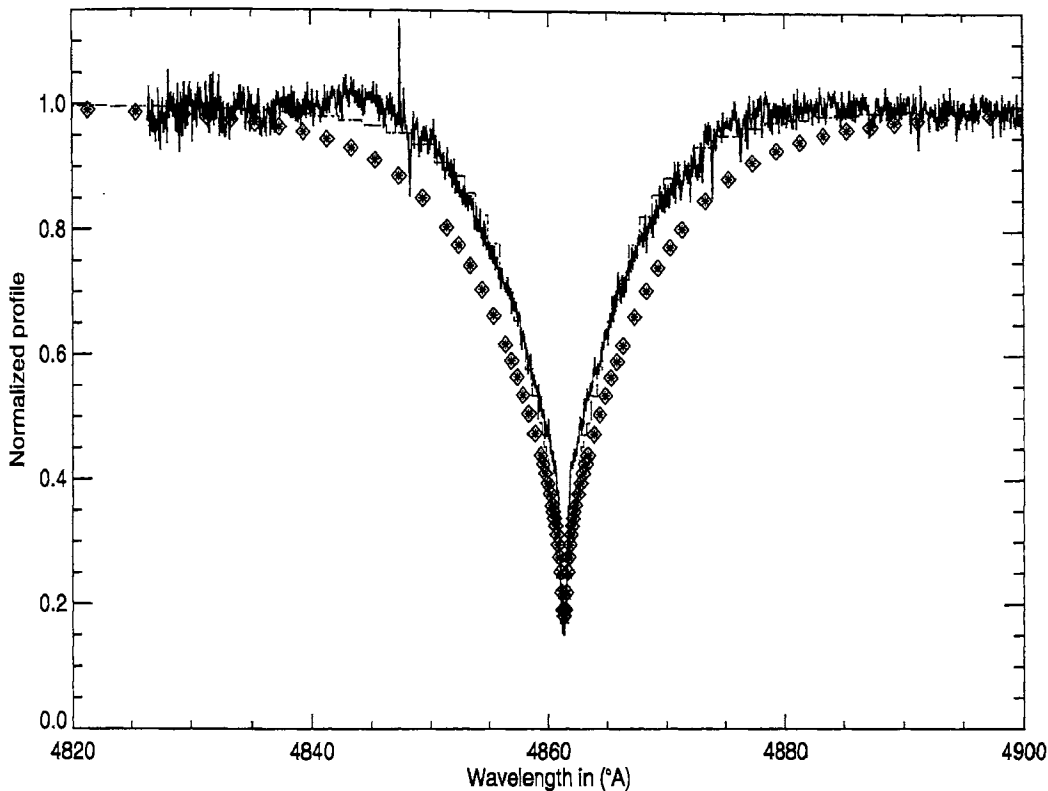


Figure 3.4: Observed  $H_\beta$  profile compared with theoretical  $H_\beta$  profiles for 2 different model atmospheric parameters for ZNG 4 in M13. Dots and dashes represent the model with  $T_{\text{eff}} = 8750$  K,  $\log g = 2.0$ ,  $[M/H] = -1.5$  and  $V_t = 2.0$  km  $s^{-1}$  which fit the profile best. Open diamonds and asterisks represent the model  $T_{\text{eff}} = 8500$  K,  $\log g = 2.5$ ,  $[M/H] = -1.5$  and  $V_t = 2.5$  km  $s^{-1}$ , which does not fit the observed profile. No noticeable differences were observed in the theoretical  $H_\beta$  profiles by considering ANOVER models for the same atmospheric parameters and are shown by dashes for the first set of parameters and asterisk in the case of second set of parameters.

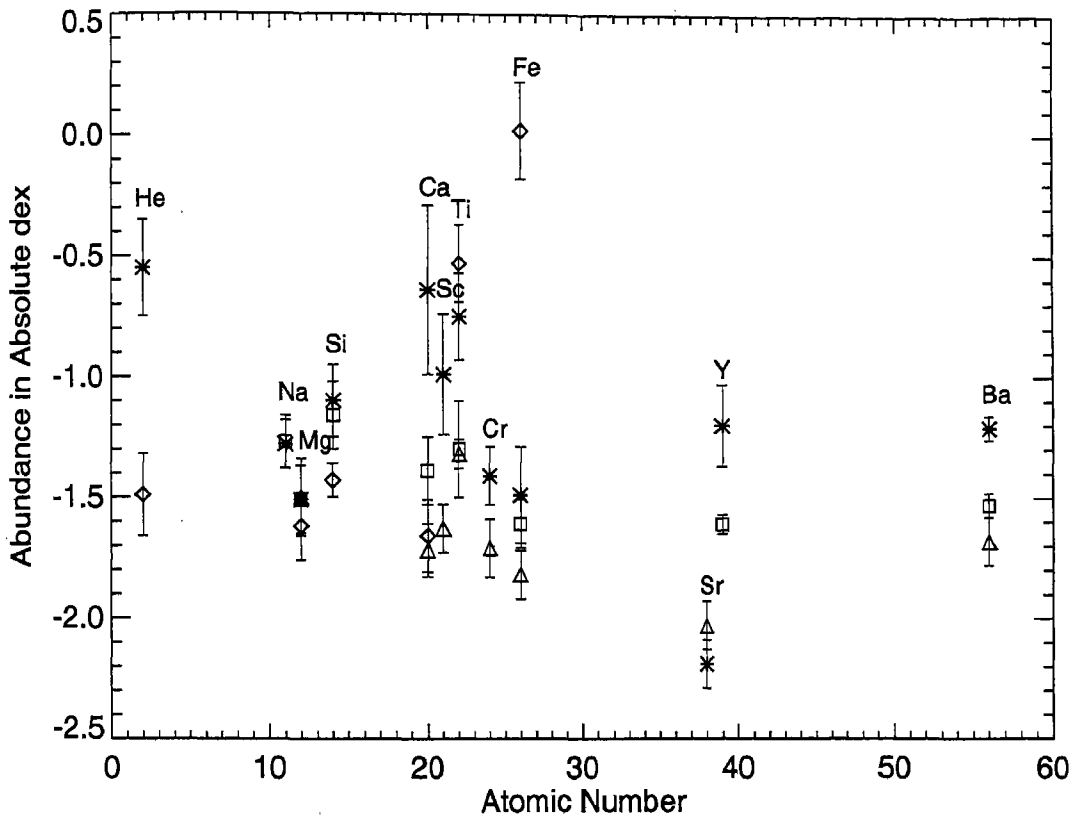


Figure 3.5: The abundances of different elements in ZNG 4 in M13 (represented by asterisk) compared with M13/ J11 ( BHB star; triangles), M13/WF4-3485 (hot BHB star; diamonds) and that of M13/ L262 (RGB star; squares) with their error bars (Table 3.3). In the cases where only upper limit of the abundances are given (3rd and 4th column of Table 3.3), those elements are not shown in the above figure. Average abundances of Y and Ba in M13 RGB stars are from Armosky et al. (1994).

However, the abundance of Ca derived from the Ca II line at 5019.97 Å is in agreement with that derived from the Ca I 4454.78 Å line. The reason for the deviation in the abundance derived from the Ca I 4226.73 Å line is not clear. It may be due to the relatively low signal to noise ratio of the data around this wavelength range. There seems to be no interstellar contribution to the Ca II line. Since the star has a radial velocity of  $-257 \text{ km s}^{-1}$ , the stellar lines are well separated from the lines of interstellar origin. The abundance of Cr and Fe ( $[\text{Fe}/\text{H}] = -1.48$  and  $[\text{Cr}/\text{Fe}] = +0.09$ ) are found to be close to the metallicity of the cluster. On the other hand, Sc is found to be overabundant ( $[\text{Sc}/\text{Fe}] = 0.51$ ). Na lines show an overabundance of 0.2 dex. We have detected one line of Sr II, two lines of Y II and two lines of Ba II. Sr seems to be underabundant ( $[\text{Sr}/\text{Fe}] = -0.70$ ), while Y and Ba are overabundant ( $[\text{Y}/\text{Fe}] = +0.29$  and  $[\text{Ba}/\text{Fe}] = +0.28$ ).

We have detected the He I line at 4471.47 Å, which yields an abundance of  $\log \epsilon(\text{He}) = 10.44$  which implies an underabundance of 0.55 dex compared to the solar value. This is in agreement with the underabundance of He found in hot BHB stars (Moehler (1999), Moehler et al. 2003 ).

We have not detected C, N and O lines in our spectrum of ZNG 4. Assuming an equivalent width of 5 mÅ as the detectable limit in our spectrum of ZNG 4, we find the upper limit of  $[\text{C}/\text{Fe}]$  to be +0.32 dex (based on the C I 5052.17 Å line ), that of  $[\text{N}/\text{Fe}]$  to be +1.15 dex ( based on the N I 4214.80 Å line ) and that of  $[\text{O}/\text{Fe}]$  to be +0.01 dex (based on the O I 6156.78 Å line ). Globular cluster stars show anticorrelation of sodium and oxygen abundances (Kraft et al. 1997). In ZNG 4 we find enhancement of sodium, therefore we expect an underabundance of oxygen. Also star to star abundance variations in the light elements C, N, O, Na, Mg and Al occur among the bright giants of a number of globular clusters (Ivans et al. 1999). The absence of C, N and O lines in our spectrum of ZNG 4 may be due to the underabundance of these elements. A much higher resolution and high signal to noise ratio spectrum of ZNG 4 may reveal the lines of C, N and O lines if present.

### 3.6 Discussion

The chemical composition of ZNG 4 shows significant deviations in element abundances from the expected metallicity of M13. Ti, Ca, Sc and Ba are found to be relatively overabundant (Figure 3.5) compared to RGB stars and cool BHB stars of M13, whereas the abundances of Mg, Cr and Fe are in agreement with the cluster metallicity.

From a study of 22 M13 G-K giants, Kraft et al. (1993, 1997) found the abundances of Fe, Sc, V and Ni to be  $[\text{Fe}/\text{H}] = -1.49$ ,  $[\text{Sc}/\text{Fe}] = -0.10$ ,  $[\text{V}/\text{Fe}] = 0.00$  and  $[\text{Ni}/\text{Fe}] = -0.04$ . They found Ca and Ti to be mildly overabundant ( $[\text{Ca}/\text{Fe}] = +0.24$  and  $[\text{Ti}/\text{Fe}] = +0.29$ ). Si was overabundant by  $+0.34$  dex. Study of M13 giants by Armosky et al. (1994) yields the average abundance of Fe, Y and Ba :  $[\text{Fe}/\text{H}] = -1.49$ ,  $[\text{Y}/\text{Fe}] = -0.12$  and  $[\text{Ba}/\text{Fe}] = -0.04$ , whereas in ZNG 4 we find significant overabundance of Ca, Sc, Ti, Y and Ba compared to that found in M13 giants. Also, overabundance of Na [ $+0.2$  dex] and absence of O lines support the anticorrelation of Na and O abundances found in M13 giants (Kraft et al. 1997).

Behr et al. (1999) have studied the BHB stars in M13 on either side of the HB gap. They find the photospheric compositions and stellar rotation rates to vary strongly as a function of  $T_{\text{eff}}$  of the stars. Among the cooler stars in their sample, at  $T_{\text{eff}}$  of 8500K, the metal abundances are in rough agreement with the canonical cluster metallicity and the hotter stars with  $T_{\text{eff}}$  greater than 10000K show a deficiency of He and enhancement of Fe, Ti, Cr by a factor of 300. However, Mg remains at the canonical cluster metallicity. In ZNG 4 also, Mg abundance is in agreement with the M13 metallicity. Abundances similar to that found in BHB stars of M13 were also found in BHB stars of M15 (Behr et al. 2000b) and BHB stars of NGC 6752 (Glaspy et al. 1989, Moehler et al. 1999). The abundance anomalies in these BHB stars are most likely due to diffusion - the gravitational settling of helium (Grestein et al. 1967) and radiative levitation of metal atoms (Michaud et al. 1983). Rotational velocities ( $v \sin i$ ) appear to have a bimodal distribution in cooler BHB stars, whereas the hotter BHB stars with  $T_{\text{eff}}$  greater than 10000K are found to be slow rotators.

However, the abundances and rotational velocity of ZNG 4 are contrary to what

is expected for stars on the red side of the HB gap at 11,000 K. It is a slow rotator ( $v \sin i = 7 \text{ km sec}^{-1}$ ). It shows underabundance of He and overabundances of Ti, Ca, Sc and Ba. In Table 3.3 and Figure 3.5, we have compared the abundances of ZNG 4 with the abundances of M13 BHB stars of  $T_{\text{eff}} 7681 \text{ K}$  (J 11) and  $T_{\text{eff}} 12,750 \text{ K}$  (WF4-3485) (Behr, 2000c) and with the abundances of the RGB star L262 (Cavallo and Nagar, 2000). In Table 3.3, the last column shows the mean RGB abundances in M13, where elements from Na to Fe are taken from Kraft et al. (1997) and Y and Ba abundances are from Armosky et al. (1994). It is evident from the abundances listed in Table 3.3 and from Figure 3.5 that ZNG 4 shows overabundance of metals compared to that of a M13 RGB star and also when compared to that of a M13 BHB star of similar temperature. These results indicate that in ZNG 4, diffusion and radiative levitation of elements may be in operation. Slowly rotating HB stars are also seen on the cooler side of HB gap, but abundance anomalies start from 11,000 K (Moehler et al. 1999, Behr et al. 2000b). This implies that ZNG 4 may have the properties of the stars on the blue side of the HB gap although it has  $T_{\text{eff}}$  of 8500 K. In this regard, more accurate determination of abundances of these elements in ZNG 4 and similar stars in M13 is needed to confirm our results and conclusions.

This may be explained in two ways. One is that, for some stars in M13, the onset of diffusion seems to start at lower  $T_{\text{eff}}$  ( $\approx 8500 \text{ K}$ ). The other argument would be that the star has evolved from the blue side of the HB gap and is moving towards the red with higher luminosity as indicated by the post-HB evolutionary tracks of Gingold (1976) and Dorman et al. (1993).

The BHB stars hotter than 11,500 K typically show strong photospheric helium depletions due to gravitational settling (Moehler et al. 2000 & 2003). The calculations of Michaud et al. (1983) indicate that helium depletion should be accompanied by photospheric enhancement of metals, since the same stable atmosphere that permits gravitational settling also permits the levitation of elements with large radiative cross sections. The depletion of helium and overabundance of some of the metals in the photosphere of ZNG 4 is in qualitative agreement with the calculations of Michaud et al. (1983).

Recently, Turcotte et al. (1998) and Richer et al. (2000) made diffusion simulations to explain the abundance patterns of chemically peculiar A and F stars. Their predicted abundance patterns are qualitatively similar to that found in ZNG 4. However, none of the recent diffusion studies treated the cases of BHB stars and post-HB stars. This phenomenon may be related to the disappearance of surface convection and hence to the formation of a stable stellar atmospheres. HB stars and post-HB stars cooler than  $T_{\text{eff}} = 6300\text{K}$  have deep convective envelopes (Sweigart 2002). Hotter than this temperature the envelope convection breaks into distinct shells associated with the ionization of H and He. Note that the surface convection disappears at  $11000\text{K}$  (Sweigart 2002) and BHB stars hotter than this show moderate to severe abundance anomalies.

ZNG 4 has a V magnitude of 13.964 (Paltrinieri et al. 1998). Considering the distance modulus of M13 to be 14.42 and  $E(B-V)$  towards M13 to be 0.02 (Kraft and Ivans 2003), we estimated the absolute magnitude ( $M_v$ ) of the star to be  $-0.522$ . For stars with  $T_{\text{eff}}$  around 8500 K, the bolometric correction (BC) is negligible (Flower 1996). Considering  $BC = 0$ , we get the bolometric magnitude ( $M_{\text{bol}}$ ) to be  $-0.522$ , which corresponds to a luminosity of  $127 L_{\odot}$  [ $\log \frac{L}{L_{\odot}} = 2.18$ ]. Using the equation connecting the mass, effective temperature and bolometric magnitude, we find the surface gravity,  $\log g = 2.6$  (assuming the mass of ZNG 4 to be  $0.5 M_{\odot}$ ), which agrees well with the value estimated from the analysis of the spectrum of ZNG 4.

The post-AGB star Barnard 29 [ $\log \frac{L}{L_{\odot}} = 3.3$ ] which is a member of M13 is more luminous than ZNG 4. The abundance pattern of ZNG 4 is very different from that of the post-AGB star Barnard 29 (Conlon et al. 1994, Moehler et al. 1998). The M13 BHB stars with  $T_{\text{eff}}$  around 8500 K have a luminosity of about  $40 L_{\odot}$ , whereas ZNG 4 is more luminous by about a factor of 3. The higher luminosity of ZNG 4 compared to BHB stars of M13 indicates that the ZNG 4 can be classified as a supra horizontal branch star. Stars which lie 1.5 magnitude above the HB stars are classified as supra horizontal branch (SHB) stars. They may be evolved blue horizontal-branch stars, the tidally stripped cores of red giants, or evolved blue stragglers (Shara et al. 1998).

The photometric studies of SHB stars in M13 (Zinn 1974) and NGC 6522 (Shara

et al. 1998) have been carried out earlier. But no detailed abundance analysis of SHB stars in globular clusters is available to compare with the abundances of ZNG 4.

### 3.7 Evolutionary status of post-HB Star

There are three different possible evolutionary paths that a Horizontal Branch star can take.

(a) Star has enough envelope mass to reach the AGB. It climbs up the AGB, evolves with double shell burning sources (Hydrogen/Helium), and usually loses mass on the AGB as well. After the envelope gets exhausted, the star moves rapidly blueward on the CMD and is a post-AGB star. The helium/carbon/oxygen core of these stars exceeds by at least a few times 0.01 solar masses the horizontal branch core mass that is found in low mass stars.

(b) Star has enough envelope mass only to evolve toward the AGB from the blue horizontal branch, but the hydrogen envelope is exhausted before the star can join the AGB and ascend on it. It then evolves blueward back to the white dwarf cooling track. These are termed post-Early AGB stars, because the “Early AGB” is a distinct phase of AGB evolution before shell flashing starts and before a bump in the AGB luminosity function occurs when the H/He shells interact. Their lifetimes predict one such star per 50 progenitor stars which are very blue HB stars within a small envelope mass range.

(c) Even more extreme blue HB stars do not have sufficient envelope to approach anywhere near the AGB, so rise above the HB in a loop before evolving directly to the WD track. These are sometimes referred to as AGB-Manque (failed AGB) stars and have direct observational counterparts in the sdO stars.

The progenitors of both (b) and (c) are termed as EHB (Extreme Horizontal Branch) stars.

These three possibilities are distinguished by (1) luminosity and (2) longevity. The post-AGB stars are relatively luminous and extremely short-lived. They cross the HR diagram in less than  $10^5$  years (only several thousand years if the core mass is



close to 0.6 solar). The post-Early AGB stars take  $10^6$  years to cross the HR diagram at significantly lower luminosity ( $L_{\text{bol}} < 1000L_{\odot}$ ) whilst the third category live for 2 to 3 times  $10^7$  years.

However, since types (b) and (c) only arise from EHB stars they are usually rare - that is except for systems like globular clusters with significant very blue HB populations such as M13, M80, NGC6752, Omega Cen etc. On the other hand if such a progenitor population does exist they are likely to be more numerous because of their relatively long lifetimes.

To sum up, a post-AGB star will have a bolometric luminosity close to or exceeding the tip of the red giant branch, whereas the others will lie below that level, and require an EHB progenitor population.

### 3.8 Conclusions

In figure 5, position of the star ZNG 4 in the  $\log T_{\text{eff}} - \log L$  plane of post-HB evolutionary track of a star with  $[\text{Fe}/\text{H}] = -1.5$  and core mass  $0.485 M_{\odot}$  (Dorman et al.1993) is shown. The position of IV 83 (BHB star of similar temperature) and Barnard 29 (post-AGB) are also shown for comparison. From the figure, we can make out that the star is evolving from BHB phase of  $T_{\text{eff}} \approx 4.3$  towards cooler asymptotic giant branch (AGB) and will possibly go through post-EAGB tracks to end up as White Dwarf.

Since ZNG 4 is a post-HB star and it has evolved from a hot BHB star stage, it may had severe abundance anomalies similar to those found in the hot BHB stars of M13 (Table 3.3). The present  $T_{\text{eff}} = 8500\text{K}$  of ZNG 4 indicates that thin layers of subsurface convection if present may have diluted the severe abundance anomalies due to diffusion and radiative levitation that took place during its hot BHB stage of evolution. It is important to derive the chemical composition of a significant sample of post-HB stars hotter than  $11000\text{K}$  and much cooler than  $11000\text{K}$  to further understand the role of diffusion, radiative levitation, rotation and convection during the post-HB stage of evolution.

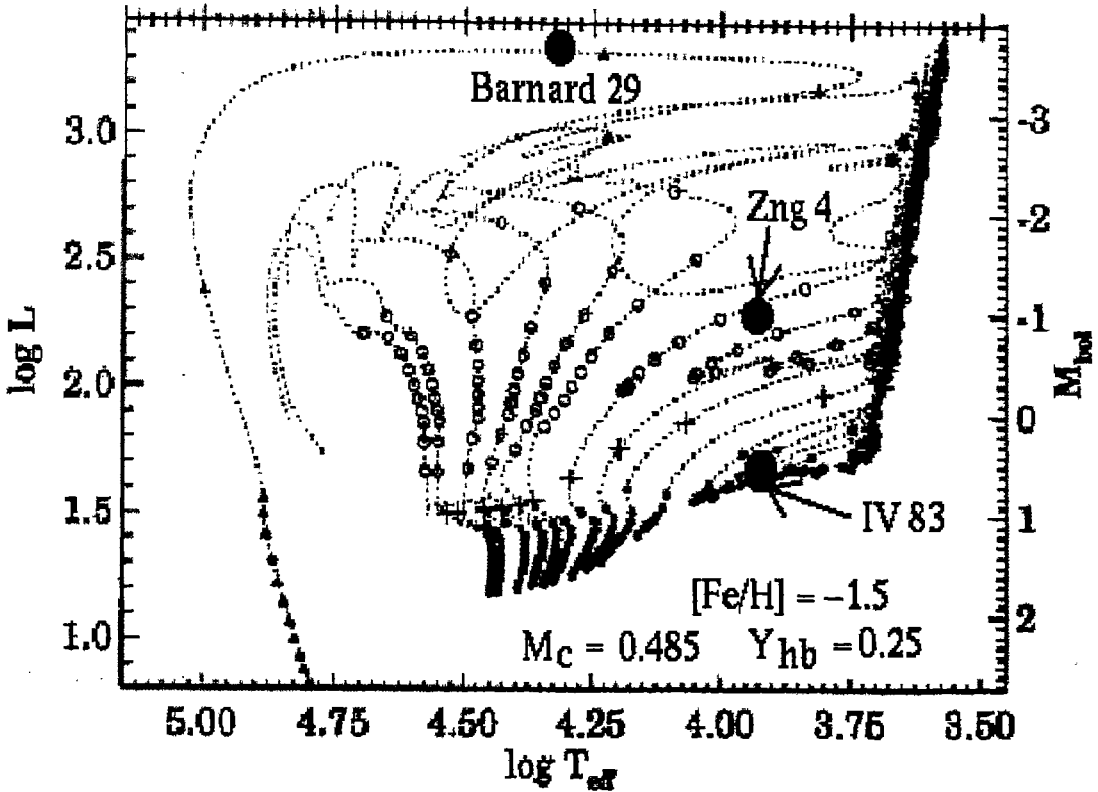


Figure 3.6: Position of ZNG 4 (in M13) in the theoretical post-HB evolutionary tracks (Dorman et al. 1993) of a star with  $[\text{Fe}/\text{H}] = -1.5$  and core mass  $0.485 M_{\odot}$ . Filled circles mark HB phase of evolution with an interval of 10 Myr. Crosses represent the core helium exhaustion point. Open circles mark the post-HB stages and are placed at an interval of 2 Myr. Filled triangles denote faster evolutionary stage after  $\log L$  reaches 3.0, with an interval of 0.1 Myr. Position of ZNG 4 in  $\log T_{\text{eff}} - \log L$  plane indicates that the star is evolving from BHB phase towards AGB and will go through post-EAGB tracks to end up as White Dwarf. Position of Barnard 29 (post-AGB) and IV 83 (BHB) are also shown for reference.

Table 1: Data for spectral lines measured in the spectrum of ZNG 4 in M13

$\lambda_{lab}$ (in $\text{\AA}$ )	LEP (eV)	log gf	EW ( $m\text{\AA}$ )	log $\epsilon$
He I				
4471.47	20.96	-0.278	11.3	10.44
Na I				
5889.95	0.00	0.117	63.9	5.05
5895.92	0.00	-0.184	40.6	5.04
Mg I				
5167.32	2.71	-1.030	31.9	6.19
5172.68	2.71	-0.402	70.2	6.09
5183.60	2.72	-0.180	85.8	6.07
Mg II				
4481.13	8.86	0.740	104.1	6.12
4481.32	8.86	0.590	80.0	5.92
Si II				
5041.02	10.07	0.291	27.5	6.59
5055.98	10.07	0.593	25.5	6.24
6347.11	8.12	0.297	84.2	6.49
6371.37	8.12	-0.003	64.1	6.48
Ca I				
4226.73	0.00	0.265	76.7	5.21
4454.78	1.90	0.335	27.7	5.71
Ca II				
5019.97	7.51	-0.501	18.6	5.77
Sc II				
4246.82	0.32	0.242	54.5	1.58
4314.08	0.62	-0.096	47.8	2.03
4320.73	0.60	-0.252	49.7	2.21
4325.00	0.59	-0.442	35.9	2.18
4374.46	0.62	-0.418	39.8	2.23

Table 1: continued

$\lambda_{\text{lab}}$ (in Å)	LEP (eV)	log gf	EW ( $m\text{Å}$ )	log $\epsilon$
Sc II				
4400.39	0.60	-0.536	32.3	2.21
4415.56	0.59	-0.668	31.5	2.32
Ti II				
4161.53	1.08	-2.160	20.8	4.27
4163.65	2.59	-0.210	76.3	4.22
4171.91	2.60	-0.270	75.0	4.27
4287.87	1.08	-1.820	38.8	4.26
4290.22	1.17	-0.930	91.1	4.16
4294.10	1.08	-0.880	95.2	4.12
4300.05	1.18	-0.490	129.9	4.43
4301.91	1.16	-1.200	78.7	4.25
4307.86	1.17	-1.100	62.6	3.93
4312.86	1.18	-1.090	77.5	4.13
4314.98	1.16	-1.120	69.8	4.04
4320.96	1.17	-1.900	43.4	4.47
4330.24	2.05	-1.800	21.6	4.57
4330.69	1.18	-2.060	24.3	4.30
4344.29	1.08	-1.930	19.8	3.99
4350.83	2.06	-1.810	12.6	4.32
4367.66	2.59	-0.870	34.9	4.28
4386.84	2.60	-0.940	27.2	4.21
4391.03	1.23	-2.240	19.2	4.38
4394.05	1.22	-1.770	37.7	4.28
4395.03	1.08	-0.510	142.4	4.62
4395.85	1.24	-1.970	31.7	4.39
4399.77	1.24	-1.220	78.3	4.31
4407.68	1.22	-2.430	10.4	4.27
4411.07	3.10	-0.670	23.0	4.18

Table 1: Continued

$\lambda_{lab}$ (in Å)	LEP (eV)	log gf	EW ( $m\text{Å}$ )	log $\epsilon$
Ti II				
4417.72	1.17	-1.230	76.0	4.23
4418.33	1.24	-1.990	25.0	4.27
4421.94	2.06	-1.580	14.6	4.16
4443.79	1.08	-0.700	118.3	4.33
4450.48	1.08	-1.510	56.7	4.20
4464.45	1.16	-1.810	39.8	4.31
4488.33	3.12	-0.510	40.0	4.36
4529.47	1.57	-1.650	27.1	4.21
4533.97	1.24	-0.540	126.3	4.42
4549.62	1.58	-0.220	102.1	3.89
4563.76	1.22	-0.790	108.1	4.32
4571.97	1.57	-0.230	69.9	3.42
4589.96	1.24	-1.620	38.7	4.14
4763.88	1.22	-2.360	18.9	4.47
4779.98	2.05	-1.260	32.9	4.24
4798.52	1.08	-2.670	12.9	4.49
4805.09	2.06	-0.960	52.1	4.24
4874.01	3.10	-0.900	18.0	4.27
4911.19	3.12	-0.650	28.4	4.28
5129.15	1.89	-1.300	33.4	4.17
5154.07	1.57	-1.780	26.9	4.29
5185.91	1.89	-1.370	26.2	4.10
5188.68	1.58	-1.050	68.5	4.20
5226.54	1.57	-1.230	52.1	4.16
5336.77	1.58	-1.630	31.9	4.25
5381.02	1.57	-1.970	21.9	4.38
Cr II				
4554.99	4.07	-1.282	14.8	4.40

Table 1: Continued

$\lambda_{lab}$ (in Å)	LEP (eV)	log gf	EW ( $m\text{Å}$ )	log $\epsilon$
Cr II				
4558.65	4.07	-0.449	44.5	4.18
4588.20	4.07	-0.627	34.6	4.20
4616.63	4.07	-1.361	15.0	4.48
4618.80	4.07	-0.840	26.1	4.25
4634.07	4.07	-0.990	19.1	4.23
4824.13	3.87	-0.970	20.6	4.11
5237.33	4.07	-1.160	13.0	4.21
Fe I				
4143.87	1.56	-0.511	23.2	6.03
4199.10	3.05	0.155	20.4	6.30
4202.03	1.49	-0.708	20.8	6.11
4260.47	2.40	0.109	22.3	5.95
4271.76	1.49	-0.164	39.6	5.93
4325.76	1.61	0.006	48.0	5.96
4383.55	1.49	0.200	59.2	5.84
4415.12	1.61	-0.615	20.5	6.08
4891.49	2.85	-0.112	15.0	6.24
4920.50	2.83	0.068	13.6	6.00
4957.60	2.81	0.233	19.4	6.00
5269.54	0.86	-1.321	8.7	5.82
5328.04	0.92	-1.466	14.3	6.24
Fe II				
4173.46	2.58	-2.740	62.2	6.42
4178.86	2.58	-2.500	43.0	5.90
4233.17	2.58	-1.900	90.5	5.99
4296.57	2.70	-3.010	16.5	5.95
4351.77	2.70	-2.020	54.1	5.66
4385.39	2.78	-2.680	31.0	6.01

Table 1: Continued

$\lambda_{lab}$ (in $\text{\AA}$ )	LEP (eV)	log gf	EW ( $m\text{\AA}$ )	log $\epsilon$
Fe II				
4416.83	2.78	-2.410	41.3	5.91
4489.18	2.83	-2.970	24.0	6.18
4491.40	2.86	-2.700	28.9	6.03
4508.29	2.86	-2.250	43.9	5.84
4515.34	2.84	-2.450	34.4	5.87
4520.22	2.81	-2.600	33.0	5.98
4522.63	2.84	-2.030	43.0	5.60
4549.47	2.83	-2.020	80.0	6.10
4555.89	2.83	-2.160	46.2	5.76
4576.34	2.84	-2.920	18.9	6.01
4582.84	2.84	-3.090	16.1	6.10
4583.84	2.81	-1.860	79.8	5.92
4629.34	2.81	-2.330	45.9	5.91
4923.93	2.89	-1.320	121.3	6.14
5018.44	2.89	-1.220	127.4	6.15
5169.03	2.89	-1.303	134.4	6.37
5197.58	3.23	-2.100	45.9	5.96
5234.62	3.22	-2.230	47.6	6.11
5276.00	3.20	-1.940	57.3	5.95
5316.61	3.15	-1.850	67.0	5.97
5362.87	3.20	-2.739	29.6	6.31
6456.38	3.90	-2.100	45.8	6.46
Sr II				
4215.52	0.00	-0.145	19.8	0.71
Y II				
4177.53	0.41	-0.160	8.98	1.09
4374.94	0.41	0.160	11.10	0.86

Table 1: Continued

$\lambda_{lab}$ (in Å)	LEP (eV)	log gf	EW ( $m\text{Å}$ )	log $\epsilon$
Ba II				
4554.03	0.00	0.170	17.03	0.95
4934.08	0.00	-0.150	8.042	0.88

Table 3.2: Chemical composition of ZNG 4 in M13

Element	no of lines	$T_{\text{eff}} = 8500 \text{ K}, \log g = 2.5$ $V_t = 2.5 \text{ km s}^{-1}$ and $[\text{Fe}/\text{H}] = -1.5$ MOOG		$T_{\text{eff}} = 8500 \text{ K}, \log g = 2.5$ $V_t = 2.5 \text{ km s}^{-1}$ and $[\text{Fe}/\text{H}] = -1.5$ WIDTH		$T_{\text{eff}} = 8750 \text{ K}, \log g = 2.0$ $V_t = 2 \text{ km s}^{-1}$ and $[\text{Fe}/\text{H}] = -1.5$ MOOG
		$[\text{X}/\text{H}] \pm \sigma$	[Ele/Fe]	$[\text{X}/\text{H}] \pm \sigma$	[Ele/Fe]	$[\text{X}/\text{H}] \pm \sigma$
		He I	1	-0.55 ± 0.20		-0.68 ± 0.20
Na I	2	-1.28 ± 0.10	+0.21	-1.30 ± 0.10	+0.20	-0.79 ± 0.11
Mg I	3	-1.46 ± 0.07	+0.03	-1.48 ± 0.05	+0.02	-1.03 ± 0.16
Mg II	2	-1.56 ± 0.14	-0.07	-1.59 ± 0.09	-0.09	-1.83 ± 0.15
Si II	4	-1.10 ± 0.15	+0.39	-1.20 ± 0.12	+0.30	-1.31 ± 0.24
Ca I	2	-0.80 ± 0.35	+0.69	-0.93 ± 0.25	+0.57	-0.09 ± 0.33
Ca II	1	-0.49 ± 0.10	+1.00	-0.62 ± 0.10	+0.88	-0.32 ± 0.10
Sc II	7	-0.99 ± 0.25	+0.50	-1.04 ± 0.25	+0.45	-0.73 ± 0.25
Ti II	51	-0.75 ± 0.18	+0.74	-0.83 ± 0.25	+0.67	-0.59 ± 0.19
Cr II	8	-1.41 ± 0.12	+0.08	-1.47 ± 0.12	+0.03	-1.38 ± 0.12
Fe I	13	-1.48 ± 0.15	+0.02	-1.53 ± 0.26	+0.02	-0.99 ± 0.14
Fe II	28	-1.50 ± 0.21	+0.00	-1.46 ± 0.22	+0.02	-1.52 ± 0.22
Sr II	1	-2.19 ± 0.10	-0.70	-2.21 ± 0.10	-0.71	-1.65 ± 0.12
Y II	2	-1.20 ± 0.17	+0.29	-1.30 ± 0.12	+0.37	-0.64 ± 0.14
Ba II	2	-1.21 ± 0.05	+0.28	-1.23 ± 0.04	+0.26	-0.61 ± 0.10



Table 3.3: Comparison of the abundances of ZNG 4 with the abundances of M13

## BHB and RGB stars

Element	ZNG 4 [Fe/H]= -1.49 $T_{\text{eff}} = 8500 \text{ K}$ $\log g = 2.5$	M13/ J11 (BHB) * [Fe/H]= -1.82 $T_{\text{eff}} = 7681 \text{ K}$ $\log g = 3.1$	M13/WF4-3485(BHB) * [Fe/H]= + 0.02 $T_{\text{eff}} = 12750 \text{ K}$ $\log g = 4.1$	M13/ L262 (RGB) * [Fe/H]= -1.61 $T_{\text{eff}} = 4160 \text{ K}$ $\log g = 0.50$	Mean RGB abundances * in M13
	[X/H]	[X/H]	[X/H]	[X/H]	[X/H]
He	-0.55	< -0.26	- 1.49 $\pm$ 0.17	...	...
Na	-1.28	...	...	-1.27 $\pm$ 0.11	-1.37 $\pm$ 0.04
Mg	-1.51	-1.50 $\pm$ 0.16	- 1.62 $\pm$ 0.14	-1.51 $\pm$ 0.14	-1.46 $\pm$ 0.03
Si	-1.10	< -1.23	- 1.43 $\pm$ 0.07	-1.16 $\pm$ 0.14	-1.30 $\pm$ 0.02
Ca	-0.64	-1.72 $\pm$ 0.11	- 1.66 $\pm$ 0.15	-1.39 $\pm$ 0.14	-1.34 $\pm$ 0.01
Sc	-0.99	-1.63 $\pm$ 0.10	< + 1.10	...	-1.67 $\pm$ 0.01
Ti	-0.75	-1.32 $\pm$ 0.06	- 0.53 $\pm$ 0.16	-1.30 $\pm$ 0.20	-1.32 $\pm$ 0.02
Cr	-1.41	-1.71 $\pm$ 0.12	< - 0.12	...	...
Fe	-1.49	-1.82 $\pm$ 0.10	+ 0.02 $\pm$ 0.20	-1.61 $\pm$ 0.10	-1.60 $\pm$ 0.01
Sr	-2.19	-2.03 $\pm$ 0.10	< + 1.75	...	...
Y	-1.20	< -0.97	< + 2.92	...	- 1.61 $\pm$ 0.04
Ba	-1.21	-1.68 $\pm$ 0.10	< + 3.26	...	- 1.53 $\pm$ 0.05

\* Abundances of M13 BHB stars are from Behr (2000c) and abundances of M13 RGB star are from Cavallo & Nagar (2000). In the last column, the mean abundances of elements from Na to Fe in M13 RGB stars are from Kraft et al (1997) and that of Y and Ba are from Armosky et al. (1994).

# Chapter 4

## Abundance analysis of the metal poor giant : LSE-202

---

### 4.1 Abstract

We are presenting the high resolution and high signal to noise ratio spectra of a halo giant ( $l = 56^{\circ}.28$ ,  $b = +24^{\circ}.03$ ) LSE 202, spanning from  $3750 \text{ \AA}$  to  $10,100 \text{ \AA}$ . The model atmosphere analysis reveals the atmospheric parameters of the star to be  $T_{\text{eff}} = 4750 \pm 250 \text{ K}$ ,  $\log g = 1.5 \pm 0.5$ ,  $[\text{Fe}/\text{H}] = -2.41$  and  $V_t = 1.9 \text{ km s}^{-1}$ . Among  $\alpha$ -process elements, Mg, Ca, Ti show moderate overabundances ( $[\text{Mg}/\text{Fe}] = +0.39$ ,  $[\text{Ca}/\text{Fe}] = +0.28$ ,  $[\text{Ti}/\text{Fe}] = +0.35$ ), where as Si shows slight deficiency ( $[\text{Si}/\text{Fe}] = -0.14$ ). Among odd  $z$  elements, Na is deficient ( $[\text{Na}/\text{Fe}] = -0.24$ ) whereas, K and Sc are overabundant compared to iron ( $[\text{K}/\text{Fe}] = +0.20$ ,  $[\text{Sc}/\text{Fe}] = +0.24$ ), V remaining with the metallicity of the star ( $[\text{V}/\text{Fe}] = -0.02$ ). Mn is slightly deficient ( $-0.29 \text{ dex}$ ), Cr and Ni goes with iron metallicity ( $[\text{Cr}/\text{Fe}] = +0.02$ ,  $[\text{Ni}/\text{Fe}] = +0.01$ ), Co being overabundant ( $[\text{Co}/\text{Fe}] = +0.40$ ). Among heavy elements, Zn shows overabundance of  $+0.30 \text{ dex}$ . The heavy elements, Ba, Sr, La and Y show deficiency ( $[\text{Ba}/\text{Fe}] = -0.43$ ,  $[\text{Sr}/\text{Fe}] = -0.26$ ,  $[\text{La}/\text{Fe}] = -0.43$  and  $[\text{Y}/\text{Fe}] = -0.38$ ), while Nd and Zr remain at metallicity of the star ( $[\text{Nd}/\text{Fe}] = +0.10$  and  $[\text{Zr}/\text{Fe}] = +0.0$ ).  $r$ -process elements, Eu

and Dy show overabundance of +0.14 and +0.25 dex respectively. The ratio [Ba/Eu] being  $-0.6$  dex shows that the heavy elemental abundances in this metal poor star is dominated by the r-process. Also, the ratio [Sr/Ba] = +0.2 dex supports the theory which predicts that these neutron-capture elements are produced by different mechanisms.

## 4.2 Introduction

The chemical compositions of the long lived stars in the halo provide us the clues for the enrichment history of our galaxy. These extreme metal-poor stars exhibit the products of nucleosynthesis from the first high-mass, zero-metallicity objects to evolve and pollute the proto-Galaxy. Results of abundance analysis of these stars can be used to probe the ejecta of the earliest supernovae and determine the nature of the stars and sites of nucleosynthesis that existed during the first epochs of star formation in the Galaxy.

Models of Big Bang cosmology yield elements only upto Boron (Kajino, Mathews & Fuller, 1990) and the theory suggests that the first heavy elements were formed in the initial stellar generations following the collapse of gas clouds of mass  $\approx 10^5 M_{\odot}$  (Couchman & Rees, 1986). Audouze & Silk (1995) proposed that, relatively few supernova are required to raise the level of the heavy elements from zero to that observed in the most metal poor halo objects.

Hence the study of chemical composition of the stars in galactic halo is required to observe the products of nucleosynthesis created in the Big Bang and in first stars. The abundance studies in the case of metal poor halo stars is a necessary tool for understanding the way our galaxy has been formed and evolved and also for understanding of the first heavy-element producing objects.

LSE 202 was discovered in The Luminous Stars Extension (LSE) survey for OB stars by Drilling and Bergeron (1995), along with a small number of bright metal deficient candidates (most of which are likely to be giants).

We took up a program to analyze the high resolution spectra of these candidate

giants, in order to understand the chemical composition of thick disk stars. LSE 202 was the first star observed under this program.

Beers et al. (2002) have carried out medium resolution (1-2 Å) spectroscopy and broadband (UBV) photometry for a sample of 39 bright stars. For LSE 202 they obtain,  $V = 10.66$ ,  $(B - V) = 0.83$  and  $(U - B) = 0.25$  from their photometry. Radial velocity was obtained using the line-by-line and cross-correlation techniques (Beers et al. 1999) and the value given is  $-384 \text{ kms}^{-1}$ . They have estimated the metallicity by spectroscopic and photometric method and they suggest a value of  $[\text{Fe}/\text{H}] = -2.19$  and they have classified it as a halo giant.

Metal-deficient giants with lower temperature have much richer absorption-line spectra than their warmer main-sequence counterparts, providing the opportunity to study many more elemental species. Thus we chose to derive the chemical composition of LSE 202, in order to further understand the heavy element compositions in the halo stars.

### 4.3 Observations

Spectra of LSE 202 was obtained with the 2.7 m telescope at the McDonald observatory, which makes use of the cross dispersed coude echelle spectrograph (Tull et al. 1995) and a CCD of  $2048 \times 2048$  pixels. Spectra were obtained with 4 exposure times (Two of them with 1500 s integration time observed on 14th July 2003 and two others with 1800 s integration time each observed on 16th July 2003). Sixty-one spectral orders were recorded, providing spectral coverage from 3650 Å to 10,100 Å, with gaps between the orders. The spectra were coadded to improve the signal to noise ratio, finally to yield  $S/N = 120$ .

The data was bias-subtracted, trimmed, flat-fielded to remove pixel to pixel variations, converted to a one-dimensional spectrum, and normalized to the continuum using standard data reduction package (NOAO IRAF). The reference spectrum of thorium-argon was used for the wavelength calibration.

## 4.4 Analysis

The spectral lines were identified using Moore's atomic multiplet table (1945). The equivalent widths of the absorption lines were measured by Gaussian fitting to the observed profiles, using the SPLIT package of IRAF. They are given in Table 4.1.

For the analysis of the spectra, excitation potential and oscillator strengths were taken from the compilation of Luck and Bond, supplemented with line information from the Vienna Atomic Line Database (<http://www.astro.univie.ac.at/vald/>). We employed the latest (2002) version of MOOG, an LTE stellar line analysis program (Snedden 1973) and for model atmospheres, we used Kurucz ATLAS (1993) models.

For the initial estimation of the temperature of the star, we used the photometric data of LSE 202 given by Beers et al. (2002). The value of  $(B - V) = 0.83$  and from the galactic coordinates of the object ( $l = 56^\circ.28$ ,  $b = +24^\circ.03$ ), we obtain  $E(B-V) = 0.047$  (Schlegel et al. 1998).  $(B - V)_0 = 0.783$  will correspond to  $T_{\text{eff}} = 4800$  K for a giant with  $[\text{Fe}/\text{H}] = -2$  (Alonso et al. 1999). For stars with metallicity lower than  $-2.0$ , this value could be slightly lower. Therefore, we used this value of  $T_{\text{eff}}$  as the initial value, and varied in steps of 250 K. Similarly  $\log g$  was varied from 0.5 to 2.5 in steps of 0.5 dex and we derived the (final) physical parameters spectroscopically by analyzing neutral (Fe I) and ionized (Fe II) lines of iron.

The stellar atmospheric parameters are determined as follows. The value of effective temperature was obtained by the method of excitation balance, constraining the abundance derived from Fe I lines to be independent of the excitation potential of individual lines. The surface gravity was then set by ionization–equilibrium, forcing abundances obtained from neutral (Fe I) and ionized (Fe II) species to be equal. The value of microturbulent velocity was adopted such that there is no correlation between the abundances determined from Fe I lines and the equivalent widths of the respective lines.

The accuracy of an equivalent width ( $W_\lambda$ ) is determined by Cayrel et al. (1998), as

$$\delta W = \frac{1.6\sqrt{w\delta x}}{S/N} \quad (4.1)$$

where 'w' is the full width at half maximum (FWHM),  $\delta x$  is the pixel size in  $\text{\AA}$  and S/N is the signal to noise ratio per pixel in the continuum. For our spectra,  $w = 0.12$  to  $0.16 \text{\AA}$ ,  $\delta x = 0.046 \text{\AA}$ ,  $S/N = 80 - 120$  : these parameters would yield  $\delta W_\lambda = 1 - 2 \text{m\AA}$ . Since the continuum normalization or blends are not taken into account in this relation, the error could be little more. Thus the accuracy of  $W_\lambda$  in our spectrum could be of the order of  $3 \text{m\AA}$ . When elements are represented by more than one line, the error in abundance caused by measurement error in  $\delta W_\lambda$  values reduces by the factor of  $\sqrt{N}$ , where N is the number of lines.

The error in estimation of  $T_{\text{eff}}$  is approximately equal to  $\pm 250$  K. Similarly  $\Delta \log g = \pm 0.5$ ,  $\Delta V_t = \pm 0.5 \text{ km s}^{-1}$ .

Table 4.1: Abundances of elements in LSE 202

T <sub>eff</sub> = 4750 K, log g = 1.5 V <sub>t</sub> = 1.9 km s <sup>-1</sup> and [Fe/H] = -2.41				Abundances in HD 122563	Abundances in BPS CS 22892-52
Element	no of lines	[X/H] ± σ	[Ele/Fe]	[Fe/H] = -2.77	[Fe/H] = -2.92
Li I			< -0.56		
Na I	02	-2.66 ± 0.23	-0.24	-0.15	-0.19
Mg I	08	-2.02 ± 0.22	+0.39	+0.51	+0.30
Al I	02	-2.30 ± 0.12	+0.12	-0.32	-0.58
Si I	02	-2.54 ± 0.19	-0.14	+0.46	+0.36
K I	01	-2.22 ± 0.14	+0.20	+0.46	+0.46
Ca I	26	-2.13 ± 0.13	+0.29	+0.29	+0.30
Ca II	02	-2.15 ± 0.15	+0.26		
Sc II	16	-2.15 ± 0.14	+0.24	+0.15	-0.10
Ti I	35	-2.10 ± 0.16	+0.31	+0.19	+0.20
Ti II	53	-2.02 ± 0.17	+0.39	+0.28	+0.16
V I	01	-2.41 ± 0.13	+0.01	+0.07	-0.05
V II	01	-2.48 ± 0.13	-0.05	+0.14	-0.03
Cr I	23	-2.49 ± 0.15	-0.08	-0.39	-0.24
Cr II	03	-2.29 ± 0.16	+0.12	-0.15	-0.15
Mn I	07	-2.61 ± 0.19	-0.29	-0.26	-0.53
Fe I	232	-2.37 ± 0.13		0.00	0.00
Fe II	20	-2.45 ± 0.12		0.00	+0.01
Co I	08	-1.98 ± 0.21	+0.40	+0.32	+0.20
Ni I	28	-2.38 ± 0.16	+0.01	+0.04	-0.07
Zn I	04	-2.11 ± 0.14	+0.30	+0.20	+0.09

Table 4.1: Abundances of heavy elements in LSE 202

T <sub>eff</sub> = 4750 K, log g = 1.5 V <sub>t</sub> = 1.9 kms <sup>-1</sup> and [Fe/H] = -2.41				Abundances in HD 122563	Abundances in BPS CS 22892-52
Element	no of lines	[X/H] ± σ	[Ele/Fe]	[Fe/H] = -2.77	[Fe/H] = -2.92
Sr II	02	-2.66 ± 0.24	-0.26	+0.17	+0.58
Y II	07	-2.78 ± 0.16	-0.38	-0.25	+0.44
Zr II	02	-2.41 ± 0.14	+0.00	+0.18	+0.73
Ba II	02	-2.85 ± 0.14	-0.43	-0.93	+0.99
La II	02	-2.86 ± 0.20	-0.43	-0.70	+1.09
Nd II	02	-2.32 ± 0.21	+0.10	-0.30	+1.33
Eu II	02	-2.27 ± 0.14	+0.14	-0.36	+1.64
Dy II	01	-2.16 ± 0.14	+0.25	...	+1.73
Ce II			< -0.425	-0.73	+1.02
Pr II			< +0.095	...	+1.30
Sm II			< +0.0350	...	+1.65
Gd II			< -0.695	...	+1.46
Tb II			< +0.165	...	+1.62
Dy II			...	...	+1.73
Ho II			< -0.305	...	+1.66
Er II			< -0.055	-0.46	+1.70
Yb II			< -1.61	-0.96	+1.42
Pb I			...	...	+1.57
Th II			...	...	+1.36
U II			...	...	< +0.9

\* Abundances of HD 122563 are from Westin et al. (2000) and abundances of BPS CS 22892-52 are from Sneden et al. (2003)

## 4.5 Results

### 4.5.1 Radial velocity

The radial velocity of LSE 202 has been derived from the wavelength shifts of several absorption lines showing no line asymmetry. These measurements (The observed velocity of  $V_r = -363.570 \pm 0.14$  kms<sup>-1</sup> will), yield an average heliocentric velocity of  $V_{\text{helio}} = -370.23 \pm 0.14$  kms<sup>-1</sup>, which transforms to a radial velocity relative to the local standard of rest  $V_{\text{lsr}} = -350.230 \pm 0.14$  kms<sup>-1</sup>. This is in agreement with the observation of Beers et al. (2002), wherein they obtain  $V_{\text{helio}} = -384$  kms<sup>-1</sup> with a quoted 1 σ error of 7 - 10 kms<sup>-1</sup>. These observations show that LSE 202 is a galactic

halo star.

## 4.5.2 Atmospheric parameters and abundances

The spectroscopic analysis yields a model with  $T_{\text{eff}} = 4750\text{K}$ ,  $\log g = 1.5$  and  $V_t = 1.9 \text{ km s}^{-1}$  and  $[\text{Fe}/\text{H}] = -2.41$ , which best fits the observed spectrum.

Table 2 lists the mean abundances of elements in LSE 202 relative to the Sun (Anders and Grevesse 1989), along with the number of lines used in the analysis and the standard deviation of abundances estimated from individual species. Uncertainties in derived abundances as a result of errors in the determination of the parameters and errors in the measurements of equivalent widths are found to be of the order of 0.12 to 0.23 dex (Table 2).

Using the derived atmospheric parameters and abundances, a synthetic spectrum was generated and plotted over the observed spectrum for verification. The observed and synthetic spectra were found to match well with the above mentioned atmospheric parameters and with the final abundances given in Table 2. Figure 2 shows the synthetic spectra overplotted on observed spectra at different wavelength region, and is found to match well.

## 4.5.3 Non LTE corrections

The assumptions of local thermodynamic equilibrium (LTE) are essentially that all transitions are only due to collisions between absorbers and that radiation is unimportant in determining energy level populations. This is fine in very dense regions where collisions are likely to dominate, but not in the case of photospheres of stars where densities are lower. Since resonance lines for alkali elements form in these outer layers, NLTE effects are thought to be important. Therefore non-LTE correction for resonant lines have been considered.

For a star with  $[\text{Fe}/\text{H}] = -2.5$ , Non LTE treatment for Na would have a correction -0.4 dex (Gehren et al. 2004) and for Al, it is approximately +0.5 dex (Gehren et al. 2004) as Al abundance is underestimated in LTE computations. For K, non-LTE



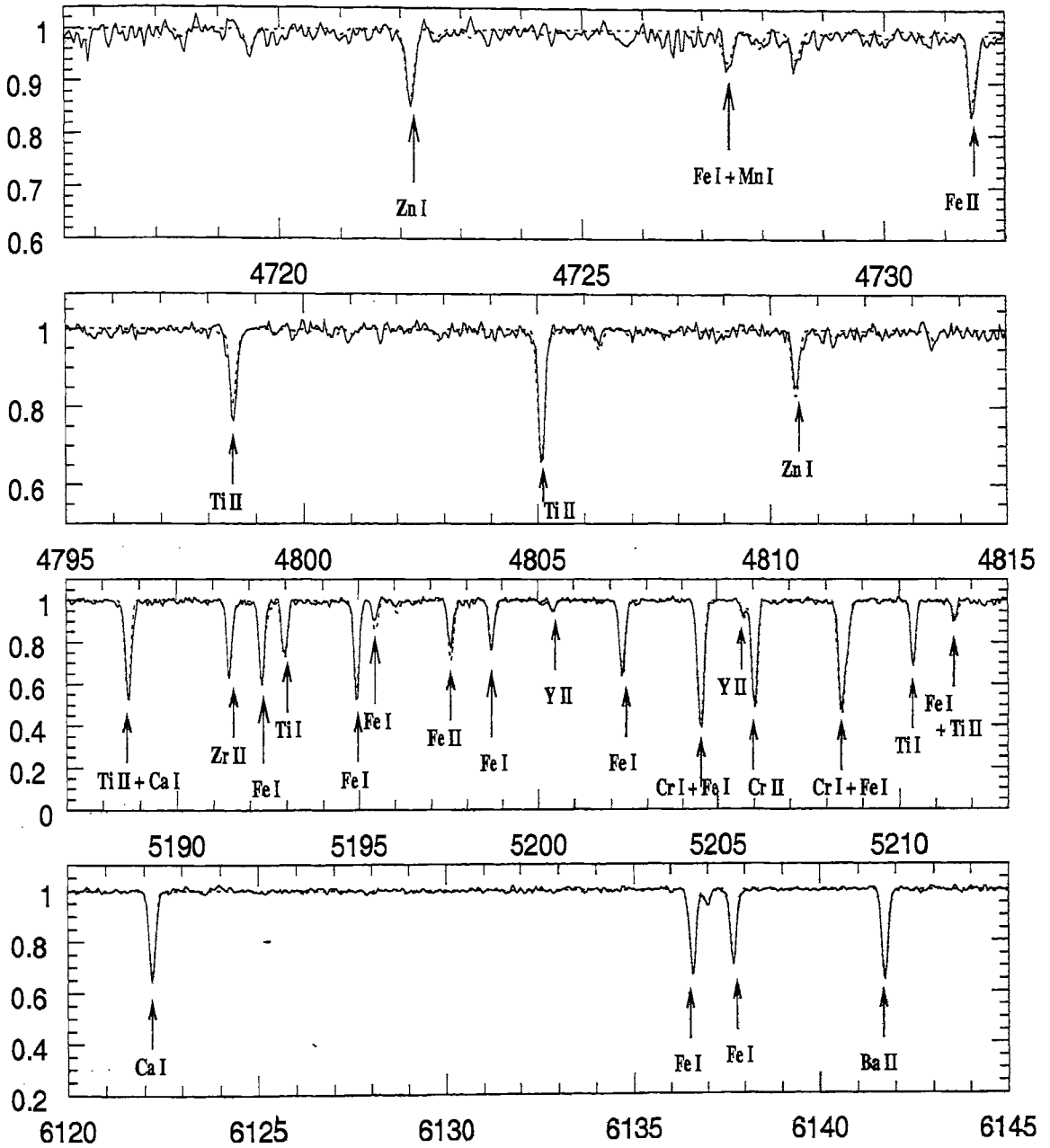


Figure 4.1: Figure shows the synthetic spectrum calculated with the atmospheric parameters ( $T_{\text{eff}} = 4750 \text{ K}$ ,  $\log g = 1.5$ ,  $V_t = 1.9 \text{ km s}^{-1}$ ) and abundances (Table 2) overplotted on the observed spectrum of LSE 202 at different wavelength regions.

correction is approximately -0.35 dex for a star with similar atmospheric parameters (Ivanova & Shimanskii, 2000).

#### 4.5.4 Hyperfine structure effects :

Hyperfine structure affects elements of odd atomic number and those with significant isotope splitting. Hyperfine splitting distributes the line opacity across a greater wavelength range and a line can grow to a greater overall strength before saturating. In such spectral lines, single line approximation is not adequate and it (ignoring the structure) would overestimate the true abundance.

Computations of Peterson (1981) and McWilliam et al. (1995) have shown that the effect could be ignored in the case of Sc, Sr, Eu and resonance lines of Al. However, for Mn and Co the effect becomes significant. Otherwise, the errors could be upto 0.6 dex.

Ryan et al. (1996) have calculated the error in abundance inferred from the resonance lines of Mn and Co through the neglect of hf structure, as a function of the observed equivalent widths.

From the plot, a correction of -0.4 dex needs to be added for Mn line at 4030 Å and -0.15 dex for Mn line at 4034 Å . Similarly for cobalt, a significant error is produced only for line at 4121 Å (of the order of -0.2 dex in value).

These corrections (correction for non-LTE and for hyperfine structure) are added for the abundances given in Table 2 and the average abundance of each element after incorporation of these corrections are given in Table 4.1.

#### 4.5.5 Elemental abundances

##### 4.5.5.1 Lithium Abundance

No lithium line was detected at 6707 Å region in the spectrum of LSE 202. Taking 5 mÅ as the detectable limit, we get the upper limit for abundance of Li to be 0.33 dex which is 3 dex below that of solar Li abundance. This shows that Li is depleted

heavily in this star.

Ryan & Deliyannis (1998a) have studied the Li abundance in metal poor stars cooler than Spite plateau (Spite & Spite 1982). They observe, stars with  $T_{\text{eff}} \geq 5700\text{K}$  have Li abundance of 2.1 dex and the cooler stars show depletion of Li by  $\approx 0.27$  dex per 100 K over the interval  $5000\text{ K} < T_{\text{eff}} < 5500\text{ K}$ . But for stars with  $T_{\text{eff}} < 4900\text{K}$ , the slope of depletion is even larger. The underabundance of Li ( $< 0.33$  dex) in LSE 202 is in agreement with that expected from cooler metal poor giants.

#### 4.5.5.2 CNO elements

Cayrel et al. (2004) have studied 30 extreme metal poor stars and find the mean value of  $[\text{C}/\text{Fe}]$  for these metal stars are approximately 0.2 dex with a dispersion of 0.37 dex. A mean value of  $[\text{O}/\text{Fe}]$  of 0.7 dex with a large dispersion of the order of 0.17 dex was found.

In our spectrum of the star, CNO lines are very weak in this cool metal poor star and the lines are below the limit of detection. We have not used the molecular lines (CN and CH) because of blending. The upper limits drawn for the abundance of these elements, assuming a  $5\text{ m}\text{\AA}$  as the detectable limit for neutral atomic lines of the elements ( C I line at  $4771.75\text{ \AA}$  and  $5052.17\text{ \AA}$ , N I lines at  $4125\text{ \AA}$  &  $4126\text{ \AA}$ , oxygen lines at  $6363\text{ \AA}$  &  $6300\text{ \AA}$  ) yield rather high abundances, as these lines are not excited in a cooler star of  $T_{\text{eff}} = 4750\text{ K}$ . Hence it is not possible to derive any meaningful information on abundance of these elements in LSE 202.

#### 4.5.5.3 Odd z elements

Among odd-z elements, Na is computed from Na D resonant lines at  $5890\text{ \AA}$  and  $5896\text{ \AA}$ . They are well separated from interstellar lines due to high radial velocity of the star. Al abundance is determined from resonant doublet ( $3944\text{ \AA}$  and  $3961\text{ \AA}$ ). Abundance obtained from  $3961\text{ \AA}$  would be more reliable, as  $3944\text{ \AA}$  might have been contaminated by CH line. Abundance of K is based on red doublet  $7665\text{ \AA}$  and  $7699\text{ \AA}$ . But  $7665\text{ \AA}$  is well within the atmospheric line region. So, we have computed abundance only from the  $7699\text{ \AA}$ . We had just two lines of V to determine

abundance, where as for the abundance measure of Sc, we had adequate lines. Results are tabulated in Table 2.

Adding the non-LTE corrections for the abundances shown in Table 2, we obtain  $[\text{Na}/\text{Fe}] = -0.24$  dex,  $[\text{Al}/\text{Fe}] = +0.12$  dex and  $[\text{K}/\text{Fe}] = 0.20$  dex. For V, we get  $[\text{V}/\text{Fe}] = -0.02$  dex and we obtain  $[\text{Sc}/\text{Fe}] = +0.24$  dex for Sc (These are presented in Table 1).

Cayrel et al. (2004), have discussed the trend of these elements with respect to the metallicity. Na decreases significantly with decreasing metallicity with a scatter of  $\approx 0.2$  dex and K & Sc seem to decrease slowly with metallicity with a moderate scatter ( $\approx 0.12$  dex), where as Al remains constant with metallicity range of  $-4.0 < [\text{Fe}/\text{H}] < -2.5$  with a scatter of 0.2 dex. The abundances of these elements in LSE 202 are in agreement with the trends of the elemental abundances in EMP stars studied by Cayrel et al. (2004).

#### 4.5.5.4 $\alpha$ -elements

Among  $\alpha$ -peak elements, we have the lines of Mg, Ca, Si and also Ti, which usually follows the trend of  $\alpha$ -elements.

In the case of metal deficient stars, the  $\alpha$ -elements behave similar to O, but with a smaller (0.5 dex) enhancement. Most of these elements show identical similar ratios. Mg is produced in core Ne burning and shell C burning. Si and Ca are formed during incomplete Si and O burning and Ti during complete and incomplete Si burning.

In our spectra, Mg shows overabundance of +0.4 dex and  $[\text{Ca}/\text{Fe}]$  yields +0.28 dex. Ti line shows overabundance of 0.35 dex following the trend of other  $\alpha$ -elements. However, Si ( $[\text{Si}/\text{Fe}] = -0.13$ ) is deficient.

#### 4.5.5.5 Fe peak elements

For the study of Fe peak elements, we have lines of Cr, Mn, Fe, Co, Ni and Zn. Cr I lines at 4339 Å, fall in the wing of Balmer line profile and thus were not considered for abundance analysis as the equivalent width measurement of these lines could be

erroneous.

Generally in EMP stars, Cr and Mn are found to be more deficient than Fe by 0.5 dex or so. [Cr/Mn] ratio is close to solar value in most metal poor stars, though Mn is an odd-z element and Cr is an even-z element (Cayrel et al. 2004).

From our observations, we find that abundance of Fe peak elements vary. Sc and Zn show overabundance ( $[\text{Sc}/\text{Fe}] = +0.24$  and  $[\text{Zn}/\text{Fe}] = +0.30$ ). Considering hyperfine splitting for Mn and Co lines and then taking the mean abundances, we obtain  $[\text{Mn}/\text{Fe}] = -0.29$  dex and  $[\text{Co}/\text{Fe}] = +0.40$  dex. Ni and Cr remains with the metallicity of the star ( $[\text{Cr}/\text{Fe}]$  and  $[\text{Ni}/\text{Fe}]$  is  $+0.02$  and  $+0.01$  respectively).

Most of these Fe-peak element abundances agree with the element trends in EMP stars obtained by Cayrel et al. (2004), except for Sc and Cr which shows an overabundance of  $+0.2$  dex.

#### 4.5.5.6 Heavy elements

The heavy element (Sr, Y and Ba) abundances in LSE 202 generally show a deficiency with respect to Fe. ( $[\text{Sr}/\text{Fe}] = -0.26$ ,  $[\text{Y}/\text{Fe}] = -0.38$ ,  $[\text{Ba}/\text{Fe}] = -0.43$ , and  $[\text{La}/\text{Fe}] = -0.43$ ). Abundance of Nd obtained from lines at  $4069 \text{ \AA}$  and  $4109 \text{ \AA}$  shows that it remains with iron metallicity.

In Table 2, the abundances of elements in LSE 202 are compared with HD 122563 (r-process poor star) and BPS CS 22892-52 (r-process rich star). Sr II, Y II and Zr II are found to be more deficient than both the stars where as Ba II, La II and Nd II are having intermediate values between these two stars.

McWilliam et al. (1995) and Ryan et al. (1996) have noted large variations in  $[\text{Sr}/\text{Fe}]$ , for stars at the same  $[\text{Fe}/\text{H}]$ . In contrast,  $[\text{Ba}/\text{Fe}]$  shows a well defined enrichment history. Ryan et al. (1998) conclude that these two elements are produced by different mechanisms. The high Sr abundance could have been produced by low-metallicity high mass stars, which later did not contribute to the evolution of Sr in the galaxy. The stars with low Sr abundance might be exhibiting the normal value where as the origin of high Sr abundance in some stars could be attributed to a weak s-process present in them.

With reference to this, [Sr/Ba] ratio in our star is +0.2 dex. The ratio is less compared to the stars HD 122563 or BPS CS 22892-52 which is of the order of 1.1 dex and 0.4 dex respectively (Table 2). This might mean that the weak s-process which could be responsible for high Sr abundance as claimed by Ryan et al. (1998), may not be operating in this star.

#### 4.5.5.7 r-process elements

The abundances of r-process elements, Zr, Eu and Dy in LSE 202 are found to be [Zr/Fe] = 0.0, [Eu/Fe] = +0.14 and [Dy/Fe] = +0.25 dex.

For some heavy elements, where we were not able to detect the lines, we could only estimate the upper limits of their abundances. We chose the heavy elemental lines and the line information (excitation potential and log gf values) from Sneden et al. (2003). The estimation on upper limits of the abundances of elements are presented, assuming an equivalent width of 5 mÅ as the detectable limit.

The results are presented in Table 4.1 and 3. (Table 4.1 presents the abundance of heavy elements and compares it with HD 122563 (Westin et al. 2000) and BPS CS 22892-52 (Sneden et al. 2003). From this we find, [Ce/Fe] < -0.43 (from line at 4137.6 Å), [Pr/Fe] < +0.10 (line at 4222.9 Å), [Sm/Fe] < 0.03 (4318.9 Å), [Gd/Fe] < -0.70 (from 3768.4 Å), [Er/Fe] < -0.05 (3938.6 Å), [Ho/Fe] < -0.30 (3810.7 Å) and [Yb/Fe] < -1.61 dex (from line at 3694.2 Å).

But for some elements like Dy (4468 Å), Pb (4057.8 Å), Th (4019.1 Å) and U (3859.6 Å), the upper limits derived from the spectra are rather high, hence no meaningful information could be provided on the abundance of these elements.

From the comparison of heavy element abundances in these three stars, we can infer that LSE 202 is s-process poor star like HD 122563 and its enrichment history is not comparable to a r-process rich star like BPS CS 22892-52.

Though the [Ba/Fe] and [Eu/Fe] abundance ratios are quite different in all the three stars, the ratio [Eu/Ba] in all are similar (+0.57 for LSE 202, +0.57 for HD 122563 and +0.67 for BPS CS 22892-52). CS 22892-52, which has high Ba abundance compared to LSE 202 and HD 122563, but having the the same [Eu/Ba] ratio might

indicate that the higher value of Ba is due to r-process synthesis.

## 4.6 Discussion and Conclusions

We have analyzed a high resolution spectrum of a metal poor giant LSE 202.

The high radial velocity of the object ( $V_{\text{hel}} = -370 \text{ kms}^{-1}$ ) shows that it is a halo star. From the analysis, we find that the model with  $[\text{Fe}/\text{H}] = -2.41$ ,  $T_{\text{eff}} = 4750 \text{ K}$ ,  $\log g = 1.5$  and  $V_t = 1.9$  fits the data best.

The abundance pattern in LSE 202 is typical of a metal poor giant.

Among odd  $z$  elements Na shows little deficiency ( $[\text{Na}/\text{Fe}] = -0.24 \text{ dex}$ ) whereas, K and Sc are slightly overabundant (+0.2 dex).

Among  $\alpha$  elements, Mg, Ca and Ti show overabundance of +0.27 to +0.4 dex. But Si shows slight deficiency of -0.14 dex.

The abundance pattern of Fe peak elements are also found to be vary. Mn shows slight deficiency ( $[\text{Mn}/\text{Fe}] = -0.29 \text{ dex}$ ), Ni remains with metallicity of Fe ( $[\text{Ni}/\text{Fe}] = +0.01 \text{ dex}$ ) whereas, Co and Zn are overabundant by a factor of +0.40 and +0.30 dex respectively.

In heavy elements, Sr, Y, Ba and La show deficiency : ( $[\text{Sr}/\text{Fe}] = -0.26$ ,  $[\text{Y}/\text{Fe}] = -0.38$ ,  $[\text{Ba}/\text{Fe}] = -0.43$  and  $[\text{La}/\text{Fe}] = -0.43$ ). Also, it shows a slight overabundance of r-process elements ( $[\text{Eu}/\text{Fe}] = +0.14$  and  $[\text{Dy}/\text{Fe}] = +0.25$ ). But the heavy elements in the star are not as enriched as BPS CS 22892-0052 (Snedden et al. 2003).

The ratio  $[\text{Eu}/\text{Ba}] = +0.58$  shows that the heavy element abundance pattern in this metal poor star is of r-process origin, which is similar to that found in other metal poor stars (Mc William et al. 1995, Ryan et al. 1996).

Table 2: Data for spectral lines measured in the spectrum of LSE 202

$\lambda_{\text{lab}}$ (in $\text{\AA}$ )	LEP (eV)	log gf	EW ( $m\text{\AA}$ )	log $\epsilon$
Na I				
5889.97	0.00	0.110	194.6	4.04
5895.94	0.00	-0.190	172.4	4.11
Mg I				
3829.36	2.71	-0.046	191.5	5.32
4057.51	4.34	-0.999	46.4	5.65
4167.28	4.34	-0.946	50.3	5.65
4703.00	4.34	-0.377	86.8	5.63
5172.70	2.71	-0.381	207.3	5.48
5183.62	2.72	-0.158	237.1	5.47
5528.42	4.34	-0.341	84.8	5.46
8806.76	4.35	-0.137	137.5	5.74
Al I				
3944.01	0.00	-0.623	133.7	3.76
3961.52	0.01	-0.323	140.9	3.59
Si I				
3905.52	1.91	-0.980	156.9	5.02
4102.94	1.91	-2.714	74.0	4.97
K I				
7698.98	0.00	-0.169	59.3	3.25
Ca I				
4289.37	1.88	-0.388	54.4	4.17
4425.44	1.88	-0.358	59.6	4.22
4434.97	1.89	-0.007	71.6	4.11
4435.69	1.89	-0.517	52.2	4.25
4455.89	1.90	-0.519	50.6	4.23
5188.85	2.93	-0.115	20.1	4.32
5261.71	2.52	-0.579	15.8	4.18
5265.56	2.52	-0.113	36.8	4.21



Table 2: continued :

$\lambda_{\text{lab}}$ (in $\text{\AA}$ )	LEP (eV)	log gf	EW ( $m\text{\AA}$ )	log $\epsilon$
Ca I				
5349.47	2.71	-0.310	17.1	4.16
5581.98	2.52	-0.555	22.8	4.33
5588.76	2.52	0.358	63.6	4.17
5590.13	2.52	-0.571	20.0	4.27
5594.47	2.52	0.097	48.7	4.18
5598.49	2.52	-0.087	37.4	4.17
5601.29	2.52	-0.523	20.6	4.24
5857.46	2.93	0.240	34.8	4.25
6102.73	1.88	-0.793	48.8	4.28
6122.23	1.89	-0.316	73.7	4.22
6162.18	1.90	-0.090	87.6	4.25
6169.56	2.52	-0.478	23.6	4.24
6439.08	2.52	0.390	72.9	4.23
6449.81	2.52	-0.502	23.7	4.25
6493.79	2.52	-0.109	39.5	4.17
6717.69	2.71	-0.524	14.8	4.23
7148.15	2.71	0.137	52.8	4.33
Ca II				
8542.09	1.70	-0.463	871.8	4.17
8662.14	1.69	-0.723	736.8	4.24
Sc II				
4246.82	0.32	0.020	122.2	0.86
4294.77	0.61	-1.634	37.3	1.05
4314.08	0.62	-0.340	95.8	0.93
4320.73	0.61	-0.474	87.6	0.86
4325.00	0.60	-0.618	82.3	0.87
4400.39	0.61	-0.780	75.7	0.88
4415.56	0.60	-0.890	72.1	0.89

Table 2: continued :

$\lambda_{\text{lab}}$ (in $\text{\AA}$ )	LEP (eV)	log gf	EW ( $m\text{\AA}$ )	log $\epsilon$
Sc II				
4670.41	1.36	-0.819	31.8	0.97
5031.02	1.36	-0.576	44.1	0.91
5239.81	1.46	-0.942	21.8	0.93
5526.79	1.77	-0.219	38.2	0.89
5657.90	1.51	-0.825	31.6	1.05
Ti I				
3904.78	0.90	0.284	35.9	2.62
3924.53	0.02	-0.881	45.2	2.91
4008.93	0.02	-1.016	34.5	2.82
4300.55	0.83	0.122	47.0	2.82
4512.73	0.84	-0.424	29.0	3.00
4518.02	0.83	-0.269	31.2	2.88
4522.80	0.82	-0.334	40.1	3.10
4533.24	0.85	0.532	65.9	2.75
4534.78	0.84	0.336	55.0	2.72
4535.57	0.83	0.162	47.8	2.75
4535.92	0.82	-0.035	52.2	3.02
4544.69	0.82	-0.464	26.1	2.95
4548.76	0.83	-0.298	29.9	2.87
4552.45	0.84	-0.284	44.6	3.15
4555.49	0.85	-0.432	20.5	2.81
4656.47	0.00	-1.289	33.3	2.93
4667.59	0.02	-1.138	44.2	3.00
4681.91	0.05	-1.015	46.9	2.96
4840.87	0.90	-0.453	21.5	2.89
4981.73	0.85	0.560	72.0	2.75
4991.07	0.84	0.436	70.3	2.82
4999.50	0.83	0.306	64.1	2.82

Table 2: continued :

$\lambda_{\text{lab}}$ (in Å)	LEP (eV)	log gf	EW ( $m\text{Å}$ )	log $\epsilon$
Ti I				
5007.21	0.82	0.168	66.7	2.99
5022.87	0.83	-0.378	25.5	2.80
5024.84	0.82	-0.546	25.1	2.95
5035.90	1.46	0.243	28.0	2.98
5038.40	1.43	0.069	16.9	2.84
5039.96	0.02	-1.074	45.7	2.91
5064.65	0.05	-0.935	48.9	2.86
5173.74	0.00	-1.062	48.1	2.90
5192.97	0.02	-0.950	47.5	2.80
5210.39	0.05	-0.828	56.8	2.87
8434.96	0.85	-0.886	19.0	2.92
Ti II				
3900.56	1.13	-0.450	135.8	3.20
3913.48	1.12	-0.530	123.5	3.01
4025.12	0.61	-1.980	89.9	2.95
4028.36	1.89	-1.000	64.0	2.92
4056.19	0.61	-3.300	29.2	2.99
4184.30	1.08	-2.510	48.5	3.11
4287.88	1.08	-2.020	75.9	3.12
4290.22	1.17	-1.120	101.0	2.92
4300.05	1.18	-0.490	121.2	2.78
4316.80	2.05	-1.420	27.5	2.74
4320.96	1.17	-1.870	71.6	2.98
4330.69	1.18	-2.060	58.8	2.93
4337.88	1.08	-1.130	107.2	2.95
4344.30	1.08	-2.090	71.1	3.08
4350.85	2.06	-1.400	25.3	2.68
4394.05	1.22	-1.770	69.9	2.90

Table 2: continued :

$\lambda_{\text{lab}}$ (in $\text{\AA}$ )	LEP (eV)	log gf	EW ( $m\text{\AA}$ )	log $\epsilon$
Ti II				
4395.03	1.08	-0.510	135.1	2.93
4395.85	1.24	-1.970	55.9	2.85
4398.27	1.22	-2.780	25.1	3.05
4399.79	1.24	-1.270	96.0	2.99
4409.22	1.24	-2.250	32.1	2.69
4409.52	1.23	-2.570	35.7	3.07
4417.72	1.17	-1.430	97.9	3.10
4418.33	1.24	-1.990	62.6	2.98
4421.95	2.06	-1.770	26.7	3.07
4443.79	1.08	-0.700	121.8	2.81
4444.56	1.12	-2.210	59.6	2.99
4450.48	1.08	-1.510	96.6	3.04
4468.51	1.13	-0.600	132.0	2.97
4470.84	1.17	-2.280	58.6	3.10
4493.51	1.08	-2.830	27.0	2.96
4501.27	1.12	-0.760	122.7	2.91
4533.97	1.24	-0.770	117.6	2.94
4544.02	1.24	-2.400	32.5	2.83
4549.81	1.18	-2.330	54.1	3.08
4657.21	1.24	-2.320	49.8	3.05
4708.66	1.24	-2.370	42.8	2.96
4762.78	1.08	-2.710	24.9	2.76
4798.52	1.08	-2.670	46.0	3.12
4865.62	1.12	-2.610	37.8	2.94
5013.68	1.58	-1.990	32.8	2.77
5129.16	1.89	-1.390	56.1	2.94
5154.06	1.57	-1.920	55.5	3.06
5185.90	1.89	-1.350	51.3	2.81

Table 2: continued :

$\lambda_{\text{lab}}$ (in $\text{\AA}$ )	LEP (eV)	log gf	EW ( $m\text{\AA}$ )	log $\epsilon$
Ti II				
5188.69	1.58	-1.210	82.1	2.84
5226.53	1.57	-1.300	78.4	2.83
5262.14	1.58	-2.106	51.7	3.19
5336.77	1.58	-1.630	62.7	2.89
5381.02	1.57	-1.970	57.6	3.12
5418.75	1.58	-2.110	42.4	3.02
V I				
4379.23	0.30	0.580	40.2	1.59
V II				
4005.71	1.82	-0.460	30.4	1.52
Cr I				
4274.81	0.00	-0.231	121.1	3.08
4289.73	0.00	-0.361	115.6	3.08
4337.57	0.97	-1.112	30.1	3.08
4344.51	1.00	-0.550	55.1	3.04
4351.06	0.97	-1.449	18.5	3.13
4496.85	0.94	-1.150	38.7	3.24
4545.95	0.94	-1.370	29.0	3.25
4646.15	1.03	-0.700	48.5	3.05
4651.29	0.98	-1.460	20.6	3.18
4652.16	1.00	-1.030	35.8	3.11
5206.02	0.94	0.019	93.1	3.00
5208.42	0.94	0.158	97.9	2.97
5247.58	0.96	-1.640	17.9	3.20
5264.16	0.97	-1.290	45.9	3.43
5265.73	0.97	-1.750	22.4	3.43
5296.69	0.98	-1.400	25.5	3.17
5298.29	0.98	-1.150	36.0	3.13

Table 2: continued :

$\lambda_{\text{lab}}$ (in $\text{\AA}$ )	LEP (eV)	log gf	EW ( $m\text{\AA}$ )	log $\epsilon$
Cr I				
5345.77	1.00	-0.980	45.0	3.15
5348.30	1.00	-1.290	34.9	3.27
5409.78	1.03	-0.720	60.6	3.18
Cr II				
4558.66	4.07	-0.660	23.3	3.32
4848.24	3.86	-1.140	19.0	3.42
Mn I				
4030.76	0.00	-0.470	130.1	2.90
4034.49	0.00	-0.811	113.0	2.88
4055.55	2.14	-0.070	28.0	2.69
4783.43	2.30	0.042	27.3	2.65
4823.53	2.32	0.144	38.6	2.79
Fe I				
3787.88	1.01	-0.859	155.6	5.15
3789.18	2.73	-1.270	40.3	5.10
3799.55	0.96	-0.846	153.3	5.05
3825.88	0.91	-0.037	301.2	5.06
3827.82	1.56	0.062	151.8	4.78
3834.22	0.96	-0.302	230.8	5.08
3840.44	0.99	-0.506	182.2	5.00
3841.05	1.61	-0.050	161.5	5.05
3849.96	1.01	-0.871	135.3	4.86
3850.82	0.99	-1.734	99.1	4.93
3865.52	1.01	-0.982	139.2	5.03
3872.50	0.99	-0.928	155.3	5.16
3878.02	0.96	-0.914	174.0	5.29
3887.05	0.91	-1.144	157.8	5.31
3895.66	0.11	-1.670	219.7	5.41

Table 2: continued :

$\lambda_{\text{lab}}$ (in $\text{\AA}$ )	LEP (eV)	log gf	EW ( $m\text{\AA}$ )	log $\epsilon$
Fe I				
3899.71	0.09	-1.531	171.9	4.89
3906.48	0.11	-2.243	130.6	5.07
3920.26	0.12	-1.746	147.1	4.84
3922.91	0.05	-1.651	164.7	4.88
3927.92	0.11	-1.590	197.4	5.17
3977.74	2.20	-1.080	73.5	4.96
3995.98	2.73	-1.450	35.5	5.13
3998.05	2.69	-0.840	69.7	5.20
4001.66	2.18	-1.880	42.9	5.06
4005.24	1.56	-0.610	122.1	4.91
4032.63	1.48	-2.440	62.8	5.20
4044.61	2.83	-1.080	42.6	5.01
4063.28	3.37	-0.804	27.6	5.04
4064.45	1.56	-3.282	23.3	5.30
4067.27	2.56	-1.419	53.0	5.24
4070.77	3.24	-0.790	37.5	5.09
4071.74	1.61	-0.022	165.6	4.98
4074.79	3.05	-0.970	33.4	4.96
4084.49	3.33	-0.590	51.0	5.26
4085.00	2.85	-1.280	47.5	5.32
4095.97	2.59	-1.400	50.0	5.18
4098.18	3.24	-0.920	30.4	5.07
4100.74	0.86	-3.179	71.9	5.37
4114.45	2.83	-1.220	37.2	5.03
4120.21	2.99	-1.170	32.1	5.06
4126.18	3.33	-0.960	25.2	5.09
4132.06	1.61	-0.650	136.8	5.22
4134.68	2.83	-0.490	66.4	4.89

Table 2: continued :

$\lambda_{\text{lab}}$ (in $\text{\AA}$ )	LEP (eV)	log gf	EW ( $m\text{\AA}$ )	log $\epsilon$
Fe I				
4137.00	3.41	-0.540	36.6	5.01
4139.93	0.99	-3.629	33.2	5.17
4143.41	3.05	-0.204	69.2	4.92
4143.87	1.56	-0.450	137.5	4.96
4147.67	1.48	-2.104	71.0	5.01
4149.37	3.33	-0.920	36.3	5.29
4150.25	3.43	-1.260	21.7	5.41
4153.90	3.40	-0.270	56.0	5.11
4154.50	2.83	-0.688	58.9	4.92
4154.80	3.37	-0.370	50.6	5.06
4156.80	2.83	-0.620	65.7	5.00
4157.78	3.42	-0.403	46.2	5.07
4158.79	3.43	-0.670	27.9	4.97
4173.92	0.99	-3.380	55.1	5.34
4174.91	0.91	-2.969	74.3	5.25
4175.64	2.85	-0.670	59.0	4.92
4181.75	2.83	-0.180	81.1	4.91
4182.38	3.02	-1.190	30.6	5.07
4187.04	2.45	-0.548	91.7	5.10
4187.79	2.43	-0.554	100.9	5.30
4195.33	3.33	-0.492	43.5	5.00
4196.21	3.40	-0.740	25.6	4.95
4199.09	3.05	0.250	87.0	4.87
4199.98	0.09	-4.750	32.2	5.18
4202.03	1.48	-0.708	127.2	4.93
4213.65	2.85	-1.290	45.4	5.25
4219.36	3.57	0.120	60.8	5.01
4220.34	3.07	-1.290	22.2	5.03



Table 2: continued :

$\lambda_{\text{lab}}$ (in $\text{\AA}$ )	LEP (eV)	log gf	EW ( $m\text{\AA}$ )	log $\epsilon$
Fe I				
4222.21	2.45	-0.967	74.4	5.07
4224.17	3.37	-0.410	38.9	4.86
4225.45	3.42	-0.500	49.0	5.21
4232.73	0.11	-4.928	25.0	5.22
4233.60	2.48	-0.604	91.1	5.16
4238.81	3.40	-0.280	45.9	4.90
4250.79	1.56	-0.710	125.2	4.96
4260.47	2.40	-0.020	115.9	5.05
4266.96	2.73	-1.680	30.7	5.21
4282.40	2.18	-0.810	100.9	5.23
4352.73	2.22	-1.260	80.7	5.21
4367.90	1.61	-2.650	45.4	5.12
4375.93	0.00	-3.031	119.5	5.24
4389.24	0.05	-4.583	52.7	5.32
4404.75	1.56	-0.142	171.1	4.99
4415.12	1.61	-0.615	131.2	4.96
4430.61	2.22	-1.659	61.3	5.16
4435.15	0.09	-4.379	66.7	5.41
4443.19	2.86	-1.020	42.3	4.90
4447.72	2.22	-1.342	82.1	5.29
4454.38	2.83	-1.250	36.7	4.99
4461.65	0.09	-3.210	113.2	5.35
4489.74	0.12	-3.966	80.5	5.33
4494.56	2.20	-1.136	84.8	5.11
4528.61	2.18	-0.822	106.9	5.29
4531.15	1.48	-2.155	84.5	5.25
4647.43	2.95	-1.310	32.7	5.09
4667.45	3.60	-0.751	17.3	4.91

Table 2: continued :

$\lambda_{\text{lab}}$ (in $\text{\AA}$ )	LEP (eV)	log gf	EW ( $m\text{\AA}$ )	log $\epsilon$
Fe I				
4678.85	3.60	-0.660	21.9	4.95
4707.27	3.24	-1.080	31.4	5.16
4710.28	3.02	-1.612	24.4	5.28
4727.39	3.69	-1.162	12.3	5.24
4733.59	1.49	-2.988	47.2	5.28
4736.77	3.21	-0.740	52.1	5.18
4741.53	2.83	-2.000	16.5	5.23
4786.81	3.02	-1.590	16.3	5.03
4789.65	3.55	-0.910	19.9	5.07
4859.74	2.88	-0.850	59.0	5.01
4871.32	2.87	-0.410	88.7	5.16
4872.14	2.88	-0.600	76.8	5.11
4890.75	2.88	-0.430	84.2	5.09
4891.49	2.85	-0.140	92.5	4.96
4903.31	2.88	-1.080	61.3	5.28
4918.99	2.87	-0.370	86.4	5.06
4920.50	2.83	0.060	105.9	5.02
4924.77	2.28	-2.220	35.2	5.22
4938.81	2.88	-1.077	58.4	5.20
4939.69	0.86	-3.340	72.2	5.31
4946.38	3.37	-1.170	30.1	5.35
4957.30	2.85	-0.408	86.8	5.08
4957.60	2.81	0.233	121.1	5.13
4966.09	3.33	-0.890	36.9	5.16
4982.52	4.10	0.144	31.5	4.92
4983.86	4.10	-0.068	25.1	4.99
4985.55	2.87	-1.332	41.3	5.13
4994.13	0.91	-3.080	78.9	5.24

Table 2: continued :

$\lambda_{\text{lab}}$ (in $\text{\AA}$ )	LEP (eV)	log gf	EW ( $m\text{\AA}$ )	log $\epsilon$
Fe I				
5001.86	3.88	0.010	40.3	4.97
5005.71	3.88	-0.180	34.9	5.06
5006.12	2.83	-0.638	77.1	5.07
5012.07	0.86	-2.642	103.1	5.28
5014.94	3.94	-0.250	23.6	4.95
5022.24	3.98	-0.530	18.5	5.14
5041.07	0.96	-3.087	67.2	5.06
5049.82	2.28	-1.420	77.5	5.19
5051.63	0.91	-2.795	96.5	5.33
5068.77	2.94	-1.230	45.4	5.18
5074.75	4.22	-0.200	22.3	5.19
5083.34	0.96	-2.958	88.0	5.35
5098.70	2.18	-2.026	57.2	5.28
5123.72	1.01	-3.068	77.0	5.28
5125.11	4.22	-0.140	22.2	5.12
5127.36	0.91	-3.307	71.3	5.29
5131.47	2.22	-2.560	26.4	5.29
5133.69	4.18	0.140	41.9	5.20
5137.38	4.18	-0.400	23.7	5.36
5139.25	3.00	-0.741	55.9	4.94
5139.46	2.94	-0.509	78.4	5.07
5141.74	2.42	-2.150	26.8	5.13
5142.93	0.96	-3.080	78.9	5.26
5150.84	0.99	-3.070	74.6	5.20
5151.91	1.01	-3.322	66.5	5.32
5162.27	4.18	0.020	33.4	5.16
5166.28	0.00	-4.195	86.7	5.37
5167.49	1.48	-1.260	130.6	5.20

Table 2: continued :

$\lambda_{\text{lab}}$ (in $\text{\AA}$ )	LEP (eV)	log gf	EW ( $m\text{\AA}$ )	log $\epsilon$
Fe I				
5171.60	1.48	-1.793	111.6	5.34
5191.45	3.04	-0.551	67.5	5.00
5192.34	3.00	-0.421	72.8	4.93
5194.94	1.56	-2.090	89.3	5.22
5198.71	2.22	-2.135	45.8	5.23
5202.34	2.18	-1.838	67.4	5.26
5208.59	3.24	-0.980	40.0	5.18
5215.18	3.27	-0.871	33.3	4.97
5216.27	1.61	-2.150	80.3	5.13
5225.53	0.11	-4.789	45.1	5.32
5232.94	2.94	-0.190	97.0	5.14
5247.05	0.09	-4.946	40.7	5.37
5250.64	2.20	-2.050	50.3	5.19
5263.30	3.27	-0.970	34.4	5.09
5266.55	3.00	-0.490	78.7	5.11
5269.54	0.86	-1.321	160.7	4.99
5273.16	3.29	-0.993	33.1	5.12
5273.37	2.48	-2.180	31.6	5.32
5281.79	3.04	-1.020	50.0	5.15
5283.62	3.24	-0.630	60.4	5.19
5302.30	3.28	-0.880	42.6	5.17
5307.36	1.61	-2.987	37.8	5.20
5324.18	3.21	-0.240	76.4	5.06
5328.04	0.91	-1.466	153.8	5.08
5328.53	1.56	-1.850	100.8	5.19
5332.90	1.56	-2.940	47.6	5.25
5339.93	3.27	-0.680	48.9	5.06
5364.87	4.45	0.220	27.1	5.12

Table 2: continued :

$\lambda_{\text{lab}}$ (in $\text{\AA}$ )	LEP (eV)	log gf	EW ( $m\text{\AA}$ )	log $\epsilon$
Fe I				
5367.47	4.42	0.350	28.5	4.98
5369.96	4.37	0.350	36.1	5.09
5371.49	0.96	-1.645	145.3	5.17
5383.37	4.31	0.500	44.7	5.03
5393.17	3.24	-0.910	47.6	5.23
5397.13	0.91	-1.993	134.3	5.26
5405.77	0.99	-1.844	135.7	5.23
5410.91	4.47	0.280	24.6	5.03
5415.20	4.39	0.500	42.1	5.07
5424.07	4.32	0.520	47.4	5.06
5429.70	0.96	-1.879	139.0	5.28
5434.52	1.01	-2.122	120.6	5.22
5455.61	1.01	-2.091	127.9	5.33
5497.52	1.01	-2.849	93.8	5.35
5501.46	0.96	-2.950	88.9	5.28
5506.78	0.99	-2.797	91.0	5.21
5569.62	3.42	-0.540	45.8	5.02
5572.84	3.40	-0.310	59.1	5.00
5576.09	3.43	-1.000	26.9	5.13
5586.76	3.37	-0.210	69.1	5.04
5615.64	3.33	-0.140	80.0	5.13
5624.54	3.42	-0.900	35.0	5.18
6065.48	2.61	-1.530	54.8	5.16
6136.61	2.45	-1.400	70.7	5.11
6137.69	2.59	-1.403	62.1	5.12
6191.56	2.43	-1.600	68.4	5.24
6213.43	2.22	-2.660	29.1	5.36
6219.28	2.20	-2.433	37.2	5.25

Table 2: continued

$\lambda_{\text{lab}}$ (in $\text{\AA}$ )	LEP (eV)	log gf	EW ( $m\text{\AA}$ )	log $\epsilon$
Fe I				
6230.73	2.56	-1.281	74.2	5.17
6246.32	3.60	-0.960	22.2	5.14
6252.55	2.40	-1.687	60.4	5.14
6335.34	2.20	-2.230	44.2	5.17
6336.84	3.69	-1.050	21.4	5.30
6393.60	2.43	-1.620	69.6	5.26
6400.00	3.60	-0.520	46.5	5.17
6408.02	3.69	-1.018	15.3	5.09
6411.65	3.65	-0.820	29.7	5.22
6421.35	2.28	-2.027	49.8	5.14
6494.98	2.40	-1.273	85.3	5.15
6593.88	2.43	-2.422	28.5	5.33
6663.45	2.42	-2.479	20.4	5.19
6750.15	2.42	-2.621	15.0	5.16
7445.75	4.26	-0.237	22.0	5.11
7495.06	4.22	-0.102	27.9	5.07
7511.02	4.18	0.099	40.0	5.05
8387.77	2.18	-1.493	102.1	5.19
8824.22	2.20	-1.540	101.2	5.19
Fe II				
4178.86	2.58	-2.480	62.3	5.08
4233.17	2.58	-2.000	81.6	5.02
4385.38	2.78	-2.570	53.7	5.18
4416.82	2.78	-2.600	39.5	4.93
4489.19	2.83	-2.970	29.4	5.14
4491.40	2.86	-2.700	32.2	4.97
4508.28	2.86	-2.210	63.0	5.07
4535.34	2.84	-2.480	49.7	5.06

Table 2: continued :

$\lambda_{\text{lab}}$ (in $\text{\AA}$ )	LEP (eV)	log gf	EW ( $m\text{\AA}$ )	log $\epsilon$
Fe II				
4522.63	2.84	-2.030	70.0	5.01
4534.17	2.86	-3.470	15.3	5.30
4549.47	2.83	-1.750	79.2	4.90
4555.89	2.83	-2.290	59.2	5.03
4666.75	2.83	-3.330	16.8	5.16
4923.93	2.89	-1.320	105.8	5.06
5018.45	2.89	-1.220	114.3	5.13
5197.56	3.23	-2.100	40.4	4.89
5234.62	3.22	-2.050	46.7	4.94
5276.00	3.20	-1.940	56.8	4.98
5316.62	3.15	-1.850	69.5	5.06
5534.83	3.24	-2.930	21.6	5.31
Co I				
3842.05	0.92	-0.770	62.7	2.78
3861.16	1.05	-0.890	58.3	2.94
3997.90	1.05	-0.870	60.7	2.93
4066.37	0.92	-1.660	40.8	3.14
4110.53	1.05	-1.080	42.1	2.73
4118.77	1.05	-0.490	70.4	2.72
4121.32	0.92	-0.320	99.3	3.15
4190.70	0.00	-3.036	23.1	3.01
Ni I				
3775.57	0.42	-1.350	98.4	3.62
3783.53	0.42	-1.310	103.9	3.72
3793.61	0.27	-2.700	57.5	3.68
3807.14	0.42	-1.180	107.3	3.66
3831.69	0.42	-2.000	92.2	4.06
4331.65	1.68	-2.100	17.8	3.77

Table 2: continued :

$\lambda_{\text{lab}}$ (in Å)	LEP (eV)	log gf	EW ( $m\text{Å}$ )	log $\epsilon$
Ni I				
4401.54	3.19	0.080	34.9	3.77
4648.66	3.42	-0.160	17.8	3.83
4714.42	3.38	0.230	35.2	3.80
4786.54	3.42	-0.170	19.3	3.87
4855.41	3.54	0.000	19.7	3.85
4866.26	3.54	-0.210	15.2	3.91
4904.41	3.54	-0.170	18.2	3.97
4980.17	3.61	-0.110	16.7	3.93
5017.58	3.54	-0.080	15.6	3.79
5035.37	3.64	0.290	23.5	3.75
5080.53	3.66	0.130	25.5	3.98
5081.11	3.85	0.300	20.1	3.89
5084.08	3.68	0.030	16.2	3.85
5137.08	1.68	-1.990	33.2	3.92
5476.91	1.83	-0.890	84.2	3.89
6643.64	1.68	-2.300	25.2	3.94
6767.77	1.83	-2.170	21.9	3.90
7122.24	3.54	0.040	25.9	3.81
Zn I				
4722.16	4.03	-0.390	24.1	2.50
4810.54	4.08	-0.170	29.3	2.45
Sr II				
4077.72	0.00	0.150	154.8	0.15
4215.54	0.00	-0.160	146.4	0.28
Y II				
4374.95	0.41	0.155	66.7	-0.57
4398.01	0.13	-0.998	24.1	-0.61
4883.69	1.08	-0.041	22.9	-0.52



Table 2: continued :

$\lambda_{\text{lab}}$ (in $\text{\AA}$ )	LEP (eV)	log gf	EW ( $m\text{\AA}$ )	log $\epsilon$
Y II				
4900.11	1.03	-0.090	19.2	-0.63
5087.42	1.08	-0.165	16.7	-0.59
5205.73	1.03	-0.342	16.4	-0.49
Zr II				
4149.22	0.80	-0.030	43.3	0.14
4208.98	0.71	-0.460	31.9	0.22
Ba II				
5853.67	0.60	-1.016	26.8	-0.70
6141.71	0.70	-0.069	71.4	-0.76
La II				
4086.71	0.00	0.163	18.9	-1.74
4333.76	0.17	0.333	27.0	-1.54
Nd II				
4069.26	0.06	-0.423	13.7	-0.72
4109.46	0.31	0.320	21.8	-0.92
Eu II				
4205.05	0.00	0.117	27.8	-1.74
4129.72	0.00	0.204	28.4	-1.80
Dy II				
4077.96	0.10	0.010	25.0	-1.07

Table 3: Estimation of upper limit for elemental abundances for Li and some of the heavy elements in LSE 202 considering 5 mÅ equivalent width as the detectable limit of weak lines in our spectrum of LSE 202

$\lambda_{\text{lab}}$ (in Å)	LEP (eV)	log gf	EW (mÅ)	log $\epsilon$
Li I				
6707.76	0.00	0.167	< 5.0	< 0.33
Ce II				
3942.15	0.00	-0.220	< 5.0	< -1.23
4137.65	0.52	0.440	< 5.0	< -1.30
Pr II				
4222.93	0.06	0.018	< 5.0	< -1.62
4408.82	0.00	-0.278	< 5.0	< -1.42
Sm II				
4318.94	0.28	-0.270	< 5.0	< -1.39
4420.53	0.33	-0.380	< 5.0	< -1.24
Gd II				
3768.40	0.08	0.360	< 5.0	< -2.00
3796.39	0.03	0.140	< 5.0	< -1.84
Tb II				
3702.85	0.13	0.440	< 5.0	< -1.93
Ho II				
3810.74	0.00	0.190	< 5.0	< -2.23
4045.47	0.00	-0.050	< 5.0	< -2.04
Er II				
3938.63	0.00	-0.520	< 5.0	< -1.55
Yb II				
3694.19	0.00	-0.300	< 5.0	< -2.95

# Chapter 5

## High resolution spectroscopy of metal poor halo giants :

### CS 29516-0041, CS 29516-0024 and CS 29522-0046

#### 5.1 Abstract

We report the detailed abundance analysis of extreme metal-poor (EMP) stars BPS CS 29516-0041, BPS CS 29516-0024 and BPS CS 29522-0046.

Our analysis of the object BPS CS 29516-0041 (BPS CS 29502 - 042) reveals the atmospheric parameters of the star to be  $T_{\text{eff}} = 5000 \pm 250$  K,  $\log g = 2.5 \pm 0.5$  dex,  $[\text{Fe}/\text{H}] = -3.0$  and  $V_t = 1.6 \text{ kms}^{-1}$ . Li abundance is less than 0.71 dex, which is underabundant compared to the lithium abundance in dwarfs (2.30 dex) of the same metallicity. Among odd-z elements, Na shows deficiency of more than 1.0 dex ( $[\text{Na}/\text{Fe}] = -1.16$ ) while K shows slight overabundance ( $[\text{K}/\text{Fe}] = +0.18$ ).  $\alpha$  process elements, Mg, Ca & Ti are nearly solar or slightly overabundant ( $[\text{Mg}/\text{Fe}] = -0.04$ ,  $[\text{Ca}/\text{Fe}] = +0.12$  and  $[\text{Ti}/\text{Fe}] = +0.08$ ). Cr and Ni go with the metallicity of the

star ( $[\text{Cr}/\text{Fe}] = -0.08$  and  $[\text{Ni}/\text{Fe}] = -0.07$ ). Ba is deficient by a factor of 0.28 dex ( $[\text{Ba}/\text{Fe}] = -0.28$ ), which is in accordance with the observations of other metal poor stars.

Analysis of the object BPS CS 29516-0024 yields,  $T_{\text{eff}} = 4750 \pm 250$  K,  $\log g = 1.0 \pm 0.5$  dex,  $[\text{Fe}/\text{H}] = -2.72$  and  $V_t = 1.7$  kms $^{-1}$ . Abundance of Li is 0.97 dex, which indicates the depletion of Li. Among odd- $z$  elements, Na is deficient compared to Fe ( $[\text{Na}/\text{Fe}] = -0.38$ ) and Sc goes with Fe metallicity ( $[\text{Sc}/\text{Fe}] = -0.04$ ).  $\alpha$  process elements, Mg, Ca and Ti show overabundances of 0.66 dex, 0.45 dex and 0.23 dex. In Fe-peak elements, Cr is underabundant by a factor of -0.32 dex whereas Ni is of iron metallicity ( $[\text{Ni}/\text{Fe}] = +0.07$ ). Heavy elements show deficiency ( $[\text{Y}/\text{Fe}] = -0.44$  and  $[\text{Ba}/\text{Fe}] = -1.04$ ).

For BPS CS 29522-0046, we obtain the atmospheric parameters to be :

$T_{\text{eff}} = 5500 \pm 250$  K,  $\log g = 3.0 \pm 0.5$  dex,  $[\text{Fe}/\text{H}] = -2.32$  and  $V_t = 1.1$  kms $^{-1}$ . Li yields an abundance of 1.89 which is slightly less compared to the Li abundance in metal poor dwarfs (2.1 dex). Na shows underabundance ( $[\text{Na}/\text{Fe}] = -0.28$ ), whereas Sc is overabundant by a factor of +0.18 dex. All  $\alpha$ -elements are enhanced ( $[\text{Mg}/\text{Fe}] = +0.55$ ,  $[\text{Ca}/\text{Fe}] = +0.45$  and  $[\text{Ti}/\text{Fe}] = +0.20$ ). Cr, the Fe-peak element is found to be slightly underabundant ( $[\text{Cr}/\text{Fe}] = -0.11$ ). The Ba abundance is found to be  $[\text{Ba}/\text{Fe}] = -0.14$ .

The elemental abundances in these stars are in accordance with the observational studies of other metal poor stars (McWilliam et al. (1995), Ryan et al. (1996), Cayrel et al. (2004), Honda et al. (2004) and Cohen et al. (2004) ).

## 5.2 Introduction

Study of chemical composition of extreme metal poor stars provides an opportunity to understand the yields of single first generation supernovae, which are presumed to have formed from primordial elements. ("Population III"). Detailed elemental abundance analysis of the stars can reveal general trends and also local deviations in element pattern of that particular star. To address the issue of heavy element yields

of SNe II, mass functions of these stars and mixing processes in the ISM, knowledge of chemical composition of large number of low metallicity stars are required.

Theoretical models speculate that the Big Bang cosmology would yield very little (if any) of elements heavier than boron. Thus, all the heavy elements were synthesized in first stellar generations (“Population III”) which are formed from collapse of gas clouds. In order to observe the products of Big Bang nucleosynthesis and to understand the star formation history of our galaxy, we need to look at the oldest and least metal enriched objects known. These candidates are not the high redshift objects, instead the most metal poor stars of the galactic halo. Thus the study of chemical abundance structure of the galactic halo provides vital clues on first heavy element producing objects and galaxy formation.

The HK objective-prism/interference-filter survey, started since 1978 (Beers, Preston & Shectman, 1985, 1992) has identified quite many extreme metal poor stars (star with metallicity below  $-2.5$  dex). Since then, there have been subsequent photometric and spectroscopic follow up of these candidate stars from high resolution echelle data (McWilliam et al. 1995, Ryan et al. 1996, Honda et al. 2004, Cohen et al. 2004). These groups have carried out the systematic survey of elemental abundances in the case of EMP stars.

In order to study the abundance pattern of the EMP stars in more detail, we chose 3 objects (BPS CS 29516-0041, BPS CS 29516-0024 and BPS CS 29502-0042) from HK prism survey (Norris et al. 1999, Bonifacio et al. 2000). Chemical composition of these stars are presented in this chapter.

BPS CS 29516-0041 ( RA :  $22^h 21^m 48.6^s$  and DEC =  $2^{\circ} 28' 27.80''$  (2000) ), which is a high galactic ( $l = 66^{\circ}.3$  and  $b = -43^{\circ}$ ) metal poor star was discovered in this HK objective-prism/interference-filter survey. The UBV photometric follow up has been carried out first by Norris et al. (1999). They obtain  $V = 12.73$ ,  $(B - V) = 0.66$  and  $(U - B) = -0.04$  for the star. Bonifacio et al. (2000) have done the UBV photometry and medium resolution spectroscopy of the star. Their observation yields  $V = 12.78$ ,  $(B - V) = 0.60$  and  $(U - B) = -0.03$  for the object. They estimate the metallicity of the star to be  $-2.45$  and suggest the luminosity class to be that of a supergiant.

BPS CS 29516-0024 ( $\alpha = 22^h26^m15.1^s$  and  $\delta = +02^{\circ}51'50''$  (2000) ) is also a high galactic latitude star ( $l = 67^{\circ}.77$  and  $b = -43^{\circ}.92$ ). Bonifacio et al. (2000) obtain  $V = 13.57$ ,  $(B - V) = 0.86$  and  $(U - B) = 0.20$  for the object. They quote  $[Fe/H]$  value of  $-2.86$  for the star and classify it under giants.

UBV photometry of the star BPS CS 29522-0046 ( $\alpha = 23^h44^m59.6^s$ ,  $\delta = +08^{\circ}46'54''$  (2000) and  $l = 96^{\circ}.47$  and  $b = -50^{\circ}.65$  ) has been carried out by Norris et al. (1999) and Bonifacio et al. (2000). Norris et al. (1999) get  $V = 12.85$ ,  $(B - V) = 0.57$  and  $(U - B) = -0.10$  for the object. The values,  $V = 12.74$ ,  $(B - V) = 0.49$  and  $(U - B) = -0.13$  were obtained by Bonifacio et al. (2000). From the medium resolution spectroscopy of the star, they classify it as a turnoff star and the metallicity is estimated to be  $-3.24$ .

In order to derive the chemical composition and understand the heavy element pattern in these metal poor stars, we carried out the analysis of their high resolution spectra. The results are reported in this chapter.

### 5.3 Observations and Analysis

A high resolution ( $\frac{\lambda}{\Delta\lambda} \approx 35,000$ ) spectra of the stars were obtained at CTIO 4m telescope, Chile. An echelle spectrograph with a grating of 31.6 l/mm and CCD of size 2K - 6K was used for this purpose. Wavelength coverage was from 4950 Å to 8220 Å.

We obtained the spectrum of BPS CS 29516-0041 on 21st June 2002, with an exposure time of 45 minutes. The average signal to noise ratio of the spectrum was around 45 and with a smoothing value of 3.0, it was increased to 75.

BPS CS 29516-0024 was observed on 22 June 2002, with two exposure times of 45 minute each. The signal to noise ratio of each of the spectrum was about 50. After co-adding the two spectra and smoothing with a value of 3.0, we obtained S/N ratio of 130.

Spectrum of BPS CS 29522-0046 was also obtained on 22nd June 2002. Two exposure times of 30 minute each were given. After co-adding and smoothing, we

could reach the S/N value of 150.

We used the standard CCD data reduction package (NOAO, IRAF) for bias subtraction, trimming and flat-fielding of the spectra to remove pixel to pixel variations. Later we converted it to a one-dimensional spectrum and normalized it to the continuum. We used thorium-argon spectrum for wavelength calibration.

The spectral lines were identified using Moore's atomic multiplet table (1945). SPLOT package in IRAF was used to measure equivalent widths of the absorption lines. The equivalent widths were measured by Gaussian fitting to the observed profiles or a multiple Gaussian fit to the blended lines.

### 5.3.1 Determination of atmospheric parameters

For all the stars, the first estimation of effective temperatures were got from the UBV photometric observation of the object from Bonifacio et al. (2000). We adopted the same extinction values for the stars, as given in their paper.

In the case of BPS CS 20516-0041, it is a giant with an estimated metallicity of  $-2.45$ . With reddening estimate of  $E(B - V) = 0.07$ , Bonifacio et al. (2000) obtain  $(B - V)_0 = 0.53$ . The value of  $(B - V)_0 = 0.53$  will correspond to a temperature of 5620 K in the case of a star with  $[Fe/H] = -2.0$  (Alonso et al. 1999). The value of  $T_{\text{eff}}$  would be slightly lower for a star which is more metal deficient than  $[Fe/H] = -2.0$ . (The color excess for the star would have been slightly (0.06) higher and thereby  $T_{\text{eff}}$  could have been of lower value, if we had considered the values from Norris et al. (1999) ).

BPS CS 29516-0024 is predicted to be a giant with  $[Fe/H] = -2.86$ . The observed value  $(B - V) = 0.86$  and ISM extinction value of  $E(B - V) = 0.10$  will yield  $(B - V)_0 = 0.76$ . From Alonso et al. (1999), we obtain the value of  $T_{\text{eff}}$  to be 4910 K. The final estimation of  $T_{\text{eff}}$  could be slightly less for more metal deficient star.

With V magnitude of 12.74 and extinction value of  $E(B - V) = 0.10$ , we obtain  $(B - V)_0 = 0.39$  for BPS CS 29522-0046. For a giant with metallicity -2,  $(B - V)_0$  of 0.39 would correspond to a  $T_{\text{eff}}$  of 5910 K (Alonso et al. 1999). But their fitting

functions unfortunately become nonphysical for turnoff stars below  $[\text{Fe}/\text{H}] \approx -2.5$ . Therefore, for BPS CS 29522-0046 which is predicted to be a turn off star with metallicity  $-3.24$ , the temperature could be much lower than that estimated from their fitting functions.

We have mainly used the excitation potential and oscillator values by compilation of Luck and Bond, supplemented by the line information (compiled as on November 2002) in the Vienna Atomic Line Database (<http://www.astro.univie.ac.at/vald/>). Kurucz (1993) grid of ATLAS models were employed and we used the latest (2002) version of MOOG, an LTE stellar line analysis program (Snedden 1973).

We obtained the value of effective temperature by the method of excitation balance, where the abundances from Fe I lines versus excitation potential of the lines were forced to have a zero slope. The surface gravity was then adjusted by the ionization- equilibrium, where abundances obtained from neutral (Fe I) and ionized (Fe II) species are equal. The microturbulent velocity was estimated with the constraint that there should be no dependence of the Fe I abundance upon equivalent widths of Fe I lines.

The results are discussed in the next few pages. The derived atmospheric parameters are given in Table 5.1 and the abundances are given in Table 2.

Table 5.1: Derived atmospheric parameters for the three BPS stars

Star	$T_{\text{eff}}$ in K	$\log g$	$V_t$ (in $\text{kms}^{-1}$ )	$[\text{Fe}/\text{H}]$
BPS CS 29516-0041	5000	2.5	1.6	-3.0
(BPS CS 29502-0042)				
BPS CS 29516-0024	4750	1.0	1.7	-2.72
BPS CS 29522-0046	5500	3.0	1.1	-2.32

Error in  $T_{\text{eff}}$  is of the order of 250 K, error in  $\log g$  is 0.5, error in  $V_t$  is around 0.5  $\text{kms}^{-1}$  and error in  $[\text{Fe}/\text{H}] = 0.5$ .



Table 2: Summary of elemental abundances in BPS CS 29516-0041, BPS CS 29516-0024 and BPS CS 29522-0046

Element	BPS CS 29516-0041		BPS CS 29516-0024		BPS CS 29522-0046	
	$T_{\text{eff}} = 5000 \text{ K}, \log g = 2.5$		$T_{\text{eff}} = 4750 \text{ K}, \log g = 1.0$		$T_{\text{eff}} = 5500 \text{ K}, \log g = 3.0$	
	$V_t = 1.6, [\text{Fe}/\text{H}] = -3.0$		$V_t = 1.7, [\text{Fe}/\text{H}] = -2.72$		$V_t = 1.1, [\text{Fe}/\text{H}] = -2.32$	
	$[\text{X}/\text{H}] \pm \sigma$	$[\text{Ele}/\text{Fe}]$	$[\text{X}/\text{H}] \pm \sigma$	$[\text{Ele}/\text{Fe}]$	$[\text{X}/\text{H}] \pm \sigma$	$[\text{Ele}/\text{Fe}]$
Li	$< -2.60 \pm 0.11$	$< +0.40$	$-2.34 \pm 0.13$	0.375	$-1.42 \pm 0.14$	+0.850
Na	$-4.16 \pm 0.12$	-1.16	$-3.10 \pm 0.10$	-0.38	$-2.55 \pm 0.12$	-0.28
Mg	$-3.04 \pm 0.26$	-0.04	$-2.06 \pm 0.19$	+0.66	$-1.72 \pm 0.10$	+0.55
K	$-2.82 \pm 0.21$	+0.18	...	...	...	...
Ca	$-2.88 \pm 0.12$	+0.12	$-2.27 \pm 0.10$	+0.45	$-1.82 \pm 0.11$	+0.45
Sc	...	...	$-2.75 \pm 0.11$	-0.04	$-2.09 \pm 0.13$	+0.18
Ti	$-2.92 \pm 0.10$	+0.08	$-2.49 \pm 0.14$	+0.23	$-2.07 \pm 0.10$	+0.20
Cr	$-3.08 \pm 0.14$	-0.08	$-3.04 \pm 0.10$	-0.32	$-2.38 \pm 0.12$	-0.11
Fe	$-3.01 \pm 0.19$	0.0	$-2.72 \pm 0.12$	0.0	$-2.27 \pm 0.15$	0.0
Ni	$-3.07 \pm 0.11$	-0.07	$-2.64 \pm 0.11$	0.075	...	...
Y	...	...	$-3.16 \pm 0.13$	-0.44	...	...
Ba	$-3.28 \pm 0.13$	-0.28	$-3.76 \pm 0.10$	-1.04	$-2.41 \pm 0.10$	-0.14

\*  $[\text{Na}/\text{Fe}]$  abundances are corrected with a flat non-LTE correction of -0.4 dex and  $[\text{K}/\text{Fe}]$  with non-LTE correction of -0.35 dex.

## 5.4 BPS CS 29516-0041 (CS 29502-042)

### 5.4.1 Radial velocity

The radial velocity of BPS CS 29516-0041 was calculated from the wavelength shifts of many absorption lines with no line asymmetry. The observed velocity of  $V_r = -169.985 \pm 0.22 \text{ kms}^{-1}$  will yield an average heliocentric velocity of  $V_{\text{helio}} = -143.445 \pm 0.22 \text{ kms}^{-1}$ , which transforms to a radial velocity relative to the local standard of rest  $V_{\text{lsr}} = -135.555 \pm 0.22 \text{ kms}^{-1}$ .

### 5.4.2 Atmospheric parameters

The plots of the abundances versus excitation potentials and abundances versus equivalent widths in the case of Fe I and Fe II lines are shown in Figure 5.1. Such plots were made by varying the  $T_{\text{eff}}$ ,  $\log g$  and  $V_t$  in steps of 250 K, 0.5 and 0.5  $\text{km s}^{-1}$  respectively to estimate the uncertainties in these parameters.

The analysis yields the stellar parameters to be  $T_{\text{eff}} = 5000 \text{ K}$ ,  $\log g = 2.5$ ,  $V_t = 1.5 \text{ kms}^{-1}$  and  $[\text{Fe}/\text{H}] = -2.99$  (Figure 5.1). The resulting abundances derived with the above atmospheric parameters, along with the line information and their equivalent width are given in Table 5.

The uncertainties in the derived parameters are of the order of 250 K for  $T_{\text{eff}}$ ,  $\log g = 0.5 \text{ dex}$  and  $V_t = 0.5 \text{ kms}^{-1}$ . The uncertainties in the derived abundances because of these errors and measurement error in equivalent widths could be of the order of 0.2 dex.

### 5.4.3 Abundances

The mean abundances of elements in BPS CS 29516-0041 relative to the Sun (Anders and Grevesse 1989) are given in Table 2, along with the standard deviation of abundances estimated from individual species.

Li line was not detectable at 6707 Å region. Considering 7mÅ as the detectable

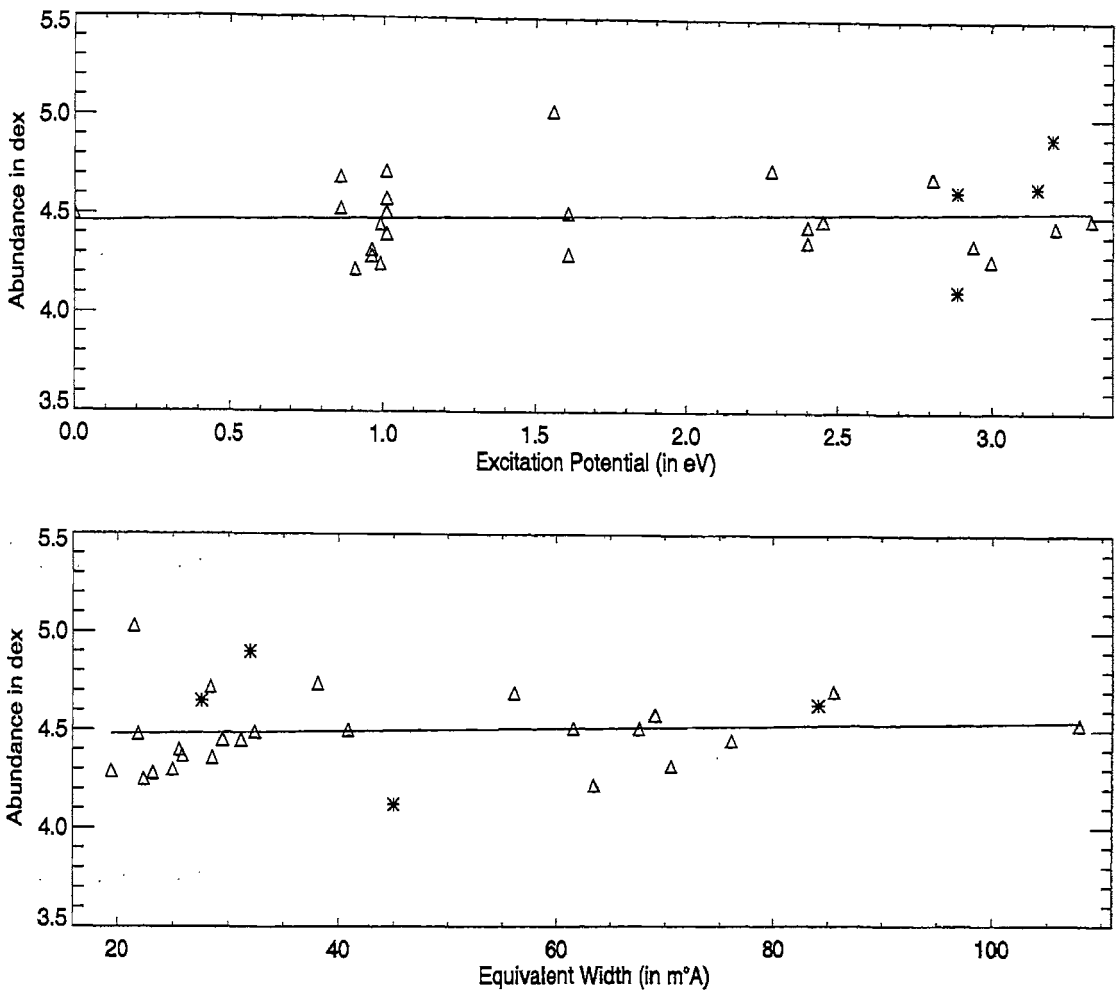


Figure 5.1: Top figure is the plot of the abundances from Fe lines versus excitation potential of the lines for the star BPS CS 29516-0041. Figure at the bottom is the plot of the abundances from Fe lines versus their equivalent widths. Triangles represent the Fe I lines and stars denote the Fe II lines.

limit in that region, we obtain Li abundance to be less than 0.71 dex. This shows that Li is depleted heavily in this star.

Among odd- $z$  elements, we could obtain lines of Na, and K. Considering non-LTE corrections for Na and K, (Gehren et al. 2004) we obtain  $[\text{Na}/\text{Fe}] = -1.16$  dex and  $[\text{K}/\text{Fe}] = +0.18$  dex.

Generally in EMP stars, even- $z$  elements show a moderate overabundances. In BPS CS 29516-0041, Mg lines go with the metallicity of the star ( $[\text{Mg}/\text{Fe}] = -0.04$  dex) whereas Ca I and Ti II lines show an overabundance of 0.1 dex ( $[\text{Ca}/\text{Fe}] = +0.12$  dex and  $[\text{Ti}/\text{Fe}] = +0.08$  dex).

From Fe-peak metal lines, we obtain  $[\text{Cr}/\text{Fe}] = -0.08$  dex and  $[\text{Ni}/\text{Fe}] = -0.07$  dex.

Because of the limited wavelength range (lack of blue region of the spectra) and low signal to noise ratio of the spectra, we are unable to detect most of the heavy element lines and derive their abundances. We detected the Ba line at 6141 Å and obtained  $[\text{Ba}/\text{Fe}] = -0.28$ , which is in agreement with that expected from the metal poor stars.

#### 5.4.3.1 Comparison with the results of Cayrel et al. (2004)

Recently Cayrel et al. (2004) have carried out the abundance analysis of 29 EMP giants, which includes BPS CS 29516-0041, the object of our study. We are comparing our results with those derived by Cayrel et al. (2004) in Table 5.3.

The slight difference in abundances obtained in our analysis and those derived by Cayrel et al. (2004) for this star may be due to the slightly different atmospheric parameters (They adopt a model temperature of 5100 K) and the quality of the spectra. Cayrel et al.'s (2004) spectra have very high resolution and high S/N ratio. The abundance differences in these two independent observations are within the error bars.

Table 5.3: Comparison of our results with those of Cayrel et al. (2004) for BPS CS 29516-0041

Element	Our results	Cayrel et al. (2004)
	$T_{\text{eff}} = 5000 \text{ K}, \log g = 2.5$ $V_t = 1.6 \text{ kms}^{-1}, [\text{Fe}/\text{H}] = -3.0$	$T_{\text{eff}} = 5100 \text{ K}, \log g = 2.5$ $V_t = 1.5 \text{ kms}^{-1}, [\text{Fe}/\text{H}] = -3.19$
	[X/Fe]	[X/Fe]
Na	-1.16	-0.85
Mg	-0.04	+0.23
K	+0.18	-0.05
Ca	+0.12	+0.22
Ti	+0.08	+0.25
Cr	-0.08	-0.37
Ni	-0.07	-0.06

Non LTE corrections of -0.4 is applied for Na and -0.35 for K

## 5.5 BPS CS 29516-0024

### 5.5.1 Radial velocity

We chose 67 absorption lines showing no line asymmetry to determine the radial velocity of BPS CS 29516-0041. The observed velocity of  $V_r = -113.32 \pm 0.15 \text{ kms}^{-1}$ , was calculated from wavelength shifts of these lines from their laboratory value. We find an average heliocentric velocity of  $V_{\text{helio}} = -86.16 \pm 0.15 \text{ kms}^{-1}$ , which transforms to a radial velocity relative to the local standard of rest  $V_{\text{lsr}} = -78.51 \pm 0.15 \text{ kms}^{-1}$ .

### 5.5.2 Atmospheric Parameters

The plots of the abundances versus excitation potentials and abundances versus equivalent widths for Fe I and Fe II lines, in the case of BPS CS 29516-0024 are shown in Figure 5.2. Such plots were made by varying the  $T_{\text{eff}}$ ,  $\log g$  and  $V_t$  in steps of 250 K, 0.5 and 0.5  $\text{kms}^{-1}$  respectively to estimate the uncertainties in these parameters.

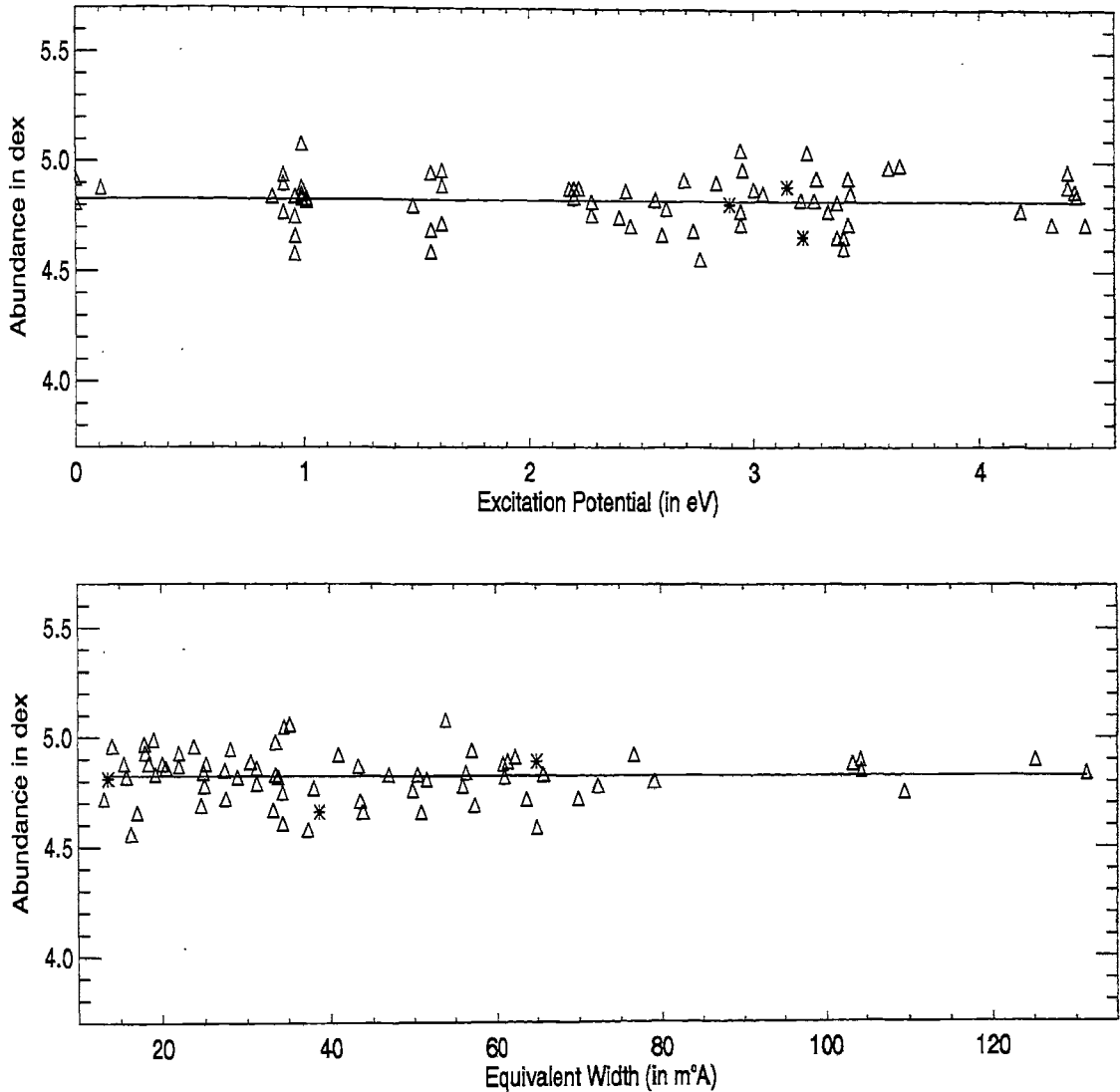


Figure 5.2: Top figure is the plot of the abundances from Fe lines versus excitation potential of the lines for the star BPS CS 29516-0024. Figure at the bottom is the plot of the abundances from Fe lines versus their equivalent widths. Triangles represent the Fe I lines and stars denote the Fe II lines.

For BPS CS 29516-0024, we obtain  $T_{\text{eff}} = 4750\text{K}$ ,  $\log g = 1.0$ ,  $V_t = 1.7\text{kms}^{-1}$  and  $[\text{Fe}/\text{H}] = -2.72$  (Figure 5.2). The resulting abundances are tabulated in Table 6. Using the derived atmospheric parameters and abundances, a synthetic spectrum was generated and plotted over the observed spectrum for verification. The observed and synthetic spectra were found to match well with the above mentioned atmospheric parameters and the final abundances as given in Table 6. A region of the observed and synthetic spectrum is shown in Figure 5.3.

### 5.5.3 Abundances

The mean abundances of elements in BPS CS 29516-0024 relative to solar abundances, are given in Table 2. Standard deviation of abundances estimated from individual species are also shown.

Li line at 6707 gives an abundance of 0.97 dex. As the line was weak ( $18.7 \text{ m}\text{\AA}$ ), hyperfine structure was not considered for the line. The abundance of Li indicates the depletion of the element compared to other metal poor dwarfs (2.30 dex).

Na lines, with non-LTE correction of -0.4 dex ( for a star with  $[\text{Fe}/\text{H}] = -2.5$ , Gehren et al. 2004) show an underabundance of -0.38 dex ( $[\text{Na}/\text{Fe}] = -0.38$ ). Sc value goes with metallicity of the star ( $[\text{Sc}/\text{Fe}] = -0.04$ )

All  $\alpha$  elements are found to be overabundant ( $[\text{Mg}/\text{Fe}] = +0.66$ ,  $[\text{Ca}/\text{Fe}] = +0.45$ ,  $[\text{Ti}/\text{Fe}] = +0.23$  ).

Among Fe peak elements, Cr shows deficiency ( $[\text{Cr}/\text{Fe}] = -0.325$ ), whereas Ni goes with Fe ( $[\text{Ni}/\text{Fe}] = +0.07$ ).

The heavy elements are deficient compared to Fe. Y yields  $[\text{Y}/\text{Fe}]$  of  $-0.44$  and Ba show deficiency of  $[\text{Ba}/\text{Fe}] = -1.045$  dex. These observation are in accordance with the general trend of heavy elements in EMP stars (McWilliam et al. (1995), Ryan et al. (1996) and Cohen et al. (2004) ).

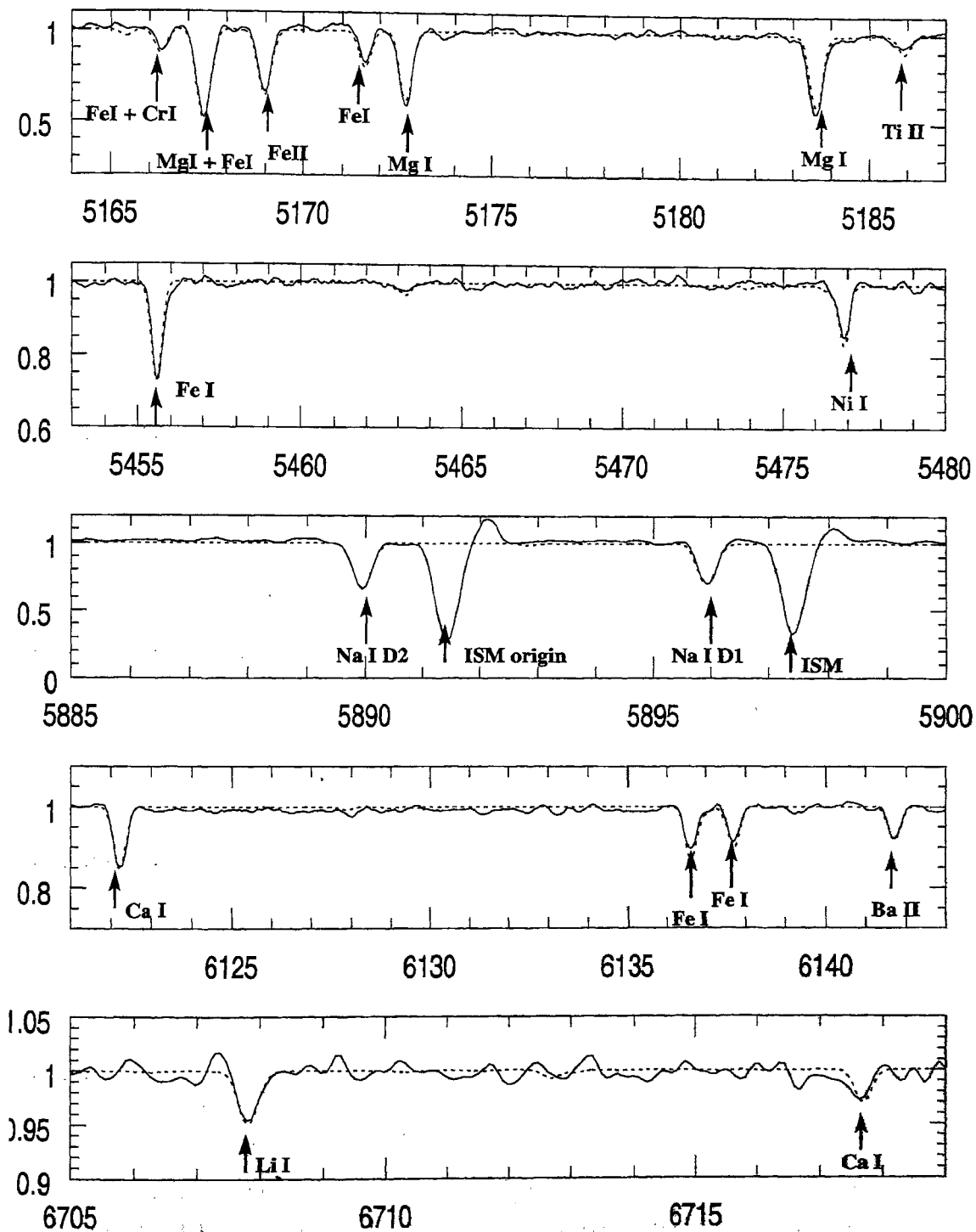


Figure 5.3: Synthetic spectra with the atmospheric model and abundances given in Table 6 are overplotted on observed spectra of the object BPS CS 29516-0024, at different regions.



Table 5.4: Comparison of our results with those of Cayrel et al. (2004) for BPS CS 29516-0024

Element	Our results	Cayrel et al. (2004)
	$T_{\text{eff}} = 4750 \text{ K}, \log g = 1.0$ $V_t = 1.7 \text{ kms}^{-1}, [\text{Fe}/\text{H}] = -2.72$	$T_{\text{eff}} = 4650 \text{ K}, \log g = 1.2$ $V_t = 1.7 \text{ kms}^{-1}, [\text{Fe}/\text{H}] = -3.06$
	[X/Fe]	[X/Fe]
Na	-0.38	-0.06
Mg	+0.66	+0.48
Ca	+0.44	+0.55
Sc	-0.04	+0.06
Ti	+0.23	+0.24
Cr	-0.32	-0.31
Ni	+0.07	-0.15

Non LTE correction of -0.4 is applied for Na

### 5.5.3.1 Comparison with the study of Cayrel et al. (2004)

The recent paper by Cayrel et al. (2004), which came out before we report our results, have done the analysis of BPS CS 29516-0024 also. In Table 5.4, we compare our results with those derived by Cayrel et al. (2004).

Abundance of Na is much lower, compared to the value obtained by Cayrel et al. (2004). (When non-LTE correction is *not* considered in both the cases, we obtain  $[\text{Na}/\text{Fe}] = +0.01$  and in their case, it is  $+0.36$  dex). There can be no interstellar contribution to these lines, as the stellar lines are well separated from lines of interstellar origin due to high radial velocity ( $\approx -113.32 \pm 0.15 \text{ kms}^{-1}$ ) of the star. Spectra synthesized in this region, found to match well with the chosen stellar parameters and Na abundances and is shown in Figure 5.3.

Among  $\alpha$ -elements, Mg and Ca abundances are 0.1 dex extra compared to the values obtained by Cayrel et al. (2004), but overabundance of Ti is similar. In Fe-peak elements, Cayrel et al. (2004) find similar value for Cr but Ni is slightly deficient

in their data.

Differences in spectral resolution and signal to noise ratio, different spectral codes and model atmospheres (We have used the code MOOG with Kurucz model atmospheres. Cayrel et al.'s (2004) analysis uses spectral analysis code "Turbospectrum" with OSMARCS model atmospheres.) might have contributed to the differences in abundances in these two independent observations. The differences are within observational errors.

## 5.6 BPS CS 29522-0046

### 5.6.1 Radial velocity

We chose around 60 good lines with no line asymmetry for the calculation of radial velocity of BPS CS 29522-0046. From the wavelength shifts of these lines, we derived the observed radial velocity of  $V_r = -135.76 \pm 0.20 \text{ kms}^{-1}$ . This yields an average heliocentric velocity of  $V_{\text{helio}} = -106.354 \pm 0.20 \text{ kms}^{-1}$ , which transforms to a radial velocity relative to the local standard of rest  $V_{\text{lsr}} = -103.414 \pm 0.20 \text{ kms}^{-1}$ .

### 5.6.2 Atmospheric parameters

Figure 5.4 shows the plot of abundances versus excitation potentials, also the plot of abundances versus equivalent widths for Fe I and Fe II lines, for BPS CS 29522-0046. The models were iterated by varying  $T_{\text{eff}}$ ,  $\log g$  and  $V_t$  in steps of 250 K, 0.5 and 0.5  $\text{kms}^{-1}$  respectively, to obtain the final plot and to estimate the uncertainties in these parameters.

We obtain,  $T_{\text{eff}} = 5500\text{K}$ ,  $\log g = 3.0$ ,  $V_t = 1.10 \text{ kms}^{-1}$  and  $[\text{Fe}/\text{H}] = -2.32$  (Figure 5.4), in the case of BPS CS 29522-0046.

Table 7 lists the line information (including wavelength, lower excitation potential and log of oscillator strengths of lines), equivalent width of each line and also the abundances resulted from individual lines using the above stellar parameters.

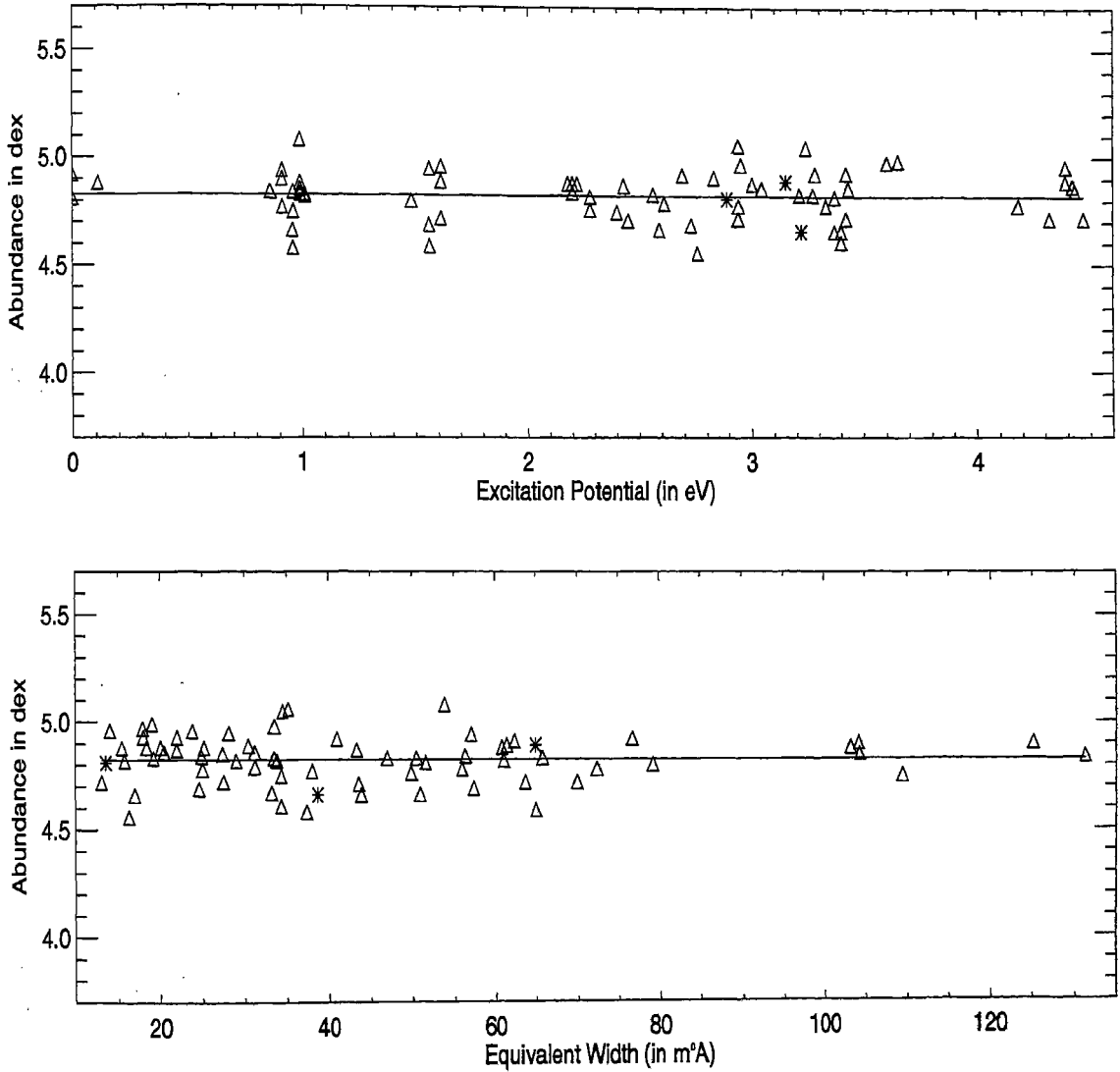


Figure 5.4: Top figure is the plot of the abundances from Fe lines versus excitation potential of the lines for the star BPS CS 29522-0046. Figure at the bottom is the plot of the abundances from Fe lines versus their equivalent widths. Triangles represent the Fe I lines and stars denote the Fe II lines.

### 5.6.3 Abundances

Table 2 lists the mean abundances of BPS CS 29522-0046 along with the other two stars studied in this chapter. Standard deviation from mean abundances for each element is also shown.

Li shows an abundance of 1.89 dex. Lambert & Reddy (2004) have studied the Li abundances in local thin disk stars. Calculating the the Li abundances with/without hyperfine structure taken into account and plotting their difference v/s equivalent width will lead to an empirical formula (Reddy, private communication)

$$\text{Li}_{\text{hfs}} = \text{Li}_{\text{no-hfs}} - (0.002 \times W_{\lambda}) + 0.0024 \quad (5.1)$$

where  $\text{Li}_{\text{hfs}}$  is the Li abundance obtained by taking hyperfine effect into consideration and  $\text{Li}_{\text{no-hfs}}$  is the Li abundance without considering hyperfine structure. This effect is minimal when the line strength is weak and could be ignored for a line whose equivalent width is less than 30 mÅ. In BPS CS 29522-0046, equivalent width of 6707 line is 30.9 mÅ. So, we have ignored this effect and have taken 1.89 dex as the Li abundance. Usually, metal poor dwarfs retain same Li abundance of 2.1 dex, down to lowest metallicities (Spite & Spite 1982). However, Ryan et al. (1999) observe Spite lithium plateau in metal poor turn off stars show a slight decreasing trend with decreasing metallicity, but which won't go below 2.0 dex. Also, they report that the scatter in Li abundances are quite minimal ( $< 0.031$  dex). However, cooler stars show depletion of Li by approximately 0.27 dex per 100 K, at the interval 5000 K  $< T_{\text{eff}} < 5500$  K (Ryan and Deliyannis, 1998a). BPS CS 29522-0046, being a giant ( $\log g = 3.0$ ), with a temperature of 5500 K, shows depletion of Li by 0.2 dex, thus confirming their observation.

Sodium, when applied a non-LTE correction of -0.4 dex (Gehren et al. 2004), would yield an abundance of  $[\text{Na}/\text{Fe}] = -0.28$ . It agrees well with the observations of stars with  $[\text{Fe}/\text{H}] = -2.0$  by McWilliam et al. (1995). Cayrel et al. (2004) have observed stars below  $[\text{Fe}/\text{H}] = -2.5$ . They plot Na abundance versus metallicity for these EMP giants and derive the slope. This slope predicts more Na abundance for a star at metallicity  $-2.0$ . This would imply that, the slope of Na abundance before and after  $[\text{Na}/\text{Fe}] = -2.5$  are not the same. McWilliam et al. (1995) have noticed

the abundance trend changing at  $[\text{Element}/\text{Fe}] = -2.4$  for 6 elements (Cr, Mn, Co, Al, Sr and Ba). Probably Na abundance also shows change with metallicity at  $-2.4$ . It would remain at the metallicity (or  $+0.2$  dex extra) for star with metallicity till  $-2.4$ , then it shows gradual decline. Further studies of Na abundance between  $-1.5$  to  $-3.5$  metallicity are required for this purpose.

Sc shows an overabundance of  $+0.18$  dex compared to iron. This is in accordance with other observations (McWilliam et al. 1995, Cayrel et al. 2004).

All  $\alpha$ -elements are overabundant with respect to iron ( $[\text{Mg}/\text{Fe}] = +0.55$ ,  $[\text{Ca}/\text{Fe}] = +0.45$  and  $[\text{Ti}/\text{Fe}] = +0.21$ ). These results are in agreement with the results obtained by Cayrel et al. (2004) for other metal poor stars.

We have only lines of Cr for Fe-peak elements and it shows abundance of  $[\text{Cr}/\text{Fe}] = -0.11$ . Again, Cr going down with metallicity of the star is an observed fact (McWilliam et al. 1995, Cayrel et al. 2004).

Among heavy elements, only Ba lines are present in this metal poor star.  $[\text{Ba}/\text{Fe}]$  shows an underabundance of  $-0.14$  dex. Underabundance of Ba is observed in most of the stars below  $[\text{Fe}/\text{H}] = -2.0$ . This star shows the onset of this trend with  $[\text{Ba}/\text{Fe}] = -0.14$  at metallicity  $-2.3$ .

## 5.7 Conclusions

We have analyzed the high resolution spectra of three metal poor stars, BPS CS 29516-0041, BPS CS 29516-0024, BPS CS 29522-0046 in this chapter.

All the stars show high radial velocities confirming that they belong to halo population.

BPS CS 29516-0041 is a cool giant and its spectra reveals the parameters of the star to be  $T_{\text{eff}} = 5000 \pm 250$  K,  $\log g = 2.5 \pm 0.5$  dex,  $[\text{Fe}/\text{H}] = -3.0$  and  $V_t = 1.6$   $\text{kms}^{-1}$ . Analysis of BPS CS 29516-0024 yields,  $T_{\text{eff}} = 4750 \pm 250$  K,  $\log g = 1.0 \pm 0.5$  dex,  $[\text{Fe}/\text{H}] = -2.72$  and  $V_t = 1.7$   $\text{kms}^{-1}$ . BPS CS 29522-0046 shows slightly higher gravity with  $T_{\text{eff}} = 5500 \pm 250$  K,  $\log g = 3.0 \pm 0.5$  dex,  $[\text{Fe}/\text{H}] = -2.32$  and  $V_t = 1.1$   $\text{kms}^{-1}$ .

All the stars show Li deficiency, but it is less pronounced in BPS CS 29522-0046.

Among odd-z elements, Na shows depletion in all the three stars, but its abundance in BPS CS 29522-0046 is higher than that predicted by the slope of abundances versus metallicity from the observations of Cayrel et al. (2004), for the stars below  $[\text{Fe}/\text{H}] = -2.5$ . Sc shows variation in abundances among stars ; ( $[\text{Sc}/\text{Fe}] = -0.04$  in BPS CS 29516-0024 and is  $+0.18$  dex in BPS CS 29522-0046).

In all the stars  $\alpha$ -elements are enhanced.

Among Fe-peak elements, Cr shows slight underabundance with respect to Fe. Ni, present in BPS CS 29516-0041 and BPS CS 29522-0046, is of iron metallicity ( $[\text{Ni}/\text{Fe}] = -0.07$  for CS 29522-046 and  $[\text{Ni}/\text{Fe}] = +0.08$  for CS 29516-024). Comparison of our studies with observations of Cayrel et al. (2004) yield slight differences of the order of 0.1 - 0.3 dex, which is within the observational uncertainties.

The heavy element Barium, shows underabundance in all the three stars. The star BPS CS 29522-0046 with ( $[\text{Fe}/\text{H}] = -2.3$ , shows the onset of this trend with  $[\text{Ba}/\text{Fe}] = -0.14$  whereas, BPS CS 29516-0024 with metallicity  $-2.7$ , shows Ba deficiency of the order of 1 dex.

On the whole, the abundance study of these three stars agree well with the studies of other extreme metal poor stars. They emphasize the need to study the elemental abundances in stars which lie on either side of ( $[\text{Fe}/\text{H}] = -2.4$ , to understand the dramatic change in the trends of abundance ratios (nucleosynthesis) around  $[\text{Fe}/\text{H}] = -2.4$  (McWilliam et al. 1995).

Table 5: Data for spectral lines measured in the spectrum of BPS CS 29516-0041

$\lambda_{lab}$ (in $\text{\AA}$ )	LEP (eV)	log gf	EW ( $m\text{\AA}$ )	log $\epsilon$
Li II				
6707.76	0.00	0.167	< 7.0	< 0.71
Na I				
5889.97	0.00	0.110	75.7	2.56
5895.94	0.00	-0.190	56.8	2.58
Mg I				
5172.70	2.71	-0.381	114.9	4.40
5183.62	2.72	-0.158	127.1	4.38
5528.42	4.34	-0.341	37.7	4.84
K I				
7698.98	0.00	-0.169	17.4	2.65
Ca I				
5588.76	2.52	0.358	16.3	3.38
5857.46	2.93	0.240	9.9	3.69
6122.23	1.89	-0.316	22.5	3.49
6162.18	1.90	-0.090	27.6	3.40
6439.08	2.52	0.390	19.1	3.39
6462.57	2.52	0.262	18.7	3.51
Ti II				
5129.16	1.89	-1.390	6.9	2.12
5188.69	1.58	-1.210	16.9	2.02
Cr I				
5409.78	1.03	-0.720	17.9	2.59
Fe I				
4957.60	2.81	0.233	85.6	4.65
5012.07	0.86	-2.642	56.1	4.67
5049.82	2.28	-1.420	38.1	4.72

Table 5: continued

$\lambda_{lab}$ (in $\text{\AA}$ )	LEP (eV)	log gf	EW ( $m\text{\AA}$ )	log $\epsilon$
Fe I				
5110.41	0.00	-3.760	40.9	4.49
5123.72	1.01	-3.068	28.4	4.71
5139.46	2.94	-0.509	28.6	4.36
5266.55	3.00	-0.490	23.2	4.27
5269.54	0.86	-1.321	107.9	4.47
5270.36	1.61	-1.510	61.6	4.48
5324.18	3.21	-0.240	31.2	4.44
5341.02	1.61	-2.060	25.0	4.29
5397.13	0.91	-1.993	63.5	4.19
5405.77	0.99	-1.844	76.1	4.39
5429.70	0.96	-1.879	70.6	4.27
5434.52	1.01	-2.122	69.1	4.54
5455.61	1.01	-2.091	67.6	4.47
5497.52	1.01	-2.849	25.6	4.39
5501.46	0.96	-2.950	19.5	4.28
5506.78	0.99	-2.797	22.4	4.24
5615.64	3.33	-0.140	32.4	4.48
6136.61	2.45	-1.400	21.9	4.47
6494.98	2.40	-1.273	29.5	4.44
Fe II				
5018.45	2.89	-1.220	45.0	4.10
5169.00	2.89	-0.870	84.2	4.56
5276.00	3.20	-1.940	32.0	4.89
5316.62	3.15	-1.850	27.6	4.65
Ni II				
5476.91	1.83	-0.890	30.0	3.19
Ba II				
6141.71	0.70	-0.069	22.9	-1.15



Table 6: Data for spectral lines measured in the spectrum of BPS CS 29516-0024

$\lambda_{lab}$ (in Å)	LEP (eV)	log gf	EW (mÅ)	log $\epsilon$
Li I				
6707.76	0.00	0.167	18.7	0.97
Na I				
5889.97	0.00	0.110	143.5	3.70
5895.94	0.00	-0.190	119.9	3.56
Mg I				
5172.70	2.71	-0.381	197.2	5.70
5183.62	2.72	-0.158	202.4	5.53
5528.42	4.34	-0.341	70.6	5.33
Ca I				
5261.71	2.52	-0.579	17.1	4.25
5581.98	2.52	-0.555	18.9	4.26
5588.76	2.52	0.358	45.2	3.93
5590.13	2.52	-0.571	10.8	3.99
5594.47	2.52	0.097	35.8	4.01
5598.49	2.52	-0.087	35.1	4.18
5601.29	2.52	-0.523	12.5	4.01
5857.46	2.93	0.240	23.7	4.05
6102.73	1.88	-0.793	31.9	4.03
6122.23	1.89	-0.316	60.0	4.08
6162.18	1.90	-0.090	67.2	4.00
6169.56	2.52	-0.478	15.0	4.02
6439.08	2.52	0.390	64.7	4.18
6462.57	2.52	0.230	54.5	4.16
6471.66	2.53	-0.653	13.1	4.12
6499.65	2.52	-0.719	14.9	4.24
7148.15	2.71	0.137	35.9	4.09
Sc II				
5526.79	1.77	-0.219	19.7	0.35

Table 6: continued

$\lambda_{lab}$ (in Å)	LEP (eV)	log gf	EW ( $m\text{Å}$ )	log $\epsilon$
Ti I				
4981.73	0.85	0.560	61.1	2.67
4991.07	0.84	0.436	55.8	2.67
4999.50	0.83	0.306	38.3	2.44
5064.65	0.05	-0.935	23.4	2.43
5173.74	0.00	-1.062	36.8	2.77
5192.97	0.02	-0.950	23.6	2.40
5210.39	0.05	-0.828	34.0	2.54
Ti II				
5154.06	1.57	-1.920	28.4	2.44
5185.90	1.89	-1.350	33.5	2.36
5188.69	1.58	-1.210	73.0	2.61
5336.77	1.58	-1.630	36.3	2.30
5381.02	1.57	-1.970	30.1	2.50
5418.75	1.58	-2.110	24.5	2.53
Cr I				
5206.02	0.94	0.019	66.0	2.59
5298.29	0.98	-1.150	17.5	2.76
5345.77	1.00	-0.980	16.9	2.59
5409.78	1.03	-0.720	24.3	2.56
Fe I				
4994.13	0.91	-3.080	57.1	4.94
5006.12	2.83	-0.638	62.4	4.91
5049.82	2.28	-1.420	49.9	4.76
5068.77	2.94	-1.230	35.2	5.06
5079.74	0.99	-3.220	53.9	5.08
5083.34	0.96	-2.958	56.4	4.84
5110.41	0.00	-3.760	76.7	4.92
5123.72	1.01	-3.068	47.0	4.83

Table 6: continued

$\lambda_{lab}$ (in $\text{\AA}$ )	LEP (eV)	log gf	EW ( $m\text{\AA}$ )	log $\epsilon$
Fe I				
5127.36	0.91	-3.307	38.0	4.77
5142.93	0.96	-3.080	37.3	4.58
5151.91	1.01	-3.322	33.8	4.82
5166.28	0.00	-4.195	51.6	4.81
5171.60	1.48	-1.793	79.2	4.80
5194.94	1.56	-2.090	57.4	4.69
5198.71	2.22	-2.135	25.2	4.88
5216.27	1.61	-2.150	61.5	4.89
5217.39	3.21	-1.070	19.2	4.83
5229.85	3.28	-1.127	18.0	4.93
5232.94	2.94	-0.190	72.4	4.78
5225.53	0.11	-4.789	20.1	4.88
5232.94	2.94	-0.190	70.0	4.72
5266.55	3.00	-0.490	60.9	4.88
5269.54	0.86	-1.321	131.3	4.84
5281.79	3.04	-1.020	31.2	4.86
5307.36	1.61	-2.987	23.8	4.96
5328.04	0.91	-1.466	125.1	4.90
5328.53	1.56	-1.850	65.0	4.59
5332.90	1.56	-2.940	28.1	4.95
5339.93	3.27	-0.680	33.5	4.83
5341.02	1.61	-1.953	63.7	4.72
5367.47	4.42	0.350	22.0	4.87
5371.49	0.96	-1.645	109.5	4.75
5393.17	3.24	-0.910	34.5	5.05
5397.13	0.91	-1.993	104.3	4.90
5404.15	4.43	0.523	27.4	4.85
5405.77	0.99	-1.844	104.4	4.85

Table 6: continued

$\lambda_{lab}$ (in $\text{\AA}$ )	LEP (eV)	log gf	EW ( $m\text{\AA}$ )	log $\epsilon$
Fe I				
5410.91	4.47	0.280	13.1	4.72
5415.20	4.39	0.500	30.5	4.89
5424.07	4.32	0.520	27.5	4.72
5445.04	4.39	-0.020	14.1	4.96
5446.92	0.99	-1.914	103.3	4.88
5497.52	1.01	-2.849	61.1	4.82
5501.46	0.96	-2.950	50.9	4.66
5506.78	0.99	-2.797	65.8	4.83
5569.62	3.42	-0.540	27.5	4.72
5572.84	3.40	-0.310	34.3	4.61
5586.76	3.37	-0.210	43.9	4.66
5602.95	3.43	-0.850	20.5	4.86
5615.64	3.33	-0.140	56.0	4.78
5624.54	3.42	-0.900	22.0	4.93
5658.82	3.40	-0.793	17.0	4.66
5709.38	3.37	-1.028	15.8	4.82
6065.48	2.61	-1.530	31.2	4.79
6136.61	2.45	-1.400	43.6	4.71
6137.69	2.59	-1.403	33.2	4.67
6191.56	2.43	-1.600	43.4	4.87
6219.28	2.20	-2.433	18.4	4.88
6230.73	2.56	-1.281	50.5	4.83
6252.55	2.40	-1.687	34.3	4.75
6265.13	2.18	-2.550	15.5	4.88
6335.34	2.20	-2.230	24.9	4.84
6400.00	3.60	-0.520	33.5	4.98
6411.65	3.65	-0.820	19.0	4.99
6421.35	2.28	-2.027	29.0	4.82

Table 6: continued

$\lambda_{lab}$ (in Å)	LEP (eV)	log gf	EW ( $m\text{Å}$ )	log $\epsilon$
Fe I				
6546.24	2.76	-1.536	16.3	4.56
6592.91	2.73	-1.473	24.6	4.69
6677.99	2.69	-1.418	41.0	4.92
7511.02	4.18	0.099	25.0	4.78
7748.27	2.95	-1.751	17.9	4.97
Fe II				
5234.62	3.22	-2.050	38.7	4.66
5316.62	3.15	-1.850	65.0	4.89
6516.08	2.89	-3.320	13.6	4.81
Ni I				
5476.91	1.83	-0.890	59.6	3.53
6643.64	1.68	-2.300	14.9	3.68
Y II				
5087.42	1.08	-0.165	11.6	-0.92
Ba II				
6141.71	0.70	-0.069	30.6	-1.62
6496.90	0.60	-0.377	22.6	-1.64

Table 7: Data for spectral lines measured in BPS CS 29522-0046

$\lambda_{lab}$ (in $\text{\AA}$ )	LEP (eV)	log gf	EW ( $m\text{\AA}$ )	log $\epsilon$
Li I				
6707.76	0.00	0.167	30.9	1.89
Na I				
5889.97	0.00	0.110	148.9	4.15
5895.94	0.00	-0.190	128.1	4.22
Mg I				
5172.70	2.71	-0.381	203.6	5.87
5183.62	2.72	-0.158	239.8	5.85
Ca I				
5588.76	2.52	0.358	48.8	4.44
5590.13	2.52	-0.571	15.7	4.59
5594.47	2.52	0.097	39.3	4.51
5598.49	2.52	-0.087	26.5	4.41
5601.29	2.52	-0.523	14.9	4.51
5857.46	2.93	0.240	31.4	4.60
6102.73	1.88	-0.793	30.5	4.53
6122.23	1.89	-0.316	58.2	4.64
6162.18	1.90	-0.090	55.3	4.37
6169.04	2.52	-0.797	10.2	4.57
6169.56	2.52	-0.478	20.0	4.60
6439.08	2.52	0.390	46.0	4.32
6449.81	2.52	-0.502	16.6	4.51
6462.57	2.52	0.262	47.7	4.48
6471.67	2.52	-0.686	14.9	4.64
6493.79	2.52	-0.109	32.1	4.52
6499.65	2.52	-0.818	15.8	4.80
6717.69	2.71	-0.524	13.1	4.59
7148.15	2.71	0.137	41.2	4.63

Table 7: continued

$\lambda_{lab}$ (in Å)	LEP (eV)	log gf	EW ( $m\text{Å}$ )	$\log \epsilon$
Sc II				
5526.79	1.77	-0.219	11.1	1.01
Ti I				
4991.07	0.84	0.436	31.7	2.97
5210.39	0.05	-0.828	14.0	2.90
Ti II				
5129.16	1.89	-1.390	18.5	2.99
5226.53	1.57	-1.300	31.2	2.88
5336.77	1.58	-1.630	17.5	2.86
Cr I				
5206.02	0.94	0.019	56.5	3.26
5208.42	0.94	0.158	66.5	3.38
5409.78	1.03	-0.720	21.5	3.23
Fe I				
5006.12	2.83	-0.638	43.8	5.21
5083.34	0.96	-2.958	37.4	5.42
5098.70	2.18	-2.026	17.9	5.26
5107.45	0.99	-3.087	24.1	5.26
5142.93	0.96	-3.080	25.3	5.25
5162.27	4.18	0.020	27.5	5.53
5171.60	1.48	-1.793	52.5	5.16
5191.45	3.04	-0.551	45.3	5.36
5192.34	3.00	-0.421	47.3	5.24
5194.94	1.56	-2.090	40.1	5.24
5215.18	3.27	-0.871	22.0	5.34
5216.27	1.61	-2.150	31.6	5.15
5226.86	3.04	-0.555	38.7	5.21
5232.94	2.94	-0.190	60.1	5.25
5266.55	3.00	-0.490	47.0	5.29

Table 7: continued

$\lambda_{lab}$ (in $\text{\AA}$ )	LEP (eV)	log gf	EW ( $m\text{\AA}$ )	log $\epsilon$
Fe I				
5269.54	0.86	-1.321	109.0	5.41
5281.79	3.04	-1.020	28.6	5.43
5302.30	3.28	-0.880	16.0	5.18
5324.18	3.21	-0.240	49.3	5.30
5328.04	0.91	-1.466	92.8	5.28
5328.53	1.56	-1.850	52.3	5.28
5339.93	3.27	-0.680	26.0	5.25
5364.87	4.45	0.220	17.4	5.30
5367.47	4.42	0.350	21.5	5.27
5383.37	4.31	0.500	28.5	5.20
5405.77	0.99	-1.844	72.4	5.21
5410.91	4.47	0.280	23.9	5.46
5415.20	4.39	0.500	30.3	5.32
5424.07	4.32	0.520	32.9	5.29
5429.70	0.96	-1.879	77.3	5.34
5445.04	4.39	-0.020	19.8	5.55
5446.92	0.99	-1.930	79.2	5.48
5506.78	0.99	-2.797	33.3	5.17
5572.84	3.40	-0.310	39.5	5.33
5576.09	3.43	-1.000	16.2	5.44
5586.76	3.37	-0.210	36.3	5.12
5615.64	3.33	-0.140	44.6	5.21
6065.48	2.61	-1.530	28.1	5.44
6136.61	2.45	-1.400	29.3	5.17
6137.69	2.59	-1.403	21.9	5.12
6191.56	2.43	-1.600	26.6	5.28
6230.73	2.56	-1.281	41.0	5.43
6252.55	2.40	-1.687	19.6	5.14



Table 7: continued

$\lambda_{lab}$ (in $\text{\AA}$ )	LEP (eV)	log gf	EW ( $m\text{\AA}$ )	log $\epsilon$
Fe I				
6393.60	2.43	-1.620	19.9	5.11
6400.00	3.60	-0.520	23.4	5.32
6411.65	3.65	-0.820	17.8	5.50
6677.99	2.69	-1.470	27.9	5.43
7445.75	4.26	-0.237	15.2	5.41
7495.06	4.22	-0.102	17.1	5.30
7511.02	4.18	0.099	27.9	5.35
Fe II				
5018.45	2.89	-1.220	80.1	5.41
5197.56	3.23	-2.100	19.5	5.04
5234.62	3.22	-2.050	20.9	5.02
5316.62	3.15	-1.850	44.5	5.33
Ba II				
5853.67	0.60	-1.016	8.2	-0.30
6141.71	0.70	-0.069	34.8	-0.27
6496.90	0.60	-0.369	28.6	-0.26

# Chapter 6

## Summery and Conclusions

We have carried out the analysis of high resolution spectra of five metal poor stars : ZNG 4 in the globular cluster M13 and halo giants LSE 202, BPS CS 29516-0041, BPS CS 29516-0024 and BPS CS 29502-042. The metallicity of these stars ranges from  $[\text{Fe}/\text{H}] = -1.5$  to  $[\text{Fe}/\text{H}] = -3.0$

Table 6.1: Atmospheric parameters of the stars observed along with their Fe and Ba abundances

Object Name	$T_{\text{eff}}$ (in K)	$\log g$	$V_t$ (in $\text{kms}^{-1}$ )	$[\text{Fe}/\text{H}]$	$[\text{Ba}/\text{Fe}]$
ZNG 4 (in M13)	8500	2.5	2.0	-1.49	+0.28
LSE 202	4750	1.5	1.9	-2.41	-0.93
BPS CS 29516-0041	5000	2.5	1.6	-3.0	-0.28
(BPS CS 29502-0042)					
BPS CS 29516-0024	4750	1.0	1.7	-2.7	-1.05
BPS CS 29522-0046	5500	3.0	1.1	-2.3	-0.14

The derived atmospheric parameters of the stars and their Fe and Ba abundances are given in Table 6.1.

## 6.1 ZNG 4 in M13

Analysis of high resolution spectrum of ZNG 4 in M13 yields,  $T_{\text{eff}} = 8500 \pm 250$  K,  $\log g = 2.5 \pm 0.5$  and  $[\text{Fe}/\text{H}] = -1.5$ . Except for magnesium, chromium and strontium, all other even Z elements show enhancement. The horizontal branch of M13 is marked by a prominent gap at 11,000 K. Stars towards the redder side of the gap show normal abundances of giants and dichotomy in rotational velocities, whereas bluer stars show underabundance of He and overabundance of heavy metals which results because of diffusion and radiative levitation. The rotational velocities of bluer HB stars are small.

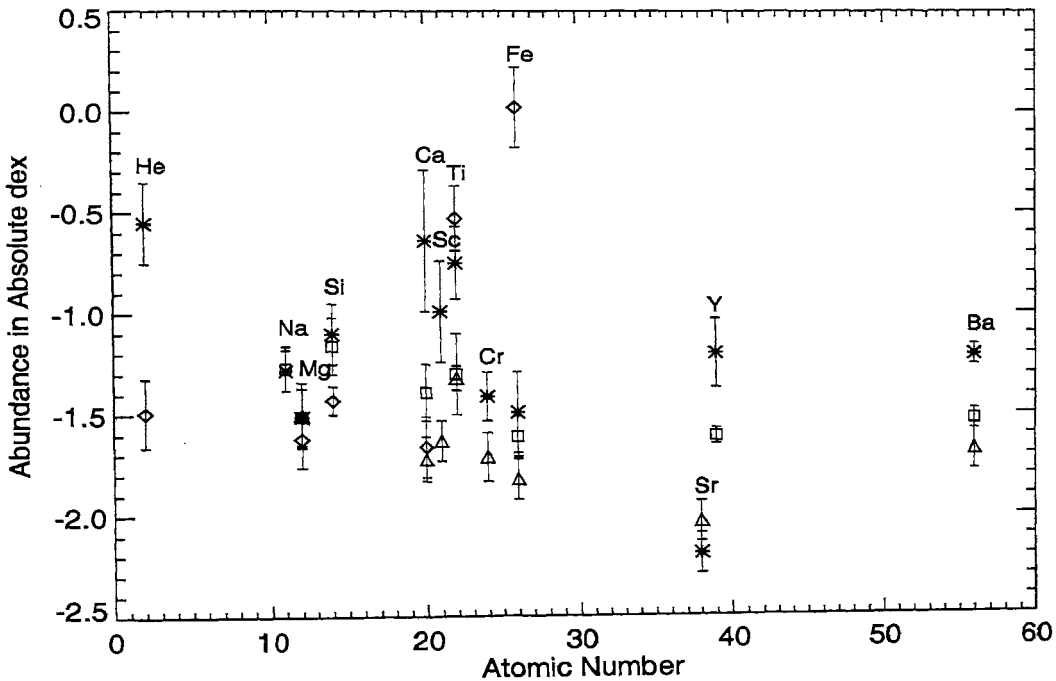


Figure 6.1: The abundances of different elements in ZNG 4 in M13 (represented by asterisk) compared with M13/J11 (BHB star; triangles), M13/WF4-3485 (hot BHB star; diamonds) and that of M13/L262 (RGB star; squares) with their error bars (Table 3.3). In the cases where only upper limit of the abundances are given (3rd and 4th column of Table 3.3), those elements are not shown in the above figure. Average abundances of Y and Ba in M13 RGB stars are from Armosky et al. (1994).

The abundances and rotational velocity of ZNG 4 is contrary to what is expected

of stars on the red side of HB gap. Being at  $T_{\text{eff}}$  of 8500 K, it shows low rotational velocity ( $v \sin i = 7 \text{ km s}^{-1}$ ), underabundance of He and overabundance of Ca, Ti, Sc and Ba (see Figure 6.1). This could either mean, the onset of diffusion of elements seem to start at lower  $T_{\text{eff}}$  or it is a star evolved from the blue side of HB gap moving towards the red with a higher luminosity.

From the luminosity and its position in the color-magnitude diagram of the cluster, we infer ZNG 4 to be a Supra Horizontal Branch (post-HB) star. The abundance pattern in ZNG 4 indicate that diffusion and radiative levitation of elements may be in operation in M13 post-HB stars even at  $T_{\text{eff}}$  of 8500K. It is important to derive the chemical compositions of significant sample of post-HB stars hotter than 11,000 K and much cooler than 11,000 K to understand the role of diffusion, radiative levitation, rotation and convection in horizontal branch stars.

Post-Early AGB (P-EAGB) stars evolve through early stages of the AGB but not the thermally pulsing stage, as the envelop is consumed from below by nuclear burning and probably from above by stellar winds (Greggio & Renzini 1990, Dorman et al. 1993). They are supposed to have evolved from extreme horizontal branch stars. Greggio & Renzini (1990), while discussing the UV upturn in elliptical galaxies point out the need to assess the size of the hot star's (for example, Post-AGB stars, P-RGB stars, accreting white dwarfs) contribution to the UV rising branch in them. But in the other hypothetical cases (such as hot HB and P-EAGB stars), they say, *it is their mere existence which has to be proven first.*

The color-magnitude diagrams of the globular clusters having blue tail with prominent HB gap (like M13, M80, NGC 6752), show stars which are above the horizontal branch (HB) and towards the left of red giant branch (RGB), called Supra Horizontal Branch (SHB) stars. Analysis of these SHB stars in globular clusters having blue tails, like ZNG 4 in M13 might provide an observational counterpart to the Post-Early AGB stars (de Boer, 1987). Thus a detailed abundance analysis of several SHB stars in globular clusters like ZNG 4 in M13, is needed to further understand the abundance anomalies.

## 6.2 LSE 202

Table 6.2: Abundances of elements in LSE 202

$T_{\text{eff}} = 4750 \text{ K}$ , $\log g = 1.5$ $V_t = 1.85 \text{ km s}^{-1}$ and $[\text{Fe}/\text{H}] = -2.41$				Abundances in HD 122563	Abundances in BPS CS 22892-52
Element	no of lines	$[\text{X}/\text{H}] \pm \sigma$	$[\text{Ele}/\text{Fe}]$	$[\text{Fe}/\text{H}] = -2.77$	$[\text{Fe}/\text{H}] = -2.92$
Li I			$< -0.56$		
Na I	02	$-2.24 \pm 0.23$	-0.24	-0.15	-0.19
Mg I	08	$-2.02 \pm 0.22$	+0.39	+0.51	+0.30
Al I	02	$\pm 0.12$	+0.12	-0.32	-0.58
Si I	02	$-2.54 \pm 0.19$	-0.14	+0.46	+0.36
K I	01	$-1.86 \pm 0.14$	+0.20	+0.46	+0.46
Ca I	26	$-2.13 \pm 0.13$	+0.29	+0.29	+0.30
Ca II	02	$-2.15 \pm 0.15$	+0.26		
Sc II	16	$-2.15 \pm 0.14$	+0.24	+0.15	-0.10
Ti I	35	$-2.10 \pm 0.16$	+0.31	+0.19	+0.20
Ti II	53	$-2.02 \pm 0.17$	+0.39	+0.28	+0.16
V I	01	$-2.41 \pm 0.13$	+0.01	+0.07	-0.05
V II	01	$-2.48 \pm 0.13$	-0.05	+0.14	-0.03
Cr I	23	$-2.49 \pm 0.15$	-0.08	-0.39	-0.24
Cr II	03	$-2.29 \pm 0.16$	+0.12	-0.15	-0.15
Mn I	07	$-2.61 \pm 0.19$	-0.29	-0.26	-0.53
Fe I	232	$-2.37 \pm 0.13$		0.00	0.00
Fe II	20	$-2.45 \pm 0.12$		0.00	+0.01
Co I	08	$-1.98 \pm 0.21$	+0.40	+0.32	+0.20
Ni I	28	$-2.38 \pm 0.16$	+0.01	+0.04	-0.07
Zn I	04	$-2.11 \pm 0.14$	+0.30	+0.20	+0.09
Sr II	02	$-2.66 \pm 0.24$	-0.26	+0.17	+0.58
Y II	07	$-2.78 \pm 0.16$	-0.38	-0.25	+0.44
Zr II	02	$-2.41 \pm 0.14$	+0.00	+0.18	+0.73
Ba II	02	$-2.85 \pm 0.14$	-0.43	-0.93	+0.99
La II	02	$-2.86 \pm 0.20$	-0.43	-0.70	+1.09
Nd II	02	$-2.32 \pm 0.21$	+0.10	-0.30	+1.33
Eu II	02	$-2.27 \pm 0.14$	+0.14	-0.36	+1.64
Dy II	01	$-2.16 \pm 0.14$	+0.25	...	+1.73

Analysis of the high resolution spectrum of the halo giant LSE 202 covering the wavelength range  $3750 \text{ \AA}$  to  $10,100 \text{ \AA}$  yields :  $T_{\text{eff}} = 4500 \pm 250 \text{ K}$ ,  $\log g = 1.0 \pm 0.5$ ,  $[\text{Fe}/\text{H}] = -2.41$  and  $V_t = 1.85 \text{ km s}^{-1}$ . All  $\alpha$ -process elements except Si show moderate overabundance of  $+0.3 \text{ dex}$  ( $[\text{Mg}/\text{Fe}] = +0.39$ ,  $[\text{Ca}/\text{Fe}] = +0.28$ ,  $[\text{Ti}/\text{Fe}] = +0.35$  and  $[\text{Si}/\text{Fe}] = -0.14$ ). Odd- $z$  elements (Na, K, Sc) are also overabundant except vanadium

( $[\text{Na}/\text{Fe}] = -0.24$ ,  $[\text{K}/\text{Fe}] = +0.20$ ,  $[\text{Sc}/\text{Fe}] = +0.24$  and  $[\text{V}/\text{Fe}] = -0.02$ ). Among Fe-peak elements, Mn shows underabundance, Cr goes with Fe and Co, Ni are slightly overabundant ( $[\text{Mn}/\text{Fe}] = -0.29$ ,  $[\text{Cr}/\text{Fe}] = +0.02$   $[\text{Co}/\text{Fe}] = +0.40$  and  $[\text{Ni}/\text{Fe}] = +0.01$ ). The heavy elements Ba, Sr, La and Y show deficiency ( $[\text{Ba}/\text{Fe}] = -0.43$ ,  $[\text{Sr}/\text{Fe}] = -0.26$ ,  $[\text{La}/\text{Fe}] = -0.43$  and  $[\text{Y}/\text{Fe}] = -0.38$ ), while Nd and Zr remain at the metallicity of the star ( $[\text{Nd}/\text{Fe}] = +0.10$  and  $[\text{Zr}/\text{Fe}] = +0.0$ ). Dy and the r-process element Eu show slight enhancement ( $[\text{Dy}/\text{Fe}] = +0.25$  and  $[\text{Eu}/\text{Fe}] = +0.14$ ), which agrees with the observations of other metal poor stars (Refer to Figure 1.7 in Introduction Chapter). With  $[\text{Ba}/\text{Eu}] = 0.6$ , we can infer that the heavy elemental abundances in this star are of r-process origin (refer to Table 6.2), similar to that found in other metal poor stars (McWilliam et al. 1995, Ryan et al. 1996).

### 6.3 BPS CS objects

Spectra of BPS CS 29516-0041 reveals the atmospheric parameters to be  $T_{\text{eff}} = 5000 \pm 250$  K,  $\log g = 2.5 \pm 0.5$  dex,  $[\text{Fe}/\text{H}] = -3.0$  and  $V_t = 1.6$  kms $^{-1}$ . Li is underabundant ( $\epsilon(\text{Li}) < 0.71$  dex). Na also shows deficiency ( $[\text{Na}/\text{Fe}] = -1.16$ ) whereas K is slightly overabundant ( $[\text{K}/\text{Fe}] = +0.18$ ).  $\alpha$ -elements show nearly solar or slightly enriched abundances ( $[\text{Mg}/\text{Fe}] = -0.04$ ,  $[\text{Ca}/\text{Fe}] = +0.12$  and  $[\text{Ti}/\text{Fe}] = +0.08$ ) and Cr, Ni goes with the metallicity of the star ( $[\text{Cr}/\text{Fe}] = -0.08$  and  $[\text{Ni}/\text{Fe}] = -0.07$ ). Ba deficiency is again observed ( $[\text{Ba}/\text{Fe}] = -0.28$ ).

We deduce  $T_{\text{eff}} = 4750 \pm 250$  K,  $\log g = 1.0 \pm 0.5$  dex,  $[\text{Fe}/\text{H}] = -2.72$  and  $V_t = 1.7$  kms $^{-1}$  for the star BPS CS 29516-0024. Li shows depletion again in this metal poor giant ( $\epsilon(\text{Li}) = 0.97$  dex). In odd-z elements, Na is underabundant again and Sc goes with metallicity of the star ( $[\text{Na}/\text{Fe}] = -0.38$  and  $[\text{Sc}/\text{Fe}] = -0.04$ ).  $\alpha$ -process elements show moderate enhancement ( $[\text{Mg}/\text{Fe}] = +0.66$ ,  $[\text{Ca}/\text{Fe}] = +0.45$  and  $[\text{Ti}/\text{Fe}] = +0.23$ ). In Fe peak elements, Cr is underabundant whereas Ni is of iron metallicity ( $[\text{Cr}/\text{Fe}] = -0.32$  and  $[\text{Ni}/\text{Fe}] = +0.08$ ). Heavy elements Y and Ba are underabundant ( $[\text{Y}/\text{Fe}] = -0.44$  and  $[\text{Ba}/\text{Fe}] = -1.04$ ).

For BPS CS 29522-0046, we obtain  $T_{\text{eff}} = 5500 \pm 250$  K,  $\log g = 3.0 \pm 0.5$  dex,

$[\text{Fe}/\text{H}] = -2.3$  and  $V_t = 1.1 \text{ kms}^{-1}$ . Abundance of Li (1.89 dex) is slightly less compared to the Li abundance in metal poor dwarfs (2.1 dex), which indicates the depletion of Li in this metal poor halo giant also. As in the case of other stars,  $\alpha$ -elements are enhanced ( $[\text{Mg}/\text{Fe}] = +0.55$ ,  $[\text{Ca}/\text{Fe}] = +0.45$  and  $[\text{Ti}/\text{Fe}] = +0.20$ ), Na is deficient ( $[\text{Na}/\text{Fe}] = -0.28$ ), whereas Sc shows overabundance of +0.18 dex. Cr shows deficiency ( $[\text{Cr}/\text{Fe}] = -0.11$ ). The heavy element, Ba is mildly depleted ( $[\text{Ba}/\text{Fe}] = -0.14$ ).

McWilliam et al. (1995) discuss, how trend of six element ratios (Cr, Mn, Co, Al, Sr and Ba) show a sudden change in slope, at a unique metallicity, near  $[\text{Fe}/\text{H}] = -2.4$ . The production of light s-element, Sr in the galaxy is not clear whereas, Ba is of r-process origin. The Ba/Eu and La/Eu ratios reveal that the first significant introduction of heavy s-process isotopes occurred at a metallicity  $[\text{Fe}/\text{H}] \approx -2.0$ . The time at which this occurred, presumably set by the lifetime of the low mass ( $\approx 1 - 2M_\odot$ ) AGB star s-process nucleosynthesis site, is of the order of  $10^{10}$  yr (Truran et al. 2002).

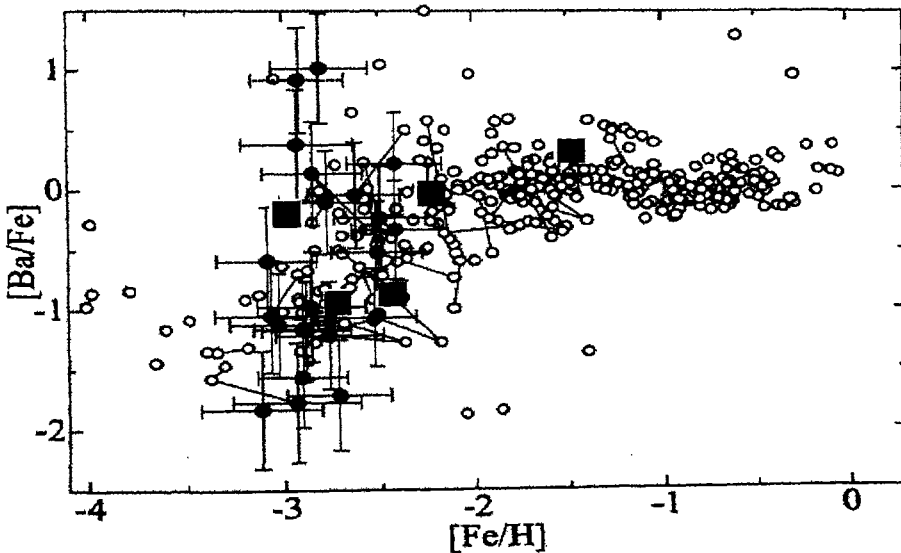


Figure 6.2: Ba abundances of the stars analyzed are overplotted on the graph showing evolution of Ba with respect to  $[\text{Fe}/\text{H}]$  of the stars. (Honda et al. 2004). Filled squares mark the Ba abundances of the stars analyzed in this thesis.

Barium, which has nearly solar ratio till  $[\text{Fe}/\text{H}] = -2.0$ , starts declining further

with decreasing metallicity (McWilliam et al. 1995). We detected Ba in all the four halo stars and its abundance confirms this trend. In BPS CS 29522-0046, which has  $[\text{Fe}/\text{H}] = -2.3$  shows the onset of this trend with  $[\text{Ba}/\text{Fe}] = -0.14$ . LSE 202 (with  $[\text{Fe}/\text{H}] = -2.4$ ) shows Ba deficiency of  $-0.44$  dex. But in the case of BPS CS 29522-0046 which has metallicity less than  $-2.7$ , Ba deficiency is about 1 dex.

Abundance studies of many more stars between  $-2.0 < [\text{Fe}/\text{H}] < -3.0$  are required to put a constraint on the distinct phase of nucleosynthesis, that could have occurred before the Galaxy reached  $[\text{Fe}/\text{H}] \approx -2.4$ .



# References

---

- Alonso, A., Arribas, S., Martínez-Roger, C., 1999, *A&AS*, 140, 261
- Anders, E., Grevesse, N., 1989, *Geochim. Cosmochim. Acta*, 53, 197
- Aoki, W., Norris, J. E., Ryan, S. G., Beers, T. C., Ando, H., 2000, *ApJ*, 536, L97
- Armosky, B. J., Sneden, C., Langer, G. E., Kraft, R. P., 1994, *AJ*, 108, 1364
- Arnett, W. D., 1971, *ApJ*, 166, 153
- Audouze, J., Silk, J., 1995, *ApJ*, 451L, 49
- Becker, S. A., Iben, I. Jr., 1979, *ApJ*, 232, 831
- Beers, T. C., Preston, G. W., Shectman, S. A., 1985, *AJ*, 90, 2089
- Beers, T. C., Preston, G. W., Shectman, S. A., 1985, *AJ*, 90, 2089
- Beers, T. C., Preston, G. W., Shectman, S. A., 1992, *AJ*, 103, 1987
- Beers, T. C., Preston, G. W., Shectman, S. A., 1992, *AJ*, 103, 1987
- Beers, T. C., Sommer-Larsen, J., 1995, *ApJS*, 96, 175
- Beers, T. C., Rossi, S., Norris, J. E., Ryan, S. G., Shefler, T., 1999, *AJ*, 117, 981

- Beers, T. C., Drilling, J. S., Rossi, S., Chiba, M., Rhee, J., Führmeister, B., Norris, J. E., von Hippel, T., 2002, *AJ*, 124, 931
- Behr, B. B., Cohen, J. G., McCarthy, J. K., Djorgovski, S. G., 1999, *ApJ*, 517L, 135
- Behr, B. B., Djorgovski, S. G., Cohen, J. G., McCarthy, J. K., Cote, P., Piotto, G., Zoccali, M., 2000a, *ApJ*, 528, 849
- Behr, B. B., Cohen, J. G., McCarthy, J. K., 2000b, *ApJ*, 531, L37
- Behr, B. B., 2000c, PhD, Thesis, California Institute of Technology.
- Bond, H. E., 1980, *ApJS*, 44, 517
- Bond, H. E., 1981, *ApJ*, 248, 606
- Bonifacio, P., Monai, S., Beers, T. C., 2000, *AJ*, 120, 2065
- Brocato, E., Matteucci, F., Mazzitelli, I., Tornambe, A., 1990, *ApJ*, 349, 458
- Burbidge, E. M., Burbidge, G. R., Fowler, W. A., Hoyle, F., 1957, *RvMP*, 29, 547
- Busso, M., Gallino, R., Wasserburg, G. J., 1999, *ARA&A*, 37, 239
- Carney, B. W., Latham, D. W., Laird, J. B., Aguilar, L. A., 1994, *AJ*, 107, 2240
- Carroll, B. W., Ostlie, D. A., 1996, *An Introduction to Modern Astrophysics*
- Castelli, F., Hack, M., 1990, *MmSAI*, 61, 595
- Cavallo, R. M., Nagar, N. M., 2000, *AJ*, 120, 1364
- Cayrel, R., 1988, *IAUS*, 132, 345
- Cayrel, R., 1996, *A&ARv*, 7, 217
- Cayrel, R., Depagne, E., Spite, M., Hill, V., Spite, F., François, P., Plez, B., Beers, T., Primas, F., Andersen, J., Barbuy, B., Bonifacio, P., Molaro, P., Nordström, B., 2004, *A&A*, 416, 1117

- Christlieb, N., Wisotzki, L., Reimers, D., Homeier, D., Koester, D., Heber, U., 2001, *A&A*, 366, 898
- Christlieb, N., Gustafsson, B., Korn, A. J., Barklem, P. S., Beers, T. C., Bessell, M. S., Karlsson, T., Mizuno-Wiedner, M., 2004, *ApJ*, 603, 708
- Cohen, J. G., Christlieb, N., McWilliam, A., Shectman, S., 2004, ( *astro-ph/0405286* )
- Conlon, E.S., Dufton, P. L., Keenan, F. P., 1994, *A&A*, 290, 897
- Couchman, H. M. P., Rees, M. J., 1986, *MNRAS*, 221, 53
- Cudworth, K. M., Monet, D. G., 1979, *AJ*, 84, 774
- de Boer, K.S., 1985, *A&A*, 142, 321
- de Boer, K, S., 1987, The second conference on faint blue stars, IAU colloquium, No.95, p95, L.Davis Press
- Dorman, B., Rood, R. T., O'Connell, R. W., 1993, *ApJ*, 419, 596
- Drilling, J. S., Bergeron, L. E., 1995, *PASP*, 107, 846
- Edmunds, M. G., Pagel, B. E. J., 1984, 3rd workshop on Stellar Nucleosynthesis Proceedings, 341
- Eggen, O. J., Lynden-Bell, D., Sandage, A. R., 1962, *ApJ*, 136, 748
- Ferraro, F. R., Paltrinieri, B., Fuci Pecci, F., Dorman, B., Rood, R.T., 1997, *ApJ*, 500, 311
- Flower, P. J., 1996, *ApJ*, 469, 355
- Gallino, R., Arlandini, C., Busso, M., Lugaro, M., Travaglio, C., Straniero, O., Chieffi, A., Limongi, M., 1998, *ApJ*, 497, 388
- Gehren, T., Liang, Y. C., Shi, J. R., Zhang, H. W., Zhao, G., 2004, *A&A*, 413, 1045

- Gingold, R. A., 1976, *ApJ*, 204, 116
- Glaspey, J.W., Michaud G., Moffat A.F.J., Demers S., 1989, *ApJ*, 339, 926
- Gonzalez, G., Wallerstein, G., 1994, *AJ*, 108, 1325
- Greenstein, G. S., Truran, J. W., Cameron, A. G. W., 1967, *Nature*, 213, 871
- Greggio, L., Renzini, A., 1990, *ApJ*, 364, 35
- Grundahl, F., Catelan, M., Landsman, W. B., et al., 1999, *ApJ*, 524, 242
- Ivanova, D. V., Shimanskii, V. V., 2000, *ARep (Astronomy reports)*, 44, 376
- Harris, H. C., Nemec, J. M., Hesser, J. E., 1983, *PASP*, 95, 256
- Honda, S., Aoki, W., Kajino, T., Ando, H., Beers, T. C., Izumiura, H., Sadakane, K., Takada-Hidai, M., 2004, *ApJ*, 607, 474,
- Ivanova, D. V., Shimansky, V. V., 2000, *AZh*, 77, 432 (English transl. *Astron. Rep.* 44, 376)
- Ivans, I. I., Sneden, C., Kraft, R. P., et al., 1999, *ApJ*, 118, 1273
- Ishimaru, Y., Wanajo, S., 1999, *ApJ*, 511L, 33
- Ishimaru, Y., Wanajo, S., Aoki, W., Ryan, S. G., 2004, *ApJ*, 600L, 47
- Kajino, T., Mathews, G. J., Fuller, G. M., 1990, *ApJ*, 364, 7
- Kraft, R. P., Sneden, C., Langer, G.E., Shetrone, M. D., 1993, *AJ*, 106, 1490
- Kraft, R. P., Sneden, C., Smith, G. H., Shetrone, M. D., Langer, G. E., Pilachowski, C. A., 1997, *AJ*, 113, 279
- Kraft, R. P., Ivans, I. I., 2003, *PASP*, 115, 143
- Kurucz, R. L., 1993, (Kurucz CD-ROMS, Cambridge: Smithsonian Astrophys. Obs.)
- Lambert, David L.; Reddy, Bacham E., 2004, *MNRAS*, 349, 757

- Majewski, S. R., 1992, *ApJS*, 78, 87
- McWilliam, A., Preston, G. W., Sneden, C., Searle, L., 1995, *AJ*, 109, 2757
- Michaud, G., Vauclair, G., Vauclair, S., 1983, *ApJ*, 267, 256
- Moehler, S., Heber, M., Lemke, M., Napiwotzki, R., 1998, *A&A*, 339, 537
- Moehler, S., 1999, *Reviews in Modern Astronomy*, 12, p281
- Moehler, S., Sweigart, A.V., Landsman, W.B., Heber, U., Catelan, M., 1999, *A&A*, 346, L1
- Moehler, S., Sweigart, A.V., Landsman, W.B., Heber, U., 2000 *A&A*, 360, 120
- Moehler, S., Landsman, W. B., Sweigart, A. V., Grundahl, F., 2003, *A&A*, 405, 135
- Moore, C. E., 1945, *A Multiplet Table of Astrophysical Interest, Part I, Table of Multiplets*, revised ed. (Princeton: Princeton Univ. Obs.)
- Morrison, H. L., Flynn, C., Freeman, K. C., 1990, *AJ*, 100, 1191
- Noguchi, K., Aoki, W., Kawanomoto, S., et al., 2002, *PASJ*, 54, 855
- Norris, J. E., Ryan, S. G., Beers, T. C., 1999, *ApJS*, 123, 639
- Paltrinieri, B., Ferraro, F. R., Carretta, E., Fusi Pecci, F., 1998, *MNRAS*, 293, 434
- Peterson, R. C., 1981, *ApJ*, 244, 989
- Peterson, R. C., 1983, *ApJ*, 275, 737
- Peterson, R. C., Rood, R.T, Crocker, D.A, 1995, *ApJ*, 453, 21
- Preston, G, W., Sneden, C., 2000, *AJ*, 120, 1014
- Rey, S-C., Yoon, S-J., Lee, Y-W., Chaboyer, B., Sarajedini, A., 2001, *AJ*, 122, 3219

- Richer J., Michaud G., Turcotte S., 2000, *ApJ* 529, 338
- Ryan, S. G., Norris, J. E., Beers, T. C., 1996, *ApJ*, 471, 254
- Ryan, S. G., Norris, J. E., Beers, T. C., 1998, Workshop on Subaru HDS : vol 1 (ed : Hidai & Ando), vol 1, 69
- Ryan, S. G., Deliyannis, C. P., 1998a, *ApJ*, 500, 398
- Ryan, S. G., Norris, J. E., Beers, T. C., 1999, *ApJ*, 523, 654
- Sandage, A., Kowal, C., 1986, *AJ*, 91, 1140
- Sandage, A., Fouts, G., 1987, *AJ*, 93, 74
- Schlegel, D. J., Finkbeiner, D. P., Davis, M., 1998, *ApJ*, 500, 525
- Shara, M. M., Drissen, L., Rich, R. M., Paresce, F., King, I. R., Meylan, G., 1998, *ApJ*, 495, 796
- Sivarani, T., Bonifacio, P., Molaro, P., Cayrel, R., Spite, M., Spite, F., Plez, B., Andersen, J., Barbuy, B., Beers, T. C., Depagne, E., Hill, V., François, P., Nordström, B., Primas, F., 2004, *A&A*, 413, 1073
- Snedden, C., 1973, *ApJ*, 184, 839
- Snedden, C., Cowan, J. J., Lawler, J. E., Ivans, I. I., Burles, S., Beers, T. C., Primas, F., Hill, V., Truran, J. W., Fuller, G. M., Pfeiffer, B., Kratz, Ki., 2003, *ApJ*, 591, 936
- Shu, F. H., 1982, *The Physical Universe – an Introduction to Astronomy*
- Snedden, C., Parthasarathy, M., 1983, *ApJ*, 267, 757
- Spite, M., Spite, F., 1978, *A&A*, 67, 23
- Spite, F., Spite, M., 1982, *A&A*, 115, 357
- Spite, M., Spite, F., 1985, *ARA&A*, 23, 225
- Spite, M., François, P., Nissen, P. E., Spite, F., 1996, *A&A*, 307, 172

- Sweigart, A. V., Mengel, J. G., Demarque, P., 1974, *A&A*, 30, 13
- Sweigart A.V., 2002, *IAU Highlights of Astronomy* 12, 293
- Trimble, V., 1983, *Reviews of Modern Physics (RvMP)*, 55, 511
- Truran, J. W., Cameron, A. G. W., 1971, *Ap&SS*, 14, 179
- Truran, J. W., 1981, *A&A*, 97, 391
- Truran, J. W., Cowan, J. J., Pilachowski, C. A., Sneden, C., 2002, *PASP*, 114, 1293
- Tull, R. G., MacQueen, P. J., Sneden, C., Lambert, D. L., 1995, *PASP*, 107, 251
- Turcotte S., Richer J., Michaud G., 1998, *ApJ* 504, 559
- Umeda, H., Nomoto, K., 2002, *ApJ*, 565, 385
- Vink, J. S., Cassisi, S., 2002, *A&A*, 392, 553
- Wallerstein, G., Iben, I. Jr., Parker, P., Boesgaard, A. M., Hale, G. M., Champagne, A. E., Barnes, C. A., Käppeler, F., Smith, Verne V., Hoffman, R. D., Timmes, F. X., Sneden, C., Boyd, R. N., Meyer, B. S., Lambert, D. L., 1997, *RvMP*, 69, 995
- Westin, J., Sneden, C., Gustafsson, B., Cowan, J. J., 2000, *ApJ*, 530, 783
- Yoshii, Y., 1981, *A&A*, 97, 280
- Yoshii, Y., Mathews, G. J., Kajino, T., 1995, *ApJ*, 447, 184
- Zinn, R. J., Newell, E. B., Gibson, J. B., 1972, *A&A*, 18, 390
- Zinn, R. J., 1974, *ApJ*, 193, 593

# List of Publications

## Accepted, Submitted and in Preparation

1. *Chemical Composition of UV-bright star ZNG 4 in the Globular Cluster M13*  
S. Ambika, M. Parthasarathy , W. Aoki, T. Fujii, Y. Nakada, Y. Ita, H. Izumiura  
2004, A&A, 417, 293
2. *Variable UV extinction by the circumstellar dust around the metal poor high galactic latitude post-AGB star HD 213985.*  
S. Ambika, M. Parthasarathy, Submitted to A&A
3. *Abundance Analysis of the metal poor giant: LSE 202.*  
S. Ambika, M. Parthasarathy & B. .E. Reddy, in preparation.
4. *High resolution spectroscopy of metal poor halo giants :*  
*BPS CS 29516-0041, BPS CS 29516-0024, BPS CS 29522-0046*  
S. Ambika, M. Parthasarathy & B. .E. Reddy, in preparation.